OPERATIONAL CHARACTERISTICS OF NANO-ELECTRO-OPTO-MECHANICAL TRANSDUCER

By

Engr. Asma Javaid

Department of Electronics,

Quaid-i-Azam University, Islamabad, 45320, Pakistan.

This dissertation is submitted for the degree of

Doctor of Philosophy

March 2022

Supervised by

Prof. Dr. Farhan Saif (SI, PoP)

Department of Electronics,

Quaid-i-Azam University, Islamabad, 45320, Pakistan.

Dedicated

to

My Parents

QUAID-I-AZAM UNIVERSITY

Department of Electronics

Author's Declaration

I, **Asma Javaid** hereby state that my PhD thesis titled

"Operational Characteristics of Nano-Electro-Opto-Mechanical Transducer" is my own work and has not been submitted previously by me for taking degree from **Department of Electronics, Quaid-i-Azam University** Or anywhere else in the country/world.

At any time if my statement is found to be incorrect even after my graduation, the university has the right to withdraw my PhD degree.

Asma Javaid

Date: 30-11-2022

QUAID-I-AZAM UNIVERSITY
Department of Electronics

QUAID-I-AZAM UNIVERSITY
ISLAMABAD

Plagiarism Undertaking

I solemnly declare that research work presented in the thesis titled,

"Operational Characteristics of Nano-Electro-Opto-Mechanical Transducer"

is solely my research work with no significant contribution from any other person. Small contribution/help wherever taken has been duly acknowledged and that complete thesis has been written by me.

I understand the zero-tolerance policy of the HEC and Quaid-i-Azam University towards plagiarism. Therefore, I as an Author of the above titled thesis, declare that no portion of my thesis has been plagiarized and any material used as reference is properly referred/cited.

I undertake that if I am found guilty of any formal plagiarism in the above titled thesis even after award of PhD degree, the University reserves the rights to withdraw/revoke my PhD degree and that HEC and the University has the right to publish my name on the HEC/University Website on which names of students are placed who submitted plagiarized thesis.
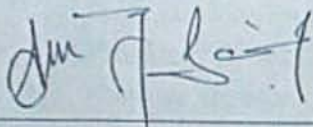
Student/Author Signature: _____

Name: **Asma Javaid**

Certificate

It is certified that the work presented in this dissertation entitled "**Operational Characteristics of Nano-Electro-Opto-Mechanical Transducer**" is accomplished by **Engr. Asma Javaid** under the supervision of **Prof. Dr. Farhan Saif** at Quaid-i-Azam University, Islamabad, Pakistan.
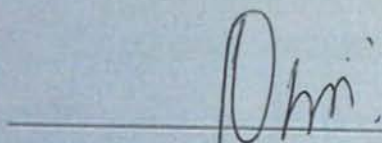
Research Supervisor:

Prof. Dr. Farhan Saif (SI, PoP)

Professor

Department of Electronics

Quaid-i-Azam University, Islamabad, Pakistan.

Submitted Through:

Prof. Dr. Qaiser Abbas Naqvi

Chairman

Department of Electronics

Quaid-i-Azam University, Islamabad, Pakistan.

Acknowledgments

In the name of Allah Almighty, the most beneficent and the most merciful. He is the one who creates the entire Universe and humans to explore His creation. I am thankful to Almighty Allah for His countless Mercy on me, the power, the help, and the courage he bestowed on me for the completion of my manuscript and making it possible for me. I would like to be beholden to my Supervisor Prof. Dr. Farhan Saif who granted me an opportunity to work with him. I am really honored for being his student. His valuable guidance and support at each and every level helped me to accomplish my work. I would not be able to finish this manuscript without his valuable suggestions and efforts.

I am thankful to my colleagues who always lent their helping hands to solve the problems which I faced during my research work. I am really obliged to my parents for their support and sacrifice in making everything possible in my life. I am thankful to all those friends and relatives who have prayed for me to complete this thesis.

<div align="right">

Engr. Asma Javaid

March 2022

</div>

Abstract

In this dissertation, we theoretically investigate the dynamics of a Nano Electro Opto-Mechanical System (NEOMS) in the presence of a strong pump field and a weak probe field. A Fabry-Perot cavity, with a fixed and partially transparent mirror at one end and a completely reflecting movable mirror MR_1 at the other end makes up the system. The Opto-mechanical coupling connects MR_1 to the intra-cavity field. The cavity also has a second moveable micro-resonator, MR_2, which is electro-statically connected to MR_1 via Coulomb coupling. To selectively pump the mechanical resonators (MR_s), mechanical driving fields ε_1 and ε_2 are used.

In NEOMS, a non-linear phenomena known as Four-Wave Mixing (FWM) is examined in the probe transmission field. This non-linearity is generated by the radiation pressure force of the intra-cavity field, produces the FWM which is analogous to the non-linear Kerr effect in optical fibers, which creates non-linear susceptibility in the medium. This non-linear effect is known as the Effective Kerr Effect, and is responsible for Four-Wave Mixing.

FWM is reported in the probe transmission field by selectively driving the mechanical resonators MR_1 and MR_2, which provides additional control of FWM. When the amplitudes and phases of the external driving fields are changed, the FWM shows consistent variations. The results reveal that changing the amplitudes and phases of external driving fields can yield significant suppression and amplification in the FWM peaks.

In the presence of Bose-Einstein Condensate (BEC) trapped inside the cavity, the FWM phenomena is also enhanced. We show that in the presence of atomic medium (BEC) in the optical cavity, the FWM intensity is significantly suppressed and amplified. By varying of atom-field coupling strength, the intensities of FWM peaks fluctuate coherently. Furthermore, we show that selected mechanical drivings fields of MR_s effectively modulate the medium-mediated FWM signal.

Furthermore, we explore another non-linear effect in an nano-transducer theoretically which is bi-stability. The opto-mechanical coupling that causes the non-linearity in NOEMS, also produces bi-stable behaviour in the mean intra-cavity photon number. We investigate the optical as well as mirror bi-stability for the NEOMS in the presence of external driving fields on the micro-resonators MR_1 and MR_2. The external driving fields can be used to control the bi-stability. We present a powerful scheme to experimentally realize an optical switch primarily based on optical bi-stability in a NEOMS. We report an optical and a mirror bi-stability as a function of input laser power, coupling frequencies and external mechanical pump fields on MR_1 and MR_2. Here, the coupling frequencies and the switchable driving fields allow a threshold value of cavity field detuning and of laser power which can be utilized in developing tunable optical switches and optical transistors.

Contents

List of Publications

1. Javaid, Asma, Sohail Ahmed, Fazal Ghafoor, Tomotake Yamakoshi, and Farhan Saif. *"Controlled Four-Wave Mixing in a Nanotransducer."* Journal of Russian Laser Research 42, no. 2 (2021): 126-135.

2. Farhan Saif, Sohail Ahmed, Asma Javaid. "*Engineering Optical and Mirror Bistability Mechanically*" (2022). (Submitted to Phys. Rev. B)

3. Sohail Ahmed, Asma Javaid, Farhan Saif. "*Controlled Four-Wave Mixing in a Nano-Electro-Opto-Mechanical Transducer with Bose-Einstein Condensate*". (In Process)

List of Figures

xv

Acronyms

BEC   Bose-Einstein Condensate

COMS   Cavity-bases Opto Mechanical System

EIT   Electro-magnetically Induced Transparency

EOMS   Electro Opto Mechanical System

FWM   Four-Wave Mixing

MR   Mechanical Resonator

NEOMS   Nano Electro Opto Mechanical System

OMIT   Opto-mechanically Induced Transparency

OMS   Opto-Mechanical System

QOMS   Quantum Opto Mechanical System

Chapter 1

Introduction

Light has been a contentious topic of debate throughout human development. Today we understand the classical and quantum effects of light. In Quantum Electronics, we study light (photons) and its interactions with matter at the microscopic and macroscopic level [1]. The Quantum mechanical systems at microscopic level includes the interaction of light with particles such as photons, atoms, and electrons,whereas at macroscopic scale it includes the dynamics of macroscopic systems with focus on nano- and micro-electronic devices.

1.1   Literature Review

The exchange of momentum between an object and the electromagnetic field produces a pressure force known as radiation pressure force. This includes the momentum of any wavelength of light or electromagnetic radiation absorbed, reflected, or otherwise emitted by materials on any scale. James Clark Maxwell devised a quantitative analysis

for the radiation pressure force, which was later detected in a laboratory in 1901 by Nichols and Hull in Dartmouth. Since that day, the radiation pressure force has been studied and used in a variety of applications, including the influencing the motion of cold atoms and subatomic particles. As only the fixed forces are provided by the light, so, the back-action of mechanical motion onto the electromagnetic field is absent in such scenarios. However, this type of two-way interaction is present in an opto-mechanical system [2].

The resonance that is the mechanical motion of the moving end mirror modifies the geometry of the optical cavity in opto-electronics. The impact of Opto-Mechanical effect is determined by the geometry of the cavity and the amplitude of mechanical motion. The incoming laser intensity is resonantly amplified when a powerful pump field is inserted into the cavity. The incoming laser field is multiplied by the cavity's optical fineness which is already in the millionth of order. This raises the radiation force by the same amount. Simultaneously, slight changes in the boundary of the cavity produce a shift in the optical resonance frequency, resulting in a swift decrease in light intensity, which reduces the radiation force. As a result, the ensuing motion interacts back on the light field and alters the radiation pressure force.

Radiation pressure is applied to particles such as electrons, atoms and molecules, and systems with very small dimensions, such as micro-resonators, and micro mirrors. In these systems an optical field interacts resulting in extremely intriguing non-linear quantum effects that are evaluated using well-developed quantum optics methods [2, 3]. These systems are widely employed in a variety of advancements, including integrated circuit sensors and actuators, as well as optical systems [4, 5]. By examining the optical

2

field that interacts with the mechanical system, the altered and changed dynamics of the mechanical system may be examined. The efficiency of these systems is determined by how they interact with their thermal environment.

1.2   Cavity fields

A powerful laser field drives the cavity in a conventional opto-mechanical system. The radiation pressure force is created by this intense field. The photons of this strong laser pump field consistently strike the mirror and export their momentum to it, exciting the moveable mirror at a resonance frequency by the continuous action of radiation pressure force. To analyze the system's dynamics and internal changes, the powerful laser beam is supplemented with a weak probe field.

1.3   The Opto-Mechanical Cavity

As demonstrated in Figure 1.1, the basic Opto-Mechanical Cavity with a high fineness and single mode optical cavity is shown. The vibrating end mirror (MR_1) is displaced from its mean location by the intra-cavity field's radiation pressure force, which alters the radiation pressure force.

A high Q Fabry-Perot cavity with a fixed mirror at one end and a moveable mirror (mechanical resonator MR_1) at the other end is considered. The cavity field is coupled to the mechanical resonator MR_1 through opto-mechanical coupling strength g_0.
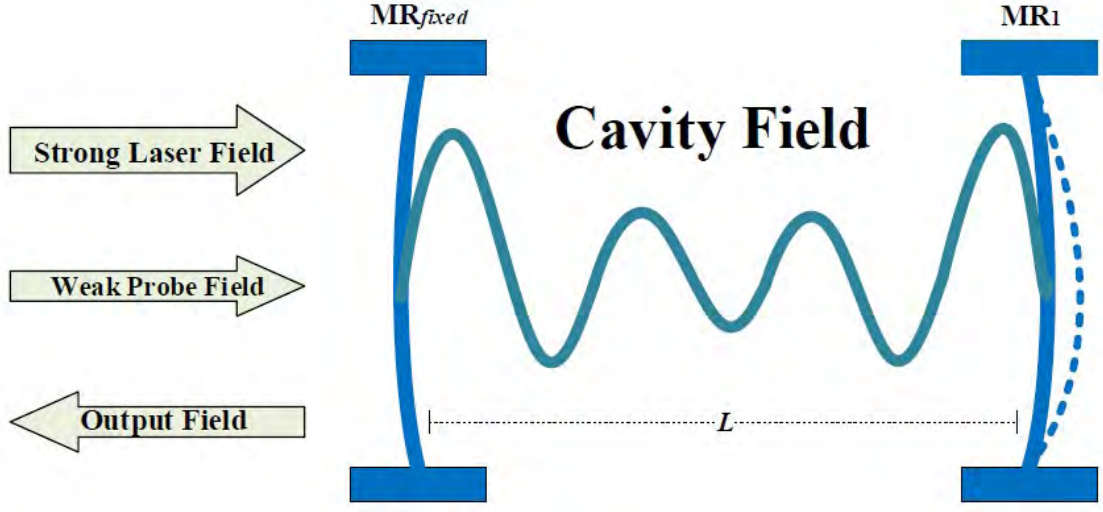
Figure 1.1: The Schematic representation of a basic Opto-Mechanical Cavity): Here, MR_1 is coupled to the cavity field through opto-mechanical interaction g_0. A strong input laser pump field of amplitude ε_l and a weak probe field of amplitude ε_p are inserted into the cavity through the fixed mirror. The length of cavity is L.

Through the fixed mirror, a strong input laser field of amplitude ε_l and a weak probe field of amplitude ε_p are pumped into the cavity. The mechanical resonator MR_1 is displaced from its mean position by the radiation pressure force, changing the cavity length. The moveable mirror compensates for this shift by exerting a back-action force on the cavity field, lowering the radiation pressure and vice versa.

1.4   Hybrid Electro-Opto-Mechanical Cavity

Hybrid quantum systems [6, 7] combine cavity-based Opto-mechanical systems with other systems such as qubits [8], mechanical membranes [9, 10], and Bose-Einstein

condensate [11]. The Quantum Electro-Opto-Mechanical System (QEMS) [12, 13] is an example of a hybrid system in which mechanical and electronic parametric parameters are extremely important. Electrostatic Coulomb interaction gives an additional degree of freedom in such systems, allowing for the resolution of side-band regimes [14, 15]. When this sort of electro-mechanical system is paired with a quantum opto-mechanical system, a novel hybrid system called as the Nano Electro Opto-Mechanical System (NEOMS) is created .

In both the classical and quantum realms, Nano Electro Opto-Mechanical Systems (NEOMS) have the potential to be effective low-noise Nano-transducers between microwave and optical signals. These type of systems provide the acuracy at nano-scale for measuring the mechanical motion of micro-resonators $(MR_{1,2})$. The mechanical vibrations of the moveable mirrors (mechanical-resonators) have a significant impact on the probe field's output signal.

This hybrid system is coupled by three different types of degrees of freedom, which are optical, electrical and mechanical. A particular Nano-Electro-Opto-Mechanical Cavity is depicted in Figure 1.2. The system contains a fixed mirror and two movable mirrors (micro-resonators) MR_1 and MR_2. The cavity composed by the MR_1 contains the optical signal i.e, cavity field and is coupled through opto-mechanical coupling strength g_o. The MR_1 is further connected to another mechanical resonator MR_2 through an electrostatic Coulomb interaction g_c. These Nano-Electro-Opto-Mechanical Systems (NEOMS) have a significant advantage over Quantum Opto-Mechanical Systems (QOMS) in the way that they offer dynamic control of the flow of light in nano-photonic structures at faster speeds and with lower power consumption.

5

Figure 1.2: The Schematic representation of the Nano-Electro-Opto-Mechanical Cavity: Here, MR_1 is coupled to the cavity field through opto-mechanical coupling g_0 and to the second mechanical resonator MR_2 through the coulomb coupling strength g_c. The length of the cavity is L while r_0 is the equilibrium distance between the two micro-resonators.

1.5 The Hybrid Electro-Opto-Mechanical Cavity with the External Driving Fields

The probe transmission field of NEOMS is further controlled by selective external driving fields of mechanical resonators MR_1 and MR_2. Selective acoustic control is used to generate symmetric and asymmetric amplifications and suppression of the output signal. The controllable motion of mechanical resonators MR_1 and MR_2 allows the switchable signal amplification and light communications. The driving fields of amplitude $|\varepsilon_1|$ and $|\varepsilon_2|$ at frequencies ω_1 and ω_2 are shined on the mechanical resonators

MR_1 and MR_2, respectively, for this purpose, as illustrated in Figure 1.3.
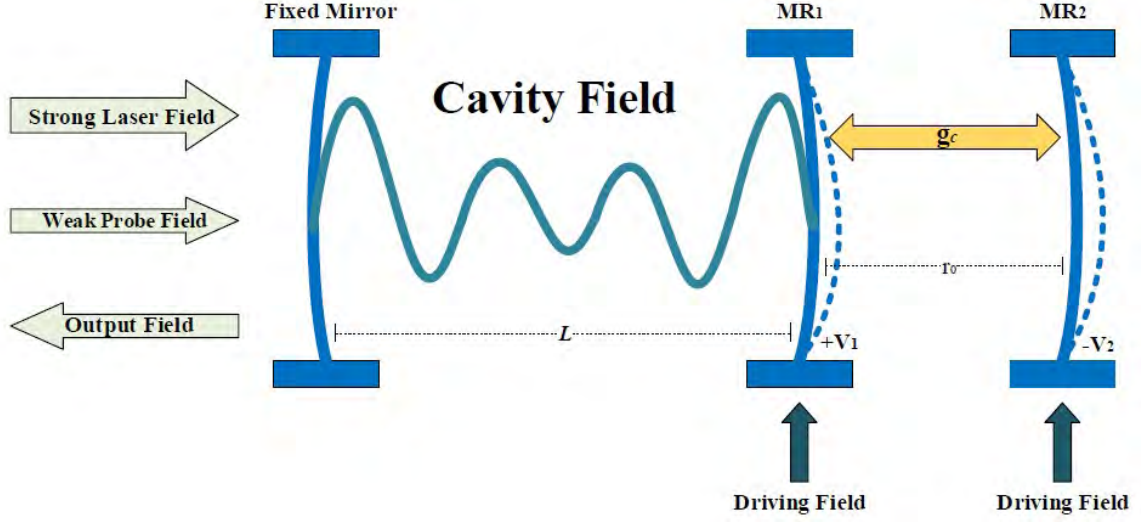
Figure 1.3: The Schematic representation of the Nano-Electro-Opto-Mechanical Cavity with external driving fields: Here, MR_1 is coupled with the cavity field through opto-mechanical coupling g_0 and to the second mechanical resonator MR_2 through the Coulomb coupling strength g_c. A strong pump field ε_l and a weak probe field ε_p is fed to the cavity. The MR_1 is charged by biased voltage $+V_1$ and the MR_2 is charged by $-V_2$. The r_0 is the equilibrium distance between MR_1 and MR_2 which are selectively driven by the arbitrary driving fields ε_1 and ε_2.

1.6 Non-linearity in Cavity-based Systems

The relative variations in photon number get lower as the input laser power increases. Another effect, namely the back-action of the vibrating end mirror onto the cavity field, which alters the radiation pressure force, kicks in at a certain point for higher laser

powers. The laser beam's inevitable photon shot noise fluctuations apply a random force on the end mirrors, imprinting some additional motion that masks the signal. The non-linearity is introduced into the cavity in this way. The effective Kerr Effect [16, 17], which derives from the radiation pressure force [6, 12], is one of these non-linearities. Because the length of the optical cavity is determined by the radiation pressure force, the conception of effective Kerr medium was developed. The opto-mechanical coupling strength g_o changes due to the intensity dependent length of the cavity. When the radiation pressure force is reduced, the mirrors' displacement increases, which causes the cavity length to increase as well, and the cycle continues.

The non-linearities are introduced into the system in this manner, which are investigated using well-developed quantum optics approaches. Four-Wave Mixing (FWM) [13, 18] electromagnetically induced transparency (EIT) [19, 20, 21, 22], opto-mechanically induced transparency (OMIT) [23, 24], optical bi-stability [25, 26], and multi-stability [27, 28] are useful tools for studying the non-linear characteristics of hybrid opto-mechanical systems.

1.7   Layout

The dynamics of a cavity-based hybrid Electro Opto-Mechanical system in the presence of a powerful pump laser are discussed in detail in this dissertation. A weak probe field is injected into the cavity in addition to the powerful pump field to scan the non-linear optical properties of the output light signal. We discuss a basic Cavity-based Opto-Mechanical System (COMS) in which a cavity field is connected to a moving-end

mirror through an opto-mechanical coupling. The partly reflecting fixed mirror injects the powerful pump laser and weak probe fields into the cavity. The outgoing intra-cavity field is used to investigate the system's dynamics. The outgoing cavity field's sudden variations in phase and amplitude provide all of the statistical information about the system's dynamics.

In the **second chapter**, the Hamiltonian of the Cavity-based System is discussed. The Hamiltonian of the Opto-Mechanical Cavity is derived. We also discussed the Hamiltonian of the hybrid Nano-Electro-Opto-Mechanical System in detail. Further the effect of external driving fields on the micro-resonators (MR_s) is considered. Then the Hamiltonian for this system is thoroughly discussed.

The **third chapter** is about the Four-Wave Mixing (FWM) which is a non-linear phenomenon. The probe transmission field of the system is used to study the inter-modulation phenomena in non-linear quantum optics known as Four-Wave Mixing (FWM). The FWM is a non-linear phenomenon generated by the effective Kerr effect of radiation pressure force. The interference of reflected and transmitted light signals to the opto-mechanical coupling field produces Four-Wave Mixing in such a system. The non-linear behaviour of Cavity-based Opto-Mechanical Systems (COMS) may be understood using FWM. In the quantum optical region, the FWM has interesting applications for creating single photons, compressed light, and entangled photons. We explore the behaviour of FWM intensity in this dissertation by externally manipulating the mechanical resonator MR_1. The switchable mechanical driving field ε_1 is applied to MR_1, providing further control of FWM signal.

We also look at the characteristics of Four-Wave Mixing light signals in a Nano

Electro Opto-Mechanical system, which is a hybrid Electro-Opto-Mechanical System (NEOMS). A second moving-end mirror MR_2 is added to the cavity in this system, which is electrostatically connected to MR_1 via Coulomb contact. By selectively controlling the two mechanical resonators MR_1 and MR_2, the behaviour of Four-Wave Mixing (FWM) intensity is investigated. Switchable mechanical drivings of MR_s offer a flexible way to implement switchable signal amplification in optical systems.

Furthermore in **fourth chapter**, we investigate the non-linear FWM phenomena in a Nano transducer (NEOMS) in the presence of Bose-Einstein condensate (BEC) trapped inside the Fabry-Perot cavity. BEC is particularly essential in exploring and analysing the underlying mysteries in several fields of experimental physics. Bose-Einstein condensate (BEC) has been discovered to be employed as "Quantum Simulators" to excite condensed matter systems [29, 30]. The Bose-Einstein condensation (BEC) has been proposed as a method for observing quantum mass acquisition [30]. We show that with the presence of atomic medium, such as Bose-Einstein condensate (BEC), in the optical cavity, FWM intensity increases. By selectively activating the mechanical resonators MR_1 and MR_2, we show that the medium-mediated FWM signal is considerably suppressed and amplified.

In the **fifth chapter**, another non-linear phenomenon has been discussed for the NEOMS with the external driving fields known as bi-stability. The optical bi-stability and mirror bi-stability has been discussed in detail. We see several tune-able parameters for controlling the bi-stability for the cavity-based system. The system maintains the bi-stable behaviour for the mean intra-cavity photon numbers with and without the external driving fields upon the micro-resonators. This bi-stable behaviour is also

observed for the position of micro-resonators. Further, the condition of optical as well as mirror bi-stability has discussed in the chapter.

The research work is concluded in the **sixth chapter**. Both of the non-linear phenomena (FWM and Bi-stability) can be controlled with different tune-able parameters for the cavity based system.

Chapter 2

The System Model and its Hamiltonian

In this chapter, we develop the theoretical model of Electro-Opto-Mechanical System under study. Let us consider an Opto-Mechanical Cavity having a fixed mirror at one end and a moveable mirror MR_1 at the other end. It is further extended with another moveable mirror MR_2 next to the MR_1. These two mirrors MR_1 and MR_2 are charged by the opposite biased voltages $+V_1$ and $-V_2$ respectively, are coupled through Coulomb interaction g_c. External driving forces are applied to these two micro-resonators.

2.1 The Opto-Mechanical System (OMS)

As illustrated in Figure 2.1, a simple Cavity-based Opto-Mechanical System (COMS) with high fineness and a single mode optical cavity is shown. The vibrating end mirror (MR_1) is displaced from its mean position by the intra-cavity field's radiation pressure

force, which alters the radiation pressure force.

A high Q Fabry-Perot cavity with a fixed mirror at one end and a moveable mirror (mechanical resonator MR_1) at the other end is considered. The cavity field is connected to the mechanical resonator MR_1 through opto-mechanical coupling g_0.
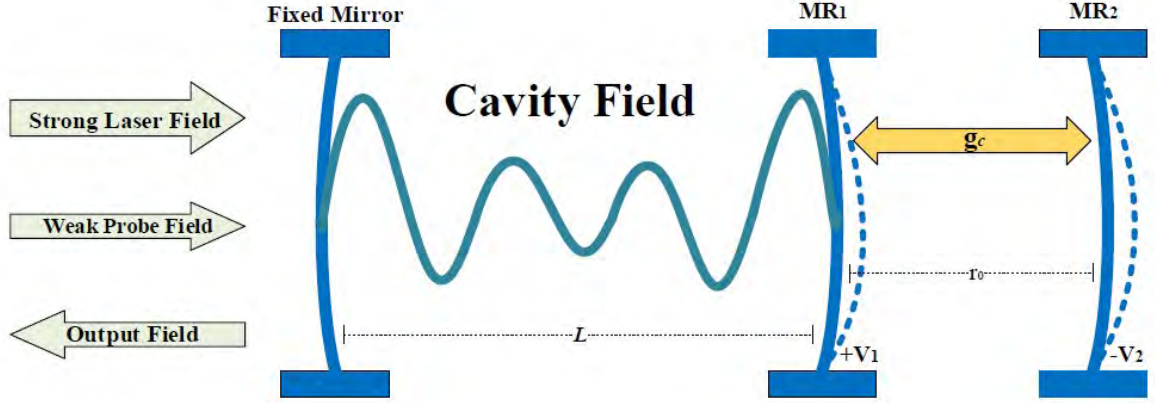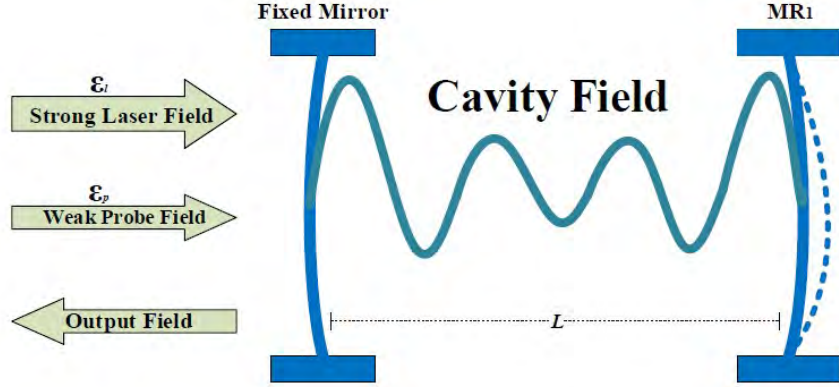

Figure 2.1: The Schematic representation of a simple Opto-Mechanical System: Here, MR_1 is coupled with the cavity field through opto-mechanical coupling g_0. A strong input laser field with amplitude ε_l and a weak probe field with amplitude ε_p are pumped to the cavity through the fixed mirror. The length of cavity is L.

Through the fixed mirror, a strong input laser field of amplitude ε_l and a weak probe field of amplitude ε_p are inserted into the cavity. The mechanical resonator MR_1 is displaced from its mean position by the radiation pressure force, changing the cavity length L. The moveable mirror MR_1 compensates for this shift by exerting a back-action force on the cavity field, lowering the radiation pressure and vice versa.

2.1.1 Hamiltonian of the OMS

Due to the radiation pressure force, the MR_1 acts as a micro-resonator and displaced from its mean position. So, we consider single mechanical mode for vibrating end mirror MR_1, modeled as harmonic oscillator with frequency ω_1, therefore the Hamiltonian of the MR_1 is given by

$$\hat{H}_{MR_1} = \hbar\omega_1 \hat{b_1}^\dagger \hat{b_1}, \tag{2.1}$$

where ω_1 is the frequency and $\hat{b_1}^\dagger$ and $\hat{b_1}$ are creation and annihilation operators of MR_1 and MR_2 respectively with $[\hat{b_1}, \hat{b_1}^\dagger] = 1$.

The cavity is driven by a strong pump field $\varepsilon_l = \sqrt{\frac{2P_l\kappa}{\hbar\omega_l}}$. A weak probe field $\varepsilon_p = \sqrt{\frac{2P_p\kappa}{\hbar\omega_p}}$ is pumped into the cavity to scan the outgoing optical signal. Here, κ is the decay rate of cavity, whereas P_l and P_p are the strong laser and weak probe field powers, respectively. The κ is same for both the frequencies i.e. ω_l and ω_p.

The Hamiltonian for the cavity has frequency ω_c. The photon creation(annihilation) operator $\hat{c}^\dagger(\hat{c})$ is coupled with the Hamiltonian of weak probe field and strong pump field. So, the total Hamiltonian of the field is

$$\hat{H}_{field} = \hbar\omega_c \hat{c}^\dagger \hat{c} - i\hbar(\hat{c}\varepsilon_p e^{i\omega_p t} - \hat{c}^\dagger \varepsilon_p^\star e^{-i\omega_p t}) + i\hbar\varepsilon_l(\hat{c}e^{i\omega_l t} - \hat{c}^\dagger e^{-i\omega_l t}). \tag{2.2}$$

The ε_l is the strong laser power induced in the cavity with $9mW$ strength. So it is considered as a real value in above equation. While ε_p is a very weak probe field used to test the non-linearity inside the cavity, is considered as a complex valued quantity whose real and imaginary parts examine the damping and oscillation of the field respectively. The range of ε_p is about 10% of the ε_l.

14

The interaction between cavity field and MR_1 has photon-phonon coupling, so the interaction Hamiltonian is given as

$$\hat{H}_{int} = -\hbar g_0 \hat{c}^\dagger \hat{c}(\hat{b}_1^\dagger + \hat{b}_1), \tag{2.3}$$

where, g_0 is opto-mechanical coupling strength which is dependent upon the length of cavity L and is given by $g_0 = (\frac{\omega_c}{L})\sqrt{\frac{\hbar}{2m_1\omega_1}}$. Here, m_1 is the mass of MR_1.

The total Hamiltonian of this Cavity-based Opto-Mechanical System is described in a rotating frame at the frequency of strong laser field ω_l by
(for $\hbar = 1$)

$$\hat{H} = \hat{H}_0 + \hat{H}_{int} + \hat{H}_{fields}, \tag{2.4}$$

where,

$$\hat{H}_0 = \Delta_c \hat{c}^\dagger \hat{c},$$
$$\hat{H}_{int} = -g_0 \hat{c}^\dagger \hat{c}(\hat{b}_1^\dagger + \hat{b}_1),$$
$$\hat{H}_{fields} = i(|\varepsilon_1|\hat{b}_1^\dagger e^{-i\delta t} + \varepsilon_l \hat{c}^\dagger + \varepsilon_p^\star \hat{c}^\dagger e^{-i\delta t} - H.c),$$

where, $\Delta_c = \omega_c - \omega_l$, with the assumption that the frequencies of the driving fields satisfy the resonance condition $\delta = \omega_p - \omega_l = \omega_1$.

2.1.2 System Model of NEOMS with External Driving Fields

Figure 2.2 depicts the basic Nano Electro Opto-Mechanical System (NEOMS), which has a fixed mirror and a moving end mirror MR_1 which combine to form an opto-mechanical system. The mechanical resonator MR_1 interacts to the cavity field via

15

radiation pressure force. A second mirror (mechanical resonator MR_2) is introduced into the cavity which interacts with the mechanical resonator MR_1 through phonon-phonon coupling.
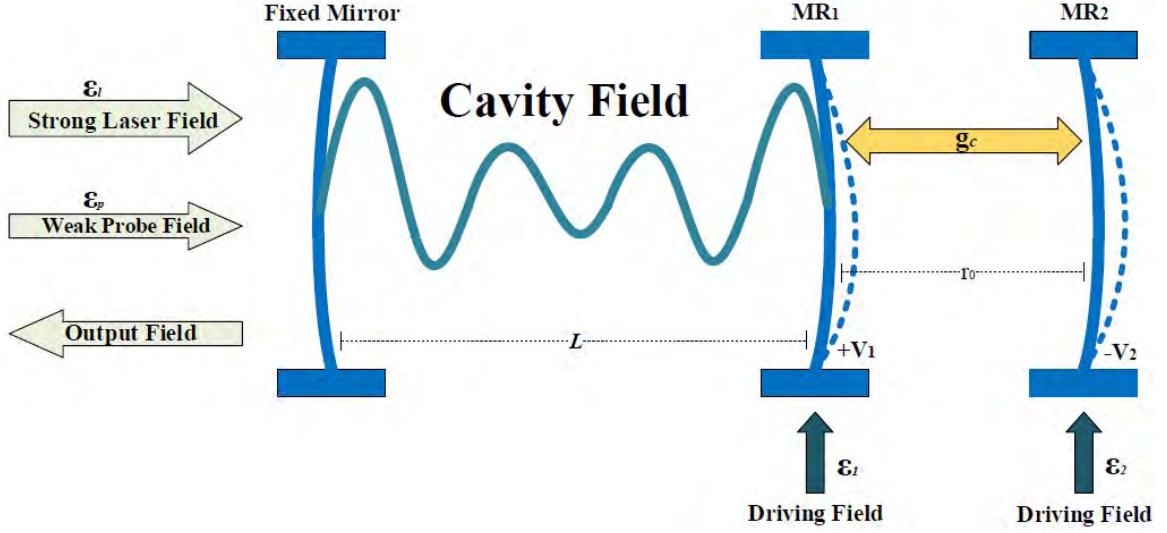
Figure 2.2: The Schematic representation of the Nano Electro Opto-Mechanical System (NEOMS): Here, MR_1 is coupled with the cavity field through opto-mechanical coupling g_0 and to the second mechanical resonator MR_2 through the Coulomb coupling strength g_c. A strong pump field ε_l and a weak probe field ε_p are pumped into the cavity. The MR_1 is charged by biased voltage $+V_1$ and MR_2 is charged by $-V_2$. The r_0 is the equilibrium distance between MR_1 and MR_2 which are selectively driven by the arbitrary driving fields ε_1 and ε_2.

The second mirror MR_2 allows more control over the cavity field and gives a lot of options for learning about non-linear processes in Cavity-based Electro-Opto-Mechanical Systems.

2.1.3 Hamiltonian of the NEOMS

We consider single mechanical mode for vibrating end mirrors, modeled as harmonic oscillators MR_1 and MR_2 with frequencies ω_1 and ω_2 respectively, therefore the Hamiltonian of the mechanical oscillators is

$$\hat{H}_{MRs} = \hbar\omega_1 \hat{b}_1^\dagger \hat{b}_1 + \hbar\omega_2 \hat{b}_2^\dagger \hat{b}_2, \tag{2.5}$$

where, ω_1 and ω_2 are oscillating frequencies and $(\hat{b}_1^\dagger)$ $\hat{b}_1$ and $(\hat{b}_2^\dagger)$ $\hat{b}_2$ are (creation)annihilation operators of MR_1 and MR_2 respectively with $[\hat{b}_i, \hat{b}_i^\dagger] = 1$.

The Hamiltonian for the cavity with frequency ω_c and bosonic creation(annihilation) operator $\hat{c}^\dagger(\hat{c})$ together with the coupled Hamiltonian of weak probe field and strong pump fields, is given by total Hamiltonian of the field as

$$\hat{H}_{field} = \hbar\omega_c \hat{c}^\dagger \hat{c} - i\hbar(\hat{c}\varepsilon_p e^{i\omega_p t} - \hat{c}^\dagger \varepsilon_p^\star e^{-i\omega_p t}) + i\hbar\varepsilon_l(\hat{c}e^{i\omega_l t} - \hat{c}^\dagger e^{-i\omega_l t}). \tag{2.6}$$

The total interaction Hamiltonian of the system is provided as the sum of the Hamiltonian for opto-mechanical coupling between cavity field and MR_1 and the Coulomb coupling between MR_1 and MR_2 as

$$\hat{H}_{int} = -\hbar g_0 \hat{c}^\dagger \hat{c}(\hat{b}_1^\dagger + \hat{b}_1) + \hbar g_c(\hat{b}_1^\dagger \hat{b}_2 + \hat{b}_1 \hat{b}_2^\dagger), \tag{2.7}$$

where, g_0 is opto-mechanical coupling strength and is given by $g_0 = \left(\frac{\omega_c}{L}\right)\sqrt{\frac{\hbar}{2m_1\omega_1}}$.

The g_c is coulomb coupling strength and is given by $g_c = \frac{k_e q_1 q_2}{r_0^3}\sqrt{\frac{\hbar}{2m_1 m_2 \omega_1 \omega_2}}$ [31, 32]. Here, k_e is the electrostatic constant. The q_1 and q_2 are the charges on MR_1 and MR_2 respectively.

The Hamiltonian for the two external driving fields with amplitudes ε_1 and ε_2 are given as

$$\hat{H}_{dr} = i\hbar(\varepsilon_1\hat{b}_1^\dagger e^{-i\omega_1 t} - \varepsilon_1\hat{b}_1 e^{i\omega_1 t}) + i\hbar(\varepsilon_2\hat{b}_2^\dagger e^{-i\omega_2 t} - \varepsilon_2\hat{b}_2 e^{i\omega_2 t}). \tag{2.8}$$

The effective Hamiltonian describing this Nano-Electro-Opto-Mechanical system is yielded in a rotating frame at the frequency of strong pump laser field ω_l by (for $\hbar = 1$)

$$\hat{H} = \hat{H}_0 + \hat{H}_{coup} + \hat{H}_{fields}, \tag{2.9}$$

where,

$$\hat{H}_0 = \Delta_c\hat{c}^\dagger\hat{c},$$
$$\hat{H}_{coup} = -g_0\hat{c}^\dagger\hat{c}(\hat{b}_1^\dagger + \hat{b}_1) + g_c(\hat{b}_1^\dagger\hat{b}_2 + \hat{b}_1\hat{b}_2^\dagger),$$
$$\hat{H}_{fields} = i(\sum_{j=1}^{2}\varepsilon_j\hat{b}_j^\dagger e^{-i\delta t} + \varepsilon_l\hat{c}^\dagger + \varepsilon_p^\star\hat{c}^\dagger e^{-i\delta t} - H.c),$$

where, $\Delta_c = \omega_c - \omega_l$ with the assumption that the frequencies of the driving fields satisfy the condition $\delta = \omega_p - \omega_l = \omega_1 = \omega_2$.

2.2   NEOMS as a Transducer

The transducers are basically quantum mechanical sensors. The NEOMS is a hybrid system consist of an opto-mechanical system and electro-mechanical system with two nano-scale movable mirrors, whereas the distance between the two is around 25 cm. This hybrid system couples the optical, electrical and mechanical degrees of freedom in a single nano-scale device that is nano-transducer. The quantum nano-transducer can

transfer the quantum information between optical and microwave modes at nano-scale. Here opto-mechanical cavity has information of cavity photons and photon-phonon interaction. While the electro-mechanical cavity has the information of Coulomb coupling, phonon-phonon interaction and nano-scale mirrors.

The moveable mirrors are called as micro-resonators because the radiation pressure force displaces them from their mean position in micro scale, but their weight is in nano-kilogram. So, we see that this hybrid system has quantum information in different modes i.e. photonic, micro-scale, and nano-scale. So the device transfers the information from one mode to another eventually working at different scales.

The non-linear effects in NEOMS are induced when the laser power is pumped into the cavity. In NEOMS,there is no medium inside the cavity but the non-linearities analogous to Kerr effect [16, 17] are present. Such non-linear effects are due to radiation pressure force. As the radiation pressure force is changed with the oscillation of micro resonators, the non-linearity in the medium also is also changed with it. Due to non-linearity, the optical response of the opto-mechanical system is altered because of the mechanical interaction, and different phenomena like OMIT [23, 24], and slow light effect [11] come into account. These effects are undesirable , depending on their technological application. But fortunately, the non-linearity effects are controllable inside the cavity by tuning different parameters. In our work, we see that FWM is controllable in NEOMS which is a non-linear phenomenon.

Chapter 3

The Controlled Four-Wave Mixing (FWM)

In this chapter, the dynamics of controlled Four-Wave Mixing (FWM) in NEOMS is discussed in detail. The FWM has been seen in the probe transmission field when two external driving fields are present on moving mirrors. By adjusting the amplitudes and phases of the external driving fields, we show that Four-Wave Mixing has controllable dynamics.

3.1 Four-Wave Mixing (FWM)

When a high-energy optical field is applied to a cavity-based system, non-linearities occur. Non-linearity exists in cavity opto-mechanical systems, just as they do in non-linear media, although the causes of these non-linearities are different in both situations. There is no medium inside the cavity in basic cavity opto-mechanical systems, although

non-linearities similar to the Kerr effect [8] are present.The radiation pressure force is the cause of such non-linear effects. With the oscillation of mechanical resonators, the radiation pressure force changes, and the non-linearity in the medium changes as well. Because of the mechanical interaction, non-linearity alters the optical response of the opto-mechanical system, resulting in phenomena such as OMIT [9, 10, 11] and slow light effect [11].

According to Huang and Agarwal [33], Four-Wave Mixing (FWM) is another non-linear phenomena that has been studied. In nonlinear quantum optics, a phenomenon known as Four-Wave Mixing (FWM) occurs when interaction between two or three wavelengths results in the creation of one or two new wavelengths. The FWM a non-linear optical phenomenon based on quantum interference and coherence that has been studied extensively since the birth of non-linear optics, is one of the most well-known non-linear optical phenomena. This has a wide range of applications, including frequency conversion [12], quantum entanglement [6], halted light [18], and fast light [34]. However, the loss of linear absorption in typical materials can only account for a tiny portion of the non-linear co-efficient. To overcome this barrier, Harris [12] demonstrated that in a three-level system, third-order susceptibility can be resonantly enhanced using electromagnetically induced transparency (EIT), implying that a highly efficient Four-Wave Mixing process based on EIT can be achieved by reducing linear absorption. Li and Xiao [13] reported an experimental finding of the amplification of non-degenerate Four-Wave Mixing based on EIT in a lambda-type three-level system of Rubidium atoms. For a five-level atomic system, Wu et al. [35] shown that suppressing photon absorption from EIT can enhance FWM. For a four-level system, Deng et al.

21

[26] suggested a strategy for opening Four-Wave Mixing (FWM) optical channels.

3.2 Controlled FWM in OMS

The model showed in Figure 2.1 of chapter two is an Opto-Mechanical System (OMS). The total Hamiltonian of OMS is also defined in equation (2.5).

For observing the non-linearity in this system, a strong laser field with frequency ω_l and a weak probe field with frequency ω_p are pumped into the optical cavity. In addition, a switchable mechanical driving field of amplitudes $|\varepsilon_1|$ is applied to the mechanical resonators MR_1 as shown in Figure 3.1.
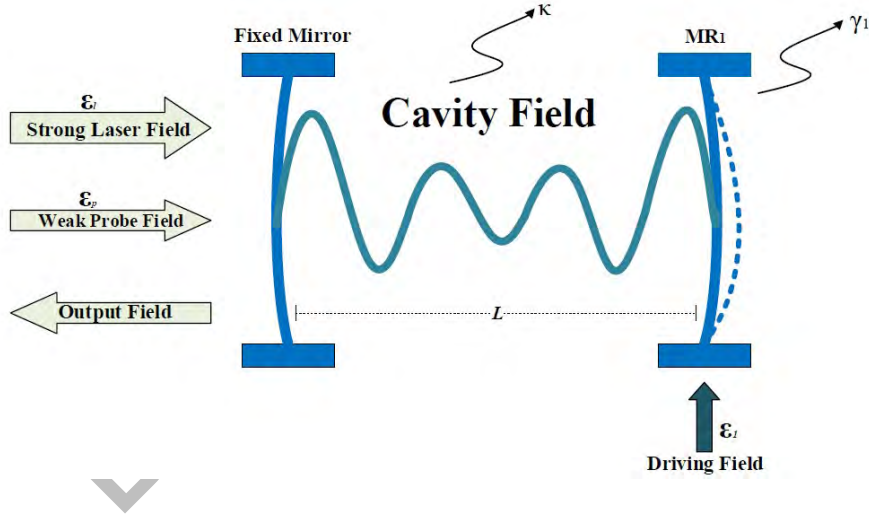
Figure 3.1: The Schematic representation of a basic Opto-Mechanical Cavity): Here, MR_1 is coupled to the cavity field through opto-mechanical interaction g_0. A strong input laser pump field of amplitude ε_l and a weak probe field of amplitude ε_p are inserted into the cavity through the fixed mirror. The length of cavity is L. The MR_1 is selectively driven by arbitrary driving field ε_1.

The Hamiltonian for the external mechanical driving field of MR_1, with amplitude $|\varepsilon_1|$ is given as

$$\hat{H}_{dr} = i\hbar|\varepsilon_1|(\hat{b}_1^\dagger e^{-i\omega_1 t} - \hat{b}_1 e^{i\omega_1 t}). \tag{3.1}$$

The total Hamiltonian of this system is described as

$$\hat{H} = \hat{H}_0 + \hat{H}_{int} + \hat{H}_{fields} + \hat{H}_{dr}. \tag{3.2}$$

The cavity field switches from excited to ground state and vice versa by using creation and annihilation operators $\hat{c}^\dagger$ and $\hat{c}$. So the cavity has some decay rate which is denoted by κ. The MR_1 also oscillates around its mean position. The creation and annihilation operators for the position of MR_1 are $b_1^\dagger$ and b_1 receptively.

So, the Heisenberg-Langevin Equations of Motion for the system can be calculated by using the standard relation

$$\frac{d\hat{O}}{dt} = -\frac{i}{\hbar}[\hat{H}, \hat{O}] + \frac{1}{2}\{\hat{\Gamma}, \hat{O}\} + \hat{N}_s. \tag{3.3}$$

Here, $\hat{O}$ is any operator of the system. The first term expresses the commutation relationship between the system's total Hamiltonian and its operator. The second term accounts for the decays associated with the operator $\hat{O}$, while the third term, the noise operator, accounts for the noise in the system. We substitute equation (3.2) in equation (3.3) to build the equation of motion as

$$\dot{\hat{c}} = -(i\Delta_c + \frac{\kappa}{2})\hat{c} + ig_0(\hat{b}_1^\dagger + \hat{b}_1)\hat{c} + \varepsilon_l + \varepsilon_p e^{-i\delta t} + \sqrt{2\kappa}\hat{c}_{in}(t),$$
$$\dot{\hat{b}_1} = -(i\omega_1 + \frac{\gamma_1}{2})\hat{b}_1 + ig_0\hat{c}^\dagger\hat{c} + |\varepsilon_1|e^{-i\delta t} + \sqrt{2\gamma_1}\hat{\zeta}_1(t), \tag{3.4}$$

where $\Delta_c = \omega_c - \omega_l$, κ and γ_1 are the decay rates related to the cavity and mechanical resonator MR_1 respectively. Here, $\hat{c}_{in}(t)$ is the input vacuum noise with zero expected

23

value, $\hat{\zeta}_1(t)$ and $\hat{\zeta}_2(t)$ are the Brownian noise operators associated with the damping of the two mechanical resonators MR_1 and MR_2. By using Markov approximation, the correlation functions of these input noise operators are given by [36]

$$\langle \hat{c}_{in}(t)\hat{c}_{in}^\dagger(t')\rangle = \delta(t - t'),$$

$$\langle \hat{\zeta}_i(t)\hat{\zeta}_i(t')\rangle = (n_{th} + 1)\delta(t - t'),$$

with $i = 1, 2$.

Here, $n_{th} = (e^{\frac{\hbar\omega}{k_B T}} - 1)^{-1}$ and k_B is the Boltzmann constant, T is the temperature of the reservoir of the mechanical resonator and ω is the frequency of thermal vibration and $\hbar\omega$ is the energy of the reservoir. Here, we use the mean-field approximation $\langle c^\dagger c\rangle \approx \langle c^\dagger\rangle\langle c\rangle$ as a mathematical tool to decouple the coupled operators. The equations of motion can be written as

$$
\begin{aligned}
\langle \dot{\hat{c}}\rangle &= -(i\Delta_c + \frac{\kappa}{2})\langle\hat{c}\rangle + ig_0(\langle\hat{b}_1\rangle^\dagger + \langle\hat{b}_1\rangle)\langle\hat{c}\rangle + \varepsilon_l + \varepsilon_p e^{-i\delta t} + \sqrt{2\kappa}\langle\hat{c}_{in}(t)\rangle, \\
\langle \dot{\hat{b}_1}\rangle &= -(i\omega_1 + \frac{\gamma_1}{2})\langle\hat{b}_1\rangle + ig_0\langle\hat{c}^\dagger\rangle\langle\hat{c}\rangle + |\varepsilon_1|e^{-i\delta t} + \sqrt{2\gamma_1}\langle\hat{\zeta}_1(t)\rangle. \quad (3.5)
\end{aligned}
$$

We calculate the Nano-Electro-Opto-Mechanical System's linear response to the weak probe field. The noise terms connected with the system average out. We linearize the dynamical equations of the system by performing calculations in the neighbourhood of steady state values, such as $\hat{c} = c_s + \delta\hat{c}$ and $\hat{b}_1 = b_{1s} + \delta\hat{b}_1$, in the case the amplitude of the pump field ε_1, is large compared to the amplitude of probe field ε_p and driving field ε_1 i.e., ε_p, $|\varepsilon_1| << \varepsilon_l$.

By setting the time derivatives of the operators in equation (3.5) to zero, we get

the system's steady state values as

$$
\begin{aligned}
c_s &= \frac{\varepsilon_l}{i\Delta_c - ig_0(b_{1s}^\star + b_{1s}) + \frac{\kappa}{2}}, \\
b_{1s} &= \frac{ig_0|c_s|^2}{i\omega_1 + \frac{\gamma_1}{2}}.
\end{aligned}
\tag{3.6}
$$

Where, c_s and b_{1s} are the steady state values of the cavity field photon numbers and the phonon number of mechanical resonator MR_1, respectively.

The fluctuation terms of the equations of motion can be simplified to

$$
\begin{aligned}
\dot{\delta\hat{c}} &= -(i\Delta + \frac{\kappa}{2})\delta\hat{c} + ig_0 c_s(\delta\hat{b}_1^\dagger + \delta\hat{b}_1) + \varepsilon_p e^{-i\delta t}, \\
\dot{\delta\hat{b}_1} &= -(i\omega_1 + \frac{\gamma_1}{2})\delta\hat{b}_1 + ig_0 c_s \delta\hat{c}^\dagger + ig_0 c_s{}^* \delta\hat{c} + |\varepsilon_1| e^{-i\delta t},
\end{aligned}
\tag{3.7}
$$

where, $\Delta = \Delta_c - g_0(b_{1s}{}^* + b_{1s})$ denotes the effective detuning.

The amplitudes of the first-order side-band modes in the system, are calculated as we consider the fluctuation terms such that,

$$
\begin{aligned}
\delta\hat{c} &= A_1{}^- e^{-i\delta t} + A_1{}^+ e^{i\delta t}, \\
\delta\hat{b}_1 &= B_1{}^- e^{-i\delta t} + B_1{}^+ e^{i\delta t}.
\end{aligned}
\tag{3.8}
$$

Substituting equation (3.7) into the set of equation (3.8), for first order side-band, we

get the following set of eight linear equations:

$$h_1{}^+A_1{}^+ = iGB_1{}^+ + iGB_1{}^{-*} + \varepsilon_p,$$

$$h_1{}^-A_1{}^- = iGB_1{}^- + iGB_1{}^{+*},$$

$$h_2{}^-B_1{}^+ = iGA_1{}^{-*} + iG^*A_1{}^+ + \varepsilon_1,$$

$$h_2{}^+B_1{}^- = iGA_1{}^{+*} + iG^*A_1{}^-,$$

$$h_1{}^+A_1{}^{-*} = -iGB_1{}^{-*} - iGB_1{}^+,$$

$$h_1{}^-A_1{}^{+*} = -iGB_1{}^{+*} - iGB_1{}^- + \varepsilon_p,$$

$$h_2{}^+B_1{}^{+*} = -iGA_1{}^{-*} - iG^*A_1{}^+,$$

$$h_2{}^-B_1{}^{-*} = -iGA_1{}^{+*} - iG^*A_1{}^- + \varepsilon_1, \tag{3.9}$$

where, we labeled $G = g_0 c_s$, $h_1{}^\pm = \pm i\Delta + \kappa/2 - i\delta$ and $h_2{}^\pm = \pm i\omega_1 + \gamma_1/2 - i\delta$.

In the above set of equations, the phase term φ_1 is introduced as $\varepsilon_1 = |\varepsilon_1|e^{-i\varphi_1}$. Equation (3.9) shows that $A_1{}^+$ is a function of weak probe field frequency δ. So, for external driving field ε_1 on MR_1, we solve the set of equation (3.9) for the value of $A_1{}^+$, we get $A_1{}^+$ as

$$A_1{}^+ = \frac{-2|G|^2(2G\varepsilon_1 e^{-i\varphi_1} - ih_2{}^-\varepsilon_p)h_1{}^+}{h_1{}^+(2i|G|^2h_2{}^-h_1{}^+ - h_1{}^-(-2i|G|^2 + h_2{}^-h_1{}^+)h_2{}^+)}$$
$$+ \frac{(G^2h_1{}^-\varepsilon_p - (2iGh_1{}^-\varepsilon_1 e^{-i\varphi_1} + (G^2 + h_1{}^-h_2{}^-)\varepsilon_p)h_1{}^+)h_2{}^+}{h_1{}^+(2i|G|^2h_2{}^-h_1{}^+ - h_1{}^-(-2i|G|^2 + h_2{}^-h_1{}^+)h_2{}^+)}. \tag{3.10}$$

26

3.2.1   Calculation of FWM

By using the standard input-output relation $\langle \hat{c}_{out}(t) \rangle = \langle \hat{c}_{in}(t) \rangle - \sqrt{2\kappa} \hat{c}$ for the system, we consider $\hat{c}_- = A_1{}^-$ and $\hat{c}_+ = A_1{}^+$, we find:

$$\langle \hat{c}_{out}(t) \rangle = (\varepsilon_l - \sqrt{2\kappa} c_s) e^{-i\omega_l t} + (\varepsilon_p - \sqrt{2\kappa} \hat{c}_-) e^{-i\omega_p t} - \sqrt{2\kappa} \hat{c}_+ e^{-i(2\omega_l - \omega_p)t}.$$

There are three frequency components ω_l, ω_p and $2\omega_l - \omega_p$. The third component $2\omega_l - \omega_p$ is a new generated frequency which corresponds to the Four-Wave Mixing (FWM) phenomenon. It is generated when two laser field photons combine with a probe field photon in the presence of opto-mechanical coupling g_o. If there is no opto-mechanical coupling g_o, there will be no FWM. The transmission of the probe field is defined by the ratio of output and input field amplitudes at the probe frequency. So, by considering only the 3rd term in output field, the intensity of the Four-Wave Mixing (FWM) is calculated as

$$FWM = \left| -\frac{\sqrt{2\kappa} A_1{}^+}{\varepsilon_p} \right|^2. \tag{3.11}$$

It is the mean-square value of the FWM signal.

For simulation purpose, we use the experimental parameters for Opto-Mechanical System (OMS) presented in [37, 38]. The length of cavity is taken $L = 25cm$ and mass of the micro-resonator MR_1 is taken as $m_1 = 145ng$. The opto-mechanical coupling strength is $g_0 = 2\pi \times 4kHz$, and other parameters are $\omega_1 = 2\pi \times 947kHz$ and $\gamma_1 = 2\pi \times 140kHz$

As in reference [38] the cavity decay rate is $\kappa = 2\pi \times 215kHz$. The cavity field frequency ω_c is calculated by the relation $\omega_c = 2\pi c/\lambda_c$, where c is speed of light and

λ_c is the wavelength of laser field. So, the value of ω_c is calculated as $1.77 \times 10^{15} Hz$. We select cavity detuning $\Delta_c = \omega_1$ and $\omega_l = \omega_c - \omega_1$, and the power of the strong laser field is taken as $9mW$. We choose the value of effective detuning as $\Delta = \omega_1$.

As we can see that the value of mechanical resonator frequency is greater than cavity decay rate i.e., $\omega_1 \gg \kappa$, hence the system remains in the resolved side-band regime [16, 39].

3.2.2 Coupling Controlled FWM
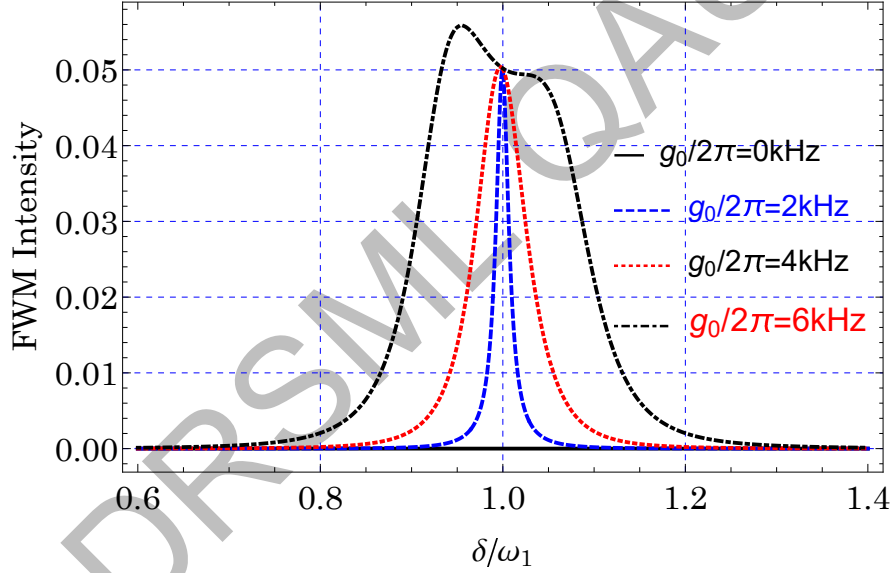
Figure 3.2: A 2-D plot for FWM Intesity (arbitrary units) vs normalized detuning δ/ω_1, for different values of opto-mechanical coupling strength g_0. The Coulomb coupling parameter is neglected, i.e $g_c = 0$. $\varepsilon_1 = 0$.

When the mechanical driving field is not applied to the micro-resonator (MR_1), i.e, $\varepsilon_1 = 0$, for lower opto-mechanical coupling levels, the FWM spectra have a single

peak., as shown in Figure 3.2.

Peaks can be seen in the Stokes ($\delta < \omega_1$) and Anti-Stokes ($\delta > \omega_1$) side-band regimes. There is no FWM signal in the output probe field when the opto-mechanical coupling is absent (see black dashed line in Figure 3.2).

When the opto-mechanical coupling g_o is introduced into the system, the FWM signal appears in the probe transmission field (blue dashed line in Figure 3.2) and the intensity of FWM signal is amplified, when the strength opto-mechanical coupling (g_o) is increased (black dot-dashed curve in Figure 3.2). For lower value of opto-mechanical coupling strengths g_o, the FWM curve has a single peak with center at $\delta = \omega_1$ (see blue dashed and red dotted curves). This feature also accounts for single photon resonance process [39]. For stronger opto-mechanical coupling strength g_o, the spectrum of the FWM intensity curve becomes broadened and splits into two asymmetric peaks (see black dot-dashed line), so, producing two-photons resonance process. The reason behind this phenomenon is that when opto-mechanical coupling g_o is increased, the cavity-mirror interaction becomes more stronger, which allows more photons to enter into the cavity in FWM which accounts for a stronger spectrum of the output signal.

3.2.3 Phase Controlled FWM

Here, we see the behavior of FWM intensity signal by keeping the opto-mechanical coupling strength constant ($g_o = 2\pi \times 4kHz$) and varying the amplitude and phase of external driving field ε_1.

In the presence of external driving field ε_1 on micro-resonator MR_1 , the peak of

FWM signal can be suppressed and amplified at Stokes side-band and at Anti-Stokes side-band regimes, respectively. The intensity of the peak of FWM signal at Anti-Stokes side-band is smaller than the intensity of the peak at Stokes side-band (see Figure 3.3a).

By increasing the phase φ_1 of the driving field on MR_1 from 0 to $\pi/4$, at Anti-Stokes side-band, the FWM spectrum greatly increases for the peak, but at the Stokes side-band, the signal is suppressed. This behavior is shown in Figure 3.3b. The reason behind this behaviour is that the effect of the opto-mechanical coupling strength g_o is enhanced by pumping the MR_1 with the external driving field ε_1.
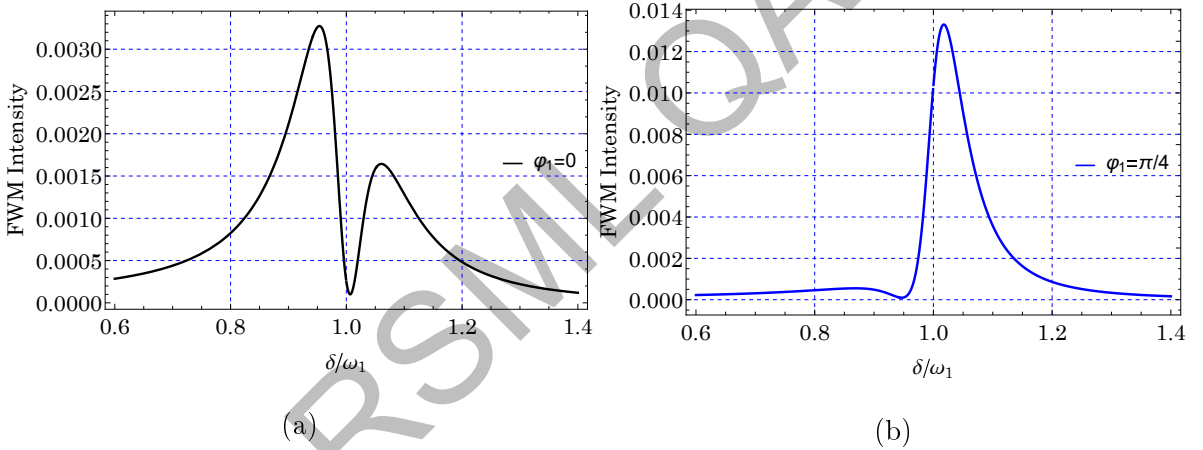
Figure 3.3: The FWM Intensity as a function of normalized detuning δ/ω_1. Only opto-mechanical coupling is present, and is kept constant, i.e, $g_0/2\pi = 4kHz$. The Coulomb coupling parameter is kept zero, i.e $g_c = 0$. $\varepsilon_1/\varepsilon_p = 0.45$. The value of phase is (a) $\varphi_1 = 0$, and (b) $\varphi_1 = \pi/4$.

In Figure 3.4a, for $\varepsilon_1/\varepsilon_p = 0.45$, the intensity of the peak the FWM signal at Stokes side-band increases while decreases at the Anti-Stokes side-band by setting the phase

30

$\varphi_1 = \pi$. When the phase angle is increased to $\varphi_1 = 3\pi/2$, the FWM intensity signals has the single peak at the resonance point. (see Figure 3.4b).

(a)

(b)
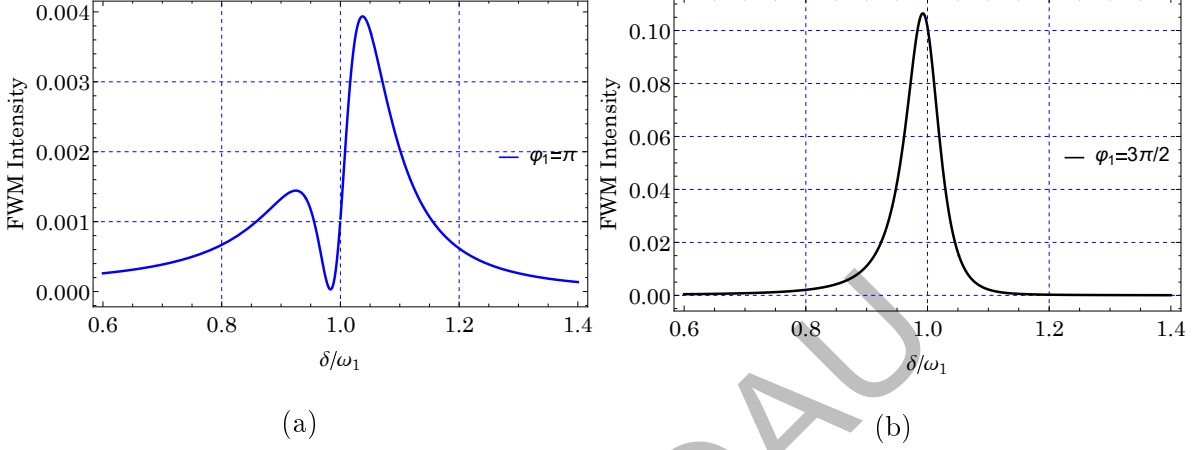
Figure 3.4: The FWM Intensity signal as a function of normalized detuning δ/ω_1. Other parameters are $\varepsilon_1/\varepsilon_p = 0.45$ and phase value for (a) is $\varphi_1 = \pi$ and (b) is $\varphi_1 = 3\pi/2$.

As the phase angle is further increased, relative suppression and amplification of the FWM signal is appeared in the observed FWM spectrum. This behaviour is due to the fact that the effective opto-mechanical coupling coefficient g_o is modified for every phase value. The periodic behavior is further confirmed by plotting the FWM across the scaled detuning δ/ω_1 and the phase φ_1 in the Figure 3.5.

The FWM signal is strong at Stokes line but the signal is very weak at Anti-Stokes line in the range of phase $\varphi_1 = \pi$ to 2π, which can be clearly seen in Figure 3.5. These periodic amplification and suppression are observed in the intensity spots shown in Figure 3.5.
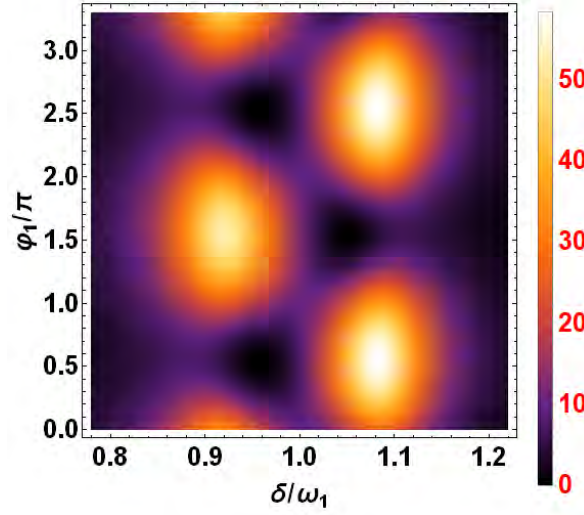
Figure 3.5: The density plot of FWM Intensity signal as a function of normalized detuning δ/ω_1 displays a periodicity as a function of phase φ_1,. Here, $\varepsilon_1/\varepsilon_p = 0.45$.

3.2.4   Amplitude controlled FWM

The FWM signal is amplified by varying the amplitude ε_1 of the mechanical driving field at MR_1.

The value of the phase is kept constant while investigating the effect of varying amplitude of mechanical driving field on the FWM signal. From Figure 3.6, it is clearly seen that the intensity of FWM spectrum increases prominently for both peaks and the intensity of FWM signal near the resonance point becomes more stronger. While in the absence of mechanical driving field, there was no FWM signal at the resonance point (see, Figure 3.2). Due to the significant enhancement in the effective opto-mechanical coupling g_0, these features observed.

In the generation of the FWM signal, the opto-mechanical coupling strength g_0 plays a central role. The external mechanical driving field enhances the opto-mechanical

32

coupling strength, which accounts for a stronger FWM intensity in the output signal.
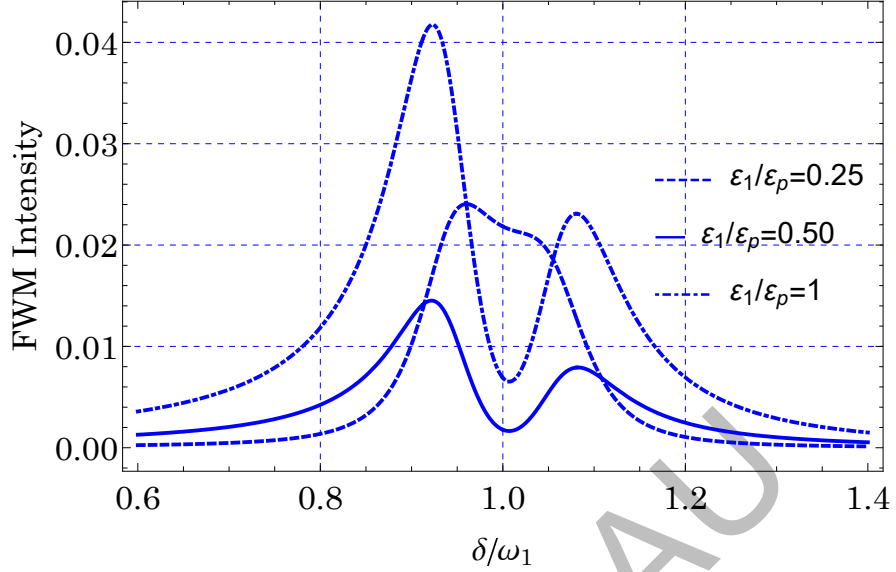
Figure 3.6: FWM Intensity as a function of normalized detuning δ/ω_1, for different values of $\varepsilon_1/\varepsilon_p$. The value of the $\varphi_1 = 0$

The intensity of both of the peaks of FWM signal increases with increase in the amplitude ε_1 of external driving field of MR_1. For the amplitude $\varepsilon_1/\varepsilon_p = 0.25$, the FWM signal is absent at the off-resonance $\delta/\omega_1 = 1$ (see blue dashed curve in Figure 3.6). When the amplitude of driving field at MR_1 is increased, the FWM signal in the off-resonance regime prominently increases (see blue line and dot-dashed curves in Figure 3.6).

3.3   Controlled FWM in NEOMS

A strong pump field of frequency ω_l and a weak probe field of frequency ω_p are applied to the optical cavity, in the presence of two external driving fields ε_1 and ε_2 applied to

the mechanical resonators MR_1 and MR_2, respectively. Due to these external driving fields, the micro-resonators oscillate around their mean position. The creation and annihilation operators for the position of MR_1 are $\hat{b}_1^\dagger$ and $\hat{b}_1$ and for MR_2 are $\hat{b}_2^\dagger$ and $\hat{b}_2$ receptively. The symbol κ describes the cavity decay rate, while γ_1 and γ_2 are the decay rates associated to MR_1 and MR_2, respectively.
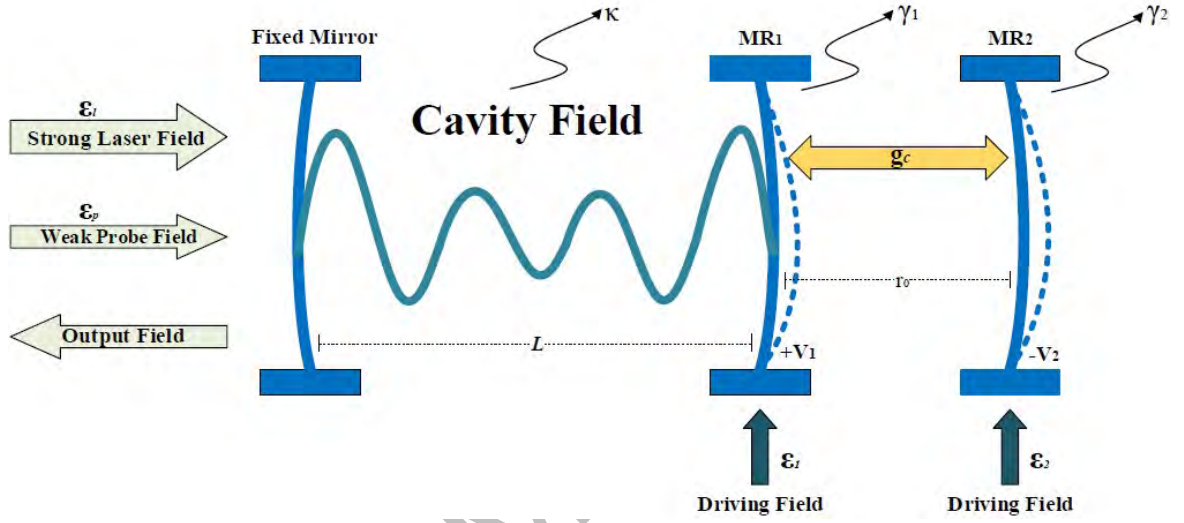
Figure 3.7: The Schematic representation of a basic Opto-Mechanical Cavity): Here, MR_1 is coupled to the cavity field through opto-mechanical interaction g_0. A strong input laser pump field of amplitude ε_l and a weak probe field of amplitude ε_p are inserted into the cavity through the fixed mirror. The L is the length of cavity. The MR_1 and MR_2 are selectively driven by ε_1 and ε_2 respectively. The κ is the cavity decay rate while γ_1 and $\gamma2$) are the decay rates associated to MR_1 and MR_2 respectively.

The total Hamiltonian describing the Nano-Electro-Opto-Mechanical system, in a

34

rotating frame at the frequency of strong pump laser field ω_l, is

$$\hat{H} = \hat{H}_0 + \hat{H}_{coup} + \hat{H}_{fields}, \qquad (3.12)$$

where, for $\hbar = 1$,

$$
\begin{aligned}
H_0 &= \Delta_c c^\dagger c, \\
H_{coup} &= -g_0 c^\dagger c (b_1{}^\dagger + b_1) + g_c(b_1{}^\dagger b_2 + b_1 b_2{}^\dagger), \\
H_{fields} &= i(\sum_{j=1}^{2} \varepsilon_j b_j{}^\dagger e^{-i\delta t} + \varepsilon_l c^\dagger + \varepsilon_p^{\star} c^\dagger e^{-i\delta t} - H.c).
\end{aligned}
$$

Where, $\Delta_c = \omega_c - \omega_l$ with the assumption that the frequencies of the driving fields satisfy the resonance condition $\delta = \omega_p - \omega_l = \omega_1 = \omega_2$.

The Heisenberg-Langevin Equation of motion for the system is

$$\frac{d\hat{O}}{dt} = -\frac{i}{\hbar}[\hat{H}, \hat{O}] + \frac{1}{2}\{\hat{\Gamma}, \hat{O}\} + \hat{N}_s. \qquad (3.13)$$

Here, $\hat{O}$ is an arbitrary operator of the system. The first term expresses the commutation relationship between the total Hamiltonian and operator $\hat{O}$. The second term accounts for the decays associated with the operator $\hat{O}$, while the third term is the noise operator, accounts for the noise in the system. We now use equation (3.12) in equation (3.13) to build the equation of motion that is

$$
\begin{aligned}
\dot{\hat{c}} &= -(i\Delta_c + \frac{\kappa}{2})\hat{c} + ig_0(\hat{b}_1^\dagger + \hat{b}_1)\hat{c} + \varepsilon_l + \varepsilon_p e^{-i\delta t} + \sqrt{2\kappa}\hat{c}_{in}(t), \\
\dot{\hat{b}_1} &= -(i\omega_1 + \frac{\gamma_1}{2})\hat{b}_1 + ig_0\hat{c}^\dagger\hat{c} - ig_c\hat{b}_2 + \varepsilon_1 e^{-i\delta t} + \sqrt{2\gamma_1}\hat{\zeta}_1(t), \\
\dot{\hat{b}_2} &= -(i\omega_2 + \frac{\gamma_2}{2})\hat{b}_2 - ig_c\hat{b}_1 + \varepsilon_2 e^{-i\delta t} + \sqrt{2\gamma_2}\hat{\zeta}_2(t). \qquad (3.14)
\end{aligned}
$$

Where, $\Delta_c = \omega_c - \omega_l$. The symbols κ and $\gamma_i (i = 1, 2)$ are decay terms related to cavity and mechanical resonators respectively MR_1 and MR_2. The $\hat{c}_{in}(t)$ is the input vacuum

35

noise with zero expected value. The $\hat{\zeta}_1(t)$ and $\hat{\zeta}_2(t)$ are the Brownian noise operators associated with the damping of the two mechanical resonators MR_1 and MR_2. By using Markov approximation, the correlation functions of these input noise operators are given by [36]

$$\langle \hat{c}_{in}(t)\hat{c}_{in}^\dagger(t')\rangle = \delta(t-t'),$$

$$\langle \hat{\zeta}_i(t)\hat{\zeta}_i(t')\rangle = (n_{th}+1)\delta(t-t'),$$

with $i = 1, 2$.

Here $n_{th} = (e^{\frac{\hbar\omega}{k_B T}}-1)^{-1}$. The k_B is the Boltzmann constant, T is the temperature of the reservoir of the mechanical resonator, ω is the frequency of thermal vibration and $\hbar\omega$ is the energy of the reservoir. Here, we use the mean-field approximation $\langle \hat{c}^\dagger \hat{c}\rangle \approx \langle \hat{c}^\dagger\rangle\langle \hat{c}\rangle$ as a mathematical tool to decouple the coupled operators. The equations of motion can be written as

$$
\begin{aligned}
\langle \dot{\hat{c}}\rangle &= -(i\Delta_c + \frac{\kappa}{2})\langle \hat{c}\rangle + ig_0(\langle \hat{b}_1\rangle^\dagger + \langle \hat{b}_1\rangle)\langle \hat{c}\rangle + \varepsilon_l + \varepsilon_p e^{-i\delta t} + \sqrt{2\kappa}\langle \hat{c}_{in}(t)\rangle, \\
\langle \dot{\hat{b}_1}\rangle &= -(i\omega_1 + \frac{\gamma_1}{2})\langle \hat{b}_1\rangle + ig_0\langle \hat{c}^\dagger\rangle\langle \hat{c}\rangle - ig_c\langle \hat{b}_2\rangle + \varepsilon_1 e^{-i\delta t} + \sqrt{2\gamma_1}\langle \hat{\zeta}_1(t)\rangle, \\
\langle \dot{\hat{b}_2}\rangle &= -(i\omega_2 + \frac{\gamma_2}{2})\langle \hat{b}_2\rangle - ig_c\langle \hat{b}_1\rangle + \varepsilon_2 e^{-i\delta t} + \sqrt{2\gamma_2}\langle \hat{\zeta}_2(t)\rangle.
\end{aligned}
\tag{3.15}
$$

We are simply interested in the Nano-Electro-Opto-Mechanical System's linear response to the weak probe field. The noise terms connected with the system are averaged to zero. The dynamical equations of the system can be linearized by adding small perturbations such as $\hat{c} = c_s + \delta\hat{c}$ and $\hat{b} = b_{is} + \delta\hat{b}_i$ $(i = 1, 2)$. The amplitudes of probe field ε_p and that of external driving fields ε_1 and ε_2 on MR_1 and MR_2 respectively, are very very small as compared to the amplitude of laser field ε_l i.e., ε_p, $\varepsilon_{1,2} << \varepsilon_l$.

36

By setting the time derivatives of the operators in equation (3.15) to zero yields the system's steady state values as

$$
\begin{aligned}
c_s &= \frac{\varepsilon_l}{i\Delta_c - ig_0({b_{1s}}^\star + b_{1s}) + \frac{\kappa}{2}}, \\
b_{1s} &= \frac{ig_0|c_s|^2 - ig_c b_{2s}}{i\omega_1 + \frac{\gamma_1}{2}}, \\
b_{2s} &= \frac{-ig_c b_{1s}}{i\omega_2 + \frac{\gamma_2}{2}},
\end{aligned}
\tag{3.16}
$$

where c_s and $b_{is}(i = 1, 2)$ are steady-state values of cavity field and mechanical resonators, respectively.

The fluctuation terms of the equations of motion can be simplified to:

$$
\begin{aligned}
\dot{\delta c} &= -(i\Delta + \frac{\kappa}{2})\delta c + ig_0 c_s(\delta b_1{}^\dagger + \delta b_1) + \varepsilon_p e^{-i\delta t}, \\
\dot{\delta b_1} &= -(i\omega_1 + \frac{\gamma_1}{2})\delta b_1 + ig_0 c_s \delta c^\dagger + ig_0 c_s{}^* \delta c - ig_c \delta b_2 + \varepsilon_1 e^{-i\delta t}, \\
\dot{\delta b_2} &= -(i\omega_2 + \frac{\gamma_2}{2})\delta b_2 - ig_c \delta b_1 + \varepsilon_2 e^{-i\delta t},
\end{aligned}
\tag{3.17}
$$

where, $\Delta = \Delta_c - g_0({b_{1s}}^* + b_{1s})$ is the effective detuning.

Following fluctuation terms are considered for determining the amplitudes of first order side-bands in the system:

$$
\delta c = A_1{}^- e^{-i\delta t} + A_1{}^+ e^{i\delta t},
$$

$$
\delta b_1 = B_1{}^- e^{-i\delta t} + B_1{}^+ e^{i\delta t},
$$

$$
\delta b_2 = B_2{}^- e^{-i\delta t} + B_2{}^+ e^{i\delta t}.
\tag{3.18}
$$

37

Substituting equation (3.18) into the set of equations equation (3.17), we get the following set of eight linear equations for first order side-bands as:

$$
\begin{aligned}
h_1{}^+ A_1{}^+ &= iGB_1{}^+ + iGB_1{}^{-*} + \varepsilon_p, \\
h_1{}^- A_1{}^- &= iGB_1{}^- + iGB_1{}^{+*}, \\
k^+ B_1{}^+ &= iGA_1{}^{-*} + iG^* A_1{}^+ + \varepsilon_1 - f\varepsilon_2, \\
k^- B_1{}^- &= iGA_1{}^{+*} + iG^* A_1{}^-, \\
h_1{}^+ A_1{}^{-*} &= -iGB_1{}^{-*} - iGB_1{}^+, \\
h_1{}^- A_1{}^{+*} &= -iGB_1{}^{+*} - iGB_1{}^- + \varepsilon_p, \\
h_2{}^+ B_1{}^{+*} &= -iGA_1{}^{-*} - iG^* A_1{}^+ + sB_1{}^+ + f\varepsilon_2, \\
h_2{}^- B_1{}^{-*} &= -iGA_1{}^{+*} - iG^* A_1{}^- + tB_1{}^- + \varepsilon_1.
\end{aligned}
\tag{3.19}
$$

Where the terms are labeled as: $G = g_0 c_s$, $h_1{}^\pm = \pm i\Delta + \kappa/2 - i\delta$, $h_2{}^\pm = \pm i\omega_1 + \gamma_1/2 - i\delta$, $h_3{}^\pm = \pm i\omega_2 + \gamma_2/2 - i\delta$, $k^\pm = h_2{}^\pm + g_c{}^2/h_3{}^\pm$, $s = g_c{}^2/h_3{}^+$, $t = g_c{}^2/h_3{}^-$ and $f = ig_c/h_3{}^+$.

By introducing the phase terms in the above set of equations as $\varepsilon_1 = \varepsilon_1 e^{-i\varphi_1}$ and $\varepsilon_2 = \varepsilon_2 e^{-i\varphi_2}$ for external driving fields ε_1 and ε_2 on micro-resonators MR_1 ans MR_2 respectively, we solve the above set of equations (equation (3.19)) for finding the value of $A_1{}^+$ as

$$
\begin{aligned}
A_1{}^+ =\ & \frac{[2i|G|^2(sk^- - st + h_2{}^- h_2{}^+ + k^+ h_2{}^+) - k^- h_1{}^- h_2{}^+(h_2{}^- + k^+)]G}{4i|G|^4(t - k^-)(s - k^+) + h_2{}^- h_2{}^+(2|G|^2 + ik^- h_1{}^-)(k^+ h_1{}^+ - 2i|G|^2)} \varepsilon_1 \\
& + \frac{[2if|G|^2(st - sk^- - tk^+ + k^- k^+ - h_2{}^- h_2{}^+) + fk^- h_1{}^- h_2{}^- h_2{}^+]G}{4i|G|^4(t - k^-)(s - k^+) + h_2{}^- h_2{}^+(2|G|^2 + ik^- h_1{}^-)(k^+ h_1{}^+ - 2i|G|^2)} \varepsilon_2 \\
& + \frac{[2|G|^2(st - sk^- - tk^+ + k^- k^+ - h_2{}^- h_2{}^+)]G^2}{4i|G|^4(t - k^-)(s - k^+) + h_2{}^- h_2{}^+(2|G|^2 + ik^- h_1{}^-)(k^+ h_1{}^+ - 2i|G|^2)} \varepsilon_p \\
& + \frac{ik^+ h_2{}^+(k^- - t)G^2 + h_2{}^- h_2{}^+(2|G|^2 k^+ + ik^- h_1{}^- k^+ - iG^2 k^- h_1{}^-)}{4i|G|^4(t - k^-)(s - k^+) + h_2{}^- h_2{}^+(2|G|^2 + ik^- h_1{}^-)(k^+ h_1{}^+ - 2i|G|^2)} \varepsilon_p.
\end{aligned}
$$

38

Here, A_1^+ is the amplitude of the FWM signal. Since $G = g_0 c_s$, so we can say that the FWM phenomenon in the output signal depends on opto-mechanical coupling g_o. If opto-mechanical coupling is neglected i.e. $g_o = 0$, the value of A_1^+ becomes zero.

3.3.1   Calculation of FWM

We choose the experimental parameters for a Nano Electro Opto-Mechanical system presented in [37, 38] and numerically study the periodic suppression and amplification in FWM signal. The length of cavity is taken $L = 25cm$ and other parameters are $g_0 = 2\pi \times 4kHz$, $g_c = 0.2MHz$, $\omega_{1,2} = 2\pi \times 947kHz$, $\gamma_{1,2} = 2\pi \times 140kHz$ and masses of the micro-resonator MR_1 and MR_2 are taken as $m_1 = m_2 = 145ng$. As presented in [38] , the cavity decay rate is $\kappa = 2\pi \times 215kHz$. The cavity field frequency is calculated by the relation $\omega_c = 2\pi c/\lambda_c$, where c is speed of light, and the value of frequency ω_c is calculated as $1.77 \times 10^{15}Hz$. We choose $\Delta_c = \omega_1$ and $\omega_l = \omega_c - \omega_1$, and the power of the laser field is taken as $9mW$. The value of effective detuning is chosen to be $\delta = \omega_1$.

The system stays in the resolved side-band regime [15] because the values of mechanical resonator frequencies are greater than cavity decay rate,i.e $\omega_{1,2} \gg \kappa$.
The FWM signal in the output field is calculated as using the relation from equation (3.11) , which follows as:

$$FWM \;\; = \;\; \left| -\frac{\sqrt{2\kappa}A_1^+}{\varepsilon_p} \right|^2 .$$

39

3.3.2 Coulomb-coupling controlled FWM

As the switchable mechanical driving fields at MR_1 and MR_2 are absent, the FWM intensity is observed to show the consistent amplifications and modifications in the output signal. By keeping the opto-mechanical coupling coefficient constant, i.e $g_0 =$
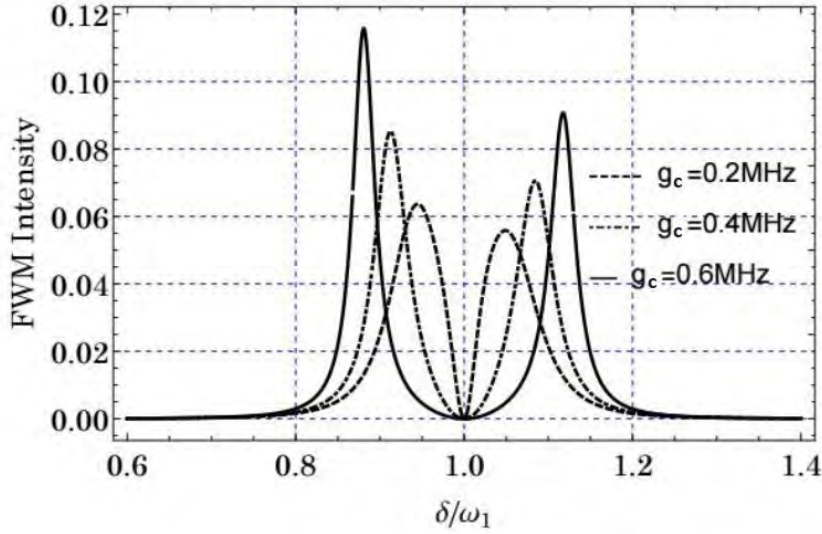
Figure 3.8: A 2-D plot for FWM Intesity signal (arbitrary units) vs normalized detuning δ/ω_1, for different values of g_c. Other parameters are $g_0/2\pi = 4kHz$, and $\varepsilon_1 = \varepsilon_2 = 0$.

$2\pi \times 4kHz$, the FWM spectrum is shown in Figure 3.8 for different values of electrostatic Coulomb coupling strength g_c. The FWM spectrum has two mode-splitting peaks. The intensity of peaks is almost same for lower values of Coulomb coupling (g_c) (see the dashed and the dot-dashed black curves in Figure 3.8), but the FWM intensity is different the higher values of g_c (see the black solid curve in Figure 3.8). The frequency shift between the two peaks is observed by the additional control of second mirror

40

(MR_2). As the value of g_c increase, this frequency shift also increases. The line width of both FWM peaks (at Stokes and Anti-Stokes lines) decreases as the Coulomb coupling is increased.

This behaviour is more clearly shown in a 3-D representation in Figure 3.9, as we plot FWM signal as a functionn of detuning δ/ω_1 and Coulomb coupling g_c.
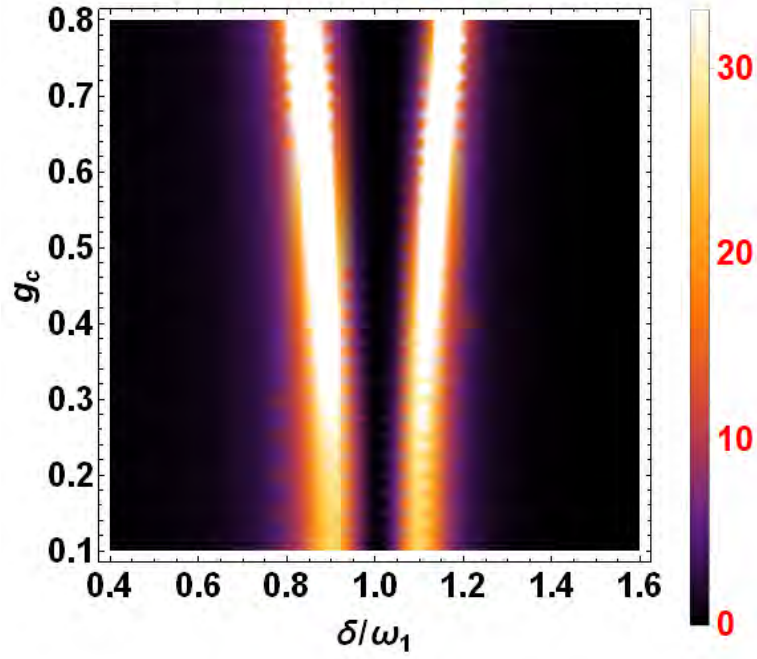
Figure 3.9: A 3-D plot for FWM Intesity (arbitrary units) as a function of normalized detuning δ/ω_1 and Coulomb coupling g_c. Other parameters are $g_0/2\pi = 4kHz$, and $\varepsilon_1 = \varepsilon_2 = 0$.

In Figure 3.9, two intensity streams, separated by the frequency shift are clearly seen. The resonance, which is responsible for the FWM signal, appears in the regions of these bright bands. The FWM signal is absent in between (off-resonant points) these intensity streams.

41

3.3.3 Phase Controlled FWM

The versatile phase control gives intuitive understanding of the non-linearity in cavity opto-mechanical systems. The extra control provided by the second mirror (MR_2) is appraised by varying the phases of the selective mechanical driving fields of MR_1 and MR_2.

Figure 3.10: A 2-D plot for FWM Intesity (arbitrary units) as a function of normalized detuning δ/ω_1, for different values of φ_2. Other parameters are $g_0/2\pi = 4kHz$, $g_c = 0.4MHz$, $\varepsilon_1 = 0$, and $\varepsilon_2/\varepsilon_p = 0.45$.

By driving the second micro-resonator (MR_2) only, i.e $\varepsilon_1/\varepsilon_p = 0$ and $\varepsilon_2/\varepsilon_p = 0.45$, two mode-splitting peaks are resulted in the FWM spectrum, which is shown in Figure 3.10. In both peaks, an asymmetrically amplified FWM signal is achieved (see, blue-dashed and black solid curves in Figure 3.10). The FWM signal is suppressed ($\varphi_2 = \pi/4$) and amplified ($\varphi_2 = \pi$) at Anti-Stokes line while the light signal is amplified

$(\varphi_2 = \pi/4)$ and suppressed $(\varphi_2 = \pi)$ at Stokes line. The science behind this asymmetric amplification and suppression is that by driving the mechanical resonator MR_2, only effective Coulomb coupling can be enhanced. That is why asymmetric amplification and suppression of the FWM signal can be achieved by selective mechanical driving of MR_2.

A 3-D representation of the phase controlled intensity of FWM signal is shown in Figure 3.11.
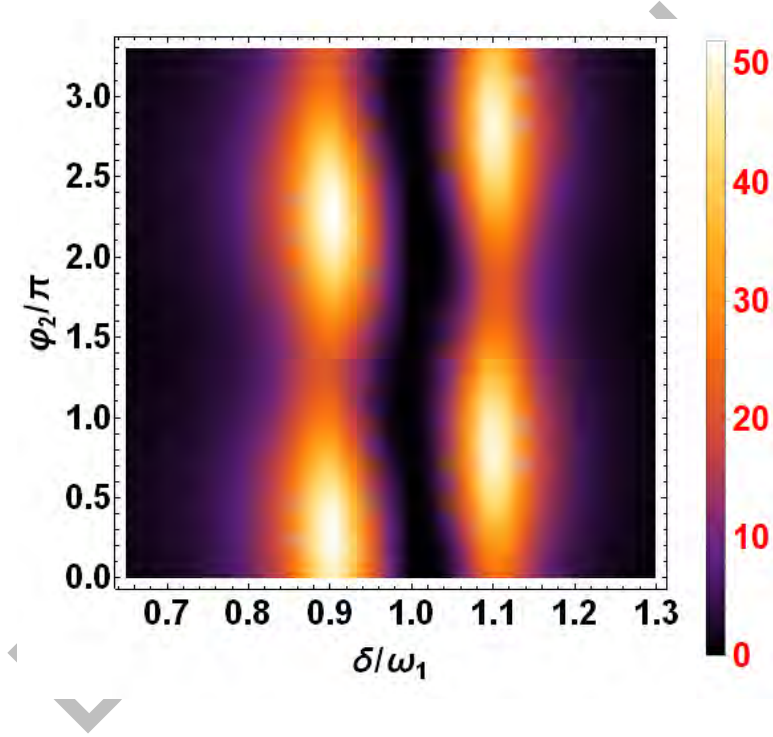
Figure 3.11: A 3-D plot for FWM Intesity (arbitrary units) as a function of normalized detuning δ/ω_1 and phase φ_2. Other parameters are $g_0/2\pi = 4kHz$, $g_c = 0.4MHz$, $\varepsilon_1 = 0$, and $\varepsilon_2/\varepsilon_p = 0.45$.

The amplification of FWM signal changes periodically with the phase φ_1 (see Figure 3.11) by driving the mechanical resonator MR_2 only. This asymmetric amplification

of the light signal is due to enhancement in the effective Coulomb coupling g_c. The FWM signal is absent in the off resonant region.

The selective mechanical driving of both mirrors MR_1 and MR_2, imparts the ability to completely block or amplify the FWM signal. To understand the FWM spectrum in the presence of mechanical driving fields on both mirrors MR_1 and MR_2, the amplitudes of both mechanical driving fields are set to $\varepsilon_1/\varepsilon_p = \varepsilon_2/\varepsilon_p = 0.45$.
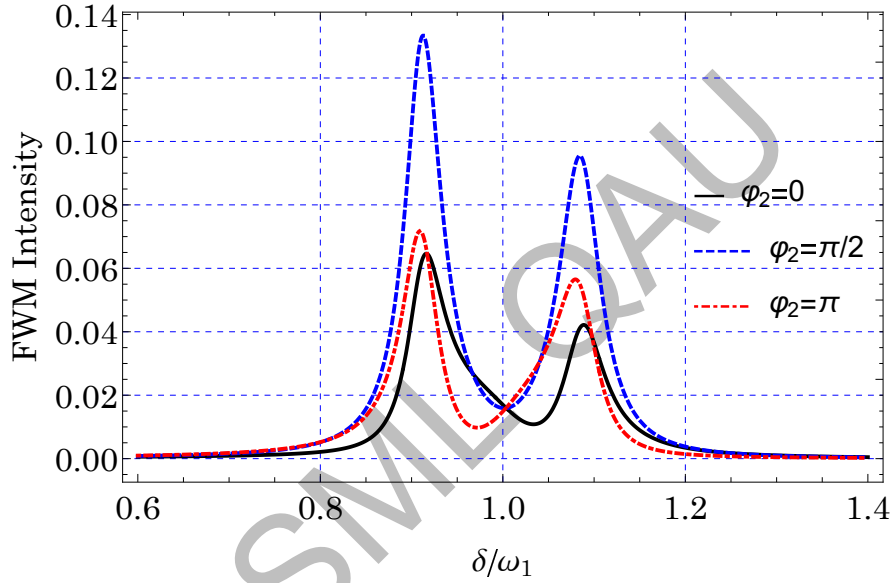
Figure 3.12: A 2-D plot for FWM Intesity (arbitrary units) as a function of normalized detuning δ/ω_1, for different values of φ_2. Other parameters are $g_0/2\pi = 4kHz$, $g_c = 0.4MHz$, $\varepsilon_1/\varepsilon_p = \varepsilon_2/\varepsilon_p = 0.45$.

Asymmetric amplifications in the FWM light signal is achieved for the phase values $\varphi_2 = 0$ and π, which is shown in Figure 3.12. The mechanical driving of both MR_1 and MR_2 is advantageous at some extent because symmetric amplification can also be observed in the FWM signal (see blue-dashed curve in Figure 3.12). A jitter variation (notch) in the FWM signal is found at the resonance point $\delta = \omega_1$. This behaviour

is due to the fact that both effective opto-mechanical coupling and Coulomb coupling strengths are enhanced by driving both MR_1 and MR_2 at the same time.
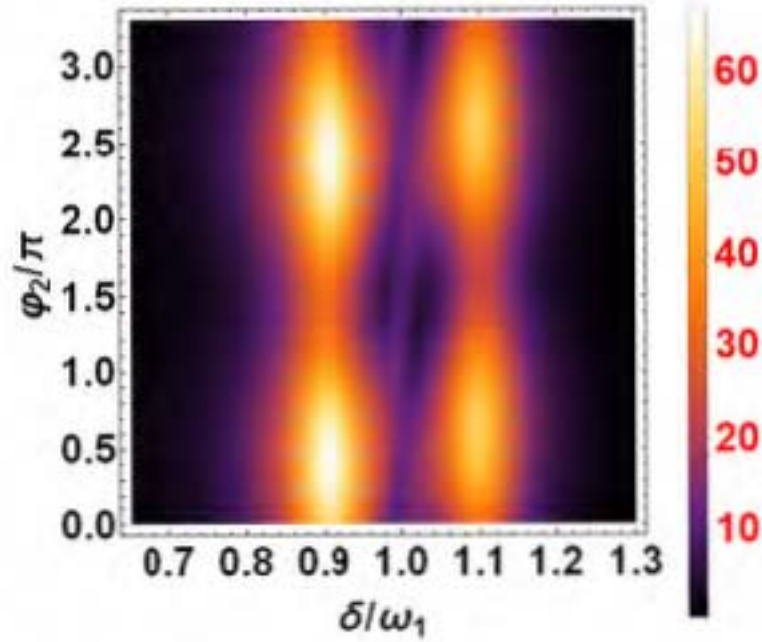
Figure 3.13: A 3-D plot for FWM Intesity (arbitrary units) as a function of normalized detuning δ/ω_1 and phase φ_2. Other parameters are $g_0/2\pi = 4kHz$, $g_c = 0.4MHz$, $\varepsilon_1 = 0$, and $\varepsilon_2/\varepsilon_p = 0.45$.

In the off resonant region ($\delta = \omega_1$), the FWM signal is not zero but has a weak signal in this area, as shown in Figure 3.13.

3.3.4   Amplitude Controlled FWM

In Figure 3.14 the FWM intensity is shown against the normalized detuning for varying amplitude of mechanical driving on MR_2. Again asymmetric amplifications and

suppressions are seen in the FWM signal around the resonance point. The FWM signal is almost blocked at the off resonant region $\delta = \omega_1$.

This ability of selective switching and amplifying the input probe signal is highly desirable in practical optical communications [40, 41, 42, 43, 44, 45, 46, 47].
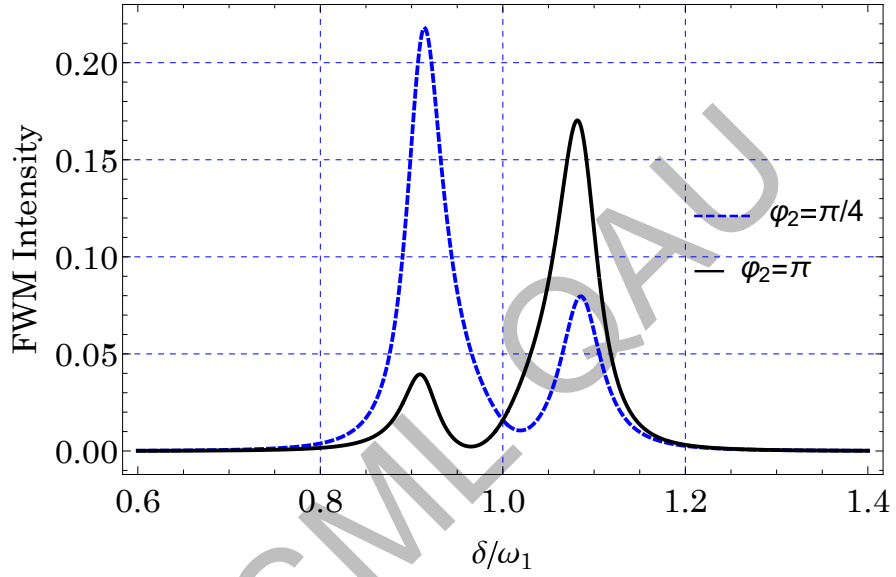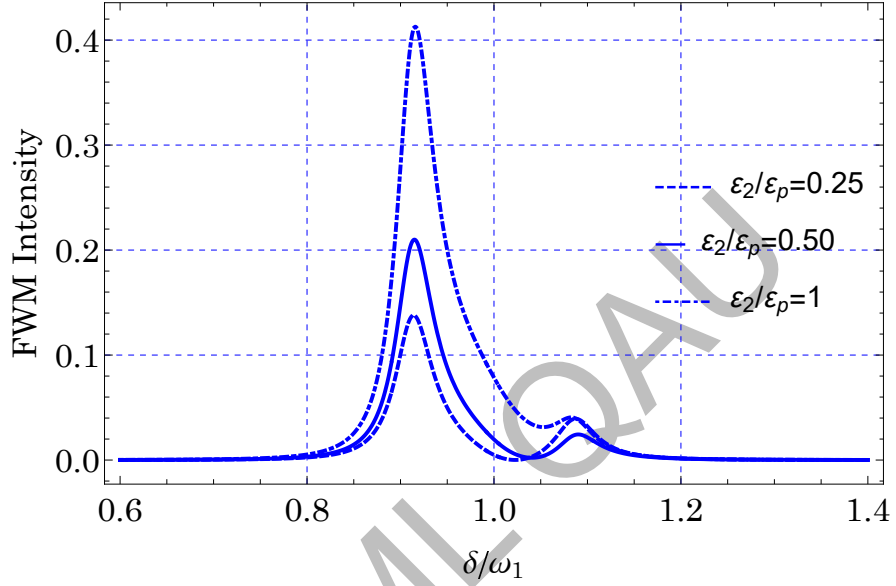

Figure 3.14: A 2-D plot for FWM Intesity (arbitrary units) as a function of normalized detuning δ/ω_1, for different values of $\varepsilon_2/\varepsilon_p$. Other parameters are $g_0/2\pi = 4kHz$, $g_c = 0.4MHz$, $\varepsilon_1 = 0$, and $\varepsilon_2/\varepsilon_p = 0.45$.

Chapter 4

Controlling FWM in NEOMS via BEC

The Bose-Einstein condensation (BEC) is a macroscopic occupation of atoms in a single quantum state. In 1924, Satyendra Nath Bose and Albert Einstein explained the condensation phenomenon. The BEC of material particles is formed when the bosons are trapped at near to absolute zero temperatures by different cooling techniques, such as laser cooling [48], evaporative cooling [49] and Sisyphus cooling [50]. The first Bose-Einstein condensate (BEC) was observed experimentally in Rubidium (Rb^{87}) by Eric Cornell, Carl Weiman [51] and co-workers in June 1995, using a combination of laser cooling and magnetic-evaporative cooling [52, 53]. Later, Wolfgang Ketterle [54] independently condensed Sodium (Na^{23}) in MIT. In the same year, at Rice University, BEC was observed in Lithium atoms by Randal Hulet [55]. Many other groups have observed Bose-Einstein condensation by using optical traps [56]. The non-linear phenomena of Electromagnetic Induced Transparency (EIT) [57, 58], Slow light [59] and fast light [60] have been experimentally observed in Bose-Einstein condensate (BEC). Bose-Einstein condensate is an ideal test bed for EIT sub and super luminal effects

which are vital in developing applications in and Optical Information Processing and Quantum Computation.

4.1 Interatomic interaction in BEC

As a result of atomic interactions, several properties of BEC enter the picture. The BEC is formed, when the de-Broglie wavelength of the atoms in the condensate is almost equal to the average inter-particle spacing. As a result, understanding the characterization of the scattering process by a single parameter, known as scattering length a. The interatomic potential is the interaction of an atom with a group of atoms in condensed phase. This potential has both an attractive as well as a repulsive component if binding is to be occur. The chemical potential is normally effective across a distance of around $1nm$, and the de-Broglie wavelength is very enormous, as much as 1000 times the distance. This indicates that collisions should be interpreted as diffracting waves from minor obstructions. As a result, the scattered field should be made up of a spherical wave defined just by its amplitude. This amplitude is actually the scattering length a.

With total number of trapped-atoms N, the condition for BEC to occur is

$$N(\frac{\hbar\omega}{k_B T})^3 = 1.2021.$$

We notice that the condensate exists at temperature $700nK$, with approximately 10^7 atoms in the optical trap [56].

48

4.2 Nature of atom-atom interaction

The inter-atomic interaction between two atoms with cross wave-functions alters the atomic pair's energy. When two atoms are close to each other, a large quantity of interaction energy occurs. The size of the energy shift is determined by the scattering length a. If an atomic pair has an unperturbed energy of E and is trapped in a volume of l^3, the energy of the condensate is $E \approx \hbar^2/ml^2$. If the number of atoms in the condensate changes, the energy of the system will be changed. Therefore, the perturbed energy ΔE will be,

$$\frac{\Delta E}{E} \approx N_0 \frac{a}{l}, \tag{4.1}$$

where N_0 is the number of atoms in the condensate and m is the mass of atom. The dilute-gas condition, is written as $N_0^{1/3} a/l << 1$.

It is possible for the scattering length a to be negative or positive. The negative sign implies that the condensate atom display an attractive inter-atomic connection, whereas the positive sign suggests that the inter-atomic interaction is repulsive. Lithium has attractive interaction while Rubidium condensate has repulsive interaction. Increasing N causes the condensate to loose energy by reducing l, which causes the density to rise, causing the condensate to no longer be a dilute gas. Instead of BEC, another form of phase transition (liquid/solid) happens. As a result, the number of atoms in a condensate exhibiting attractive interactions is limited to total number of trapped-atoms N.

4.3 System Model

Let us discuss the enhanced FWM signal in the presence of an atomic medium, i.e Bose-Einstein condensate (BEC). In the presence of switchable mechanical driving fields on mechanical resonators MR_1 and MR_2, we investigate the adaptability of a trapped Bose-Einstein condensate (BEC) in a Nano Electro opto-mechanical system. The effects of atomic medium (BEC) on the strength of the FWM signal will be explored numerically using appropriate experimental parameters. A Nano Electro Opto-Mechanical System (NEOMS) with a Bose-Einstein condensate trapped inside the optical cavity accompanied by the additional control of mechanical driving fields ε_1 and ε_2, is shown in Figure 4.1.

4.4 Mathematical Treatment

We assume that the atomic density is so high that two-body atom-atom interactions are impossible to ignore, and that on-site kinetic energy and atom hopping are significant. To completely characterise the dynamics of Bose-Einstein condensate in NEOMS, we will employ the Bose-Hubbard Model (BHM) [61]. From the microscopic second-quantized Hamiltonian,

$$
\begin{aligned}
\hat{H} = \int dx \hat{\psi}^\dagger(x) [-\frac{\hbar^2}{2m} \nabla^2 + V(x)] \hat{\psi}(x) \\
+ \frac{\lambda}{2} \int d^3 x \hat{\psi}^\dagger(x) \hat{\psi}^\dagger(x) \hat{\psi}(x) \hat{\psi}(x),
\end{aligned}
\tag{4.2}
$$

where, $\lambda = 4\pi a_{sc}\hbar^2/2m$ with a_s as s-wave scattering length and m is the mass of the condensate, and $\hat{V}(x) = U_0 \hat{c}^\dagger \hat{c} \cos^2(kx)$ (here k is the wave number) with $U_0 = g_a{}^2/\Delta_a$
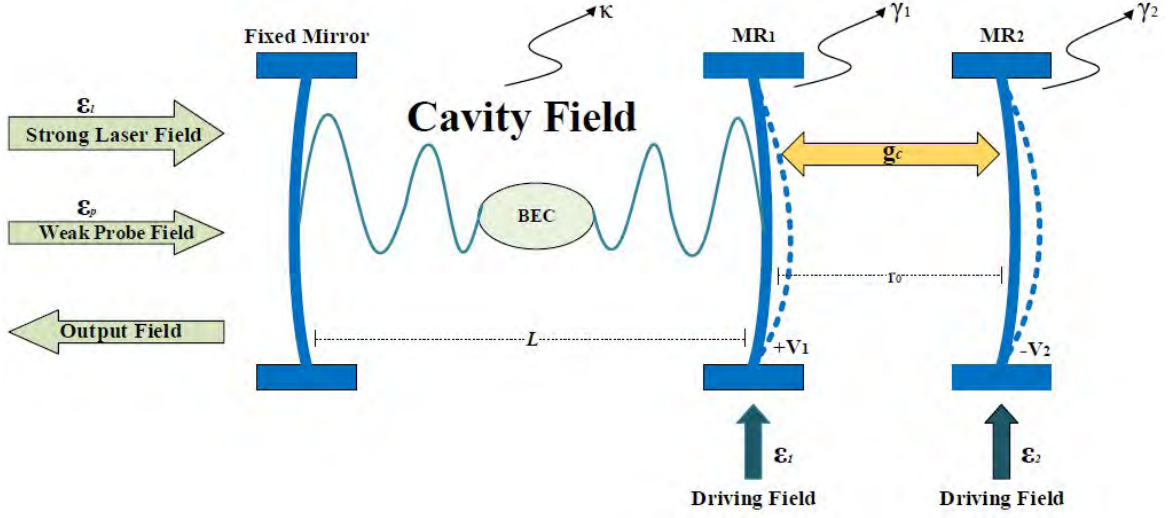
Figure 4.1: The Schematic description of NEOMS with BEC trapped inside the optical cavity: Here, MR_1 is coupled with the cavity through opto-mechanical coupling and optical field is coupled with two level N-atoms of BEC with atomic coupling stregnth g_a , and mechanical resonators MR_1 and MR_2 are coupled through the coulomb coupling strength g_c. The ε_1 and ε_2 are external driving fields on MR_1 and MR_2 respectively. The L is the length of the cavity while r_0 is the equilibrium distance between two micro-resonators.

(here g_a is atomic coupling strength and Δ_a is the atomic detuning).

Now, expanding the field operator $\hat{\psi}(x)$ in terms of Wannier functions, i.e

$$\hat{\psi}(x) = \sum_{i,n} \omega_n(x - x_i)\hat{b}_i,$$

we can write the opto-mechanical Bose-Hubbard Hamiltonian (OMBH) for the system

presented in the work by assuming nearest neighbor approximation [62].

$$\hat{H}_{BH} = \frac{U}{2} \sum_j (\hat{b}_j^\dagger \hat{b}_j^\dagger \hat{b}_j \hat{b}_j) + \sum_j \hat{b}_j^\dagger \hat{b}_j (E_0 + \hbar U_0 (V_{cl} + \hat{c}^\dagger \hat{c}) J_0)$$
$$+ \sum_j (\hat{b}_{j+1}^\dagger \hat{b}_j + \hat{b}_{j+1} \hat{b}_j^\dagger)(E + \hbar U_0 (V_{cl} + \hat{c}^\dagger \hat{c}) J). \tag{4.3}$$

The first term of equation (4.3) represents the atom-atom interaction, second term is the Hamiltonian of on-site kinetic energy and tunneling energy and the third term represents kinetic energy and the tunneling (hopping) energy of atoms from one lattice site to another neighbouring sites. The U is two-body atom-atom interaction energy, $\hat{b}_j^\dagger$ and $\hat{b}_j$ are bosonic creation and annihilation operators at the j_{th} site, E_0 is the on-site kinetic energy. Moreover, U_0 is the height of the optical lattice potential per photon, V_{cl} is the classical potential added to the system and J_0 is the tunneling energy. The relations for these terms are given as

$$
\begin{aligned}
U &= \frac{4\pi a_{sc} \hbar^2}{2m} \int d^3 x |\omega(x - x_j)|^4, \\
E_0 &= \int d^3 x \omega(x - x_j)(-\frac{\hbar^2 \Delta^2}{2m}) \omega(x - x_j), \\
J_0 &= \int d^3 x \omega(x - x_j) \cos^2(kx) \omega(x - x_j), \\
U_0 &= \frac{g_a{}^2}{\Delta_a}.
\end{aligned}
\tag{4.4}
$$

We use nearest neighbour approximation, so that we can neglect the third term of equation4.2, and only considering the first two terms, the total Hamiltonian of the system in a rotating frame with laser frequency ω_l in the presence of input pump field ε_l, weak probe field ε_p and selective mechanical drivings of mechanical resonators MR_1

and MR_2, can be written as

$$\hat{H}_T = \frac{U}{2}\sum_j(\hat{b}_j^\dagger\hat{b}_j^\dagger\hat{b}_j\hat{b}_j) + \sum_j\hat{b}_j^\dagger\hat{b}_j(E_0 + \hbar U_0(V_{cl} + \hat{c}^\dagger\hat{c})J_0)$$
$$+\Delta_c\hat{c}^\dagger\hat{c} - g_0\hat{c}^\dagger\hat{c}(\hat{b}_1^\dagger + \hat{b}_1) + g_c(\hat{b}_1^\dagger\hat{b}_2 + \hat{b}_1\hat{b}_2^\dagger)$$
$$+i(\sum_{k=1}^{2}\varepsilon_k\hat{b}_k^\dagger e^{-i\delta t} + \varepsilon_l\hat{c}^\dagger + \varepsilon_p^\star\hat{c}^\dagger e^{-i\delta t} - H.c). \tag{4.5}$$

For a detailed investigation of dynamics of the system, photon losses are included along with the decay rate connected to the condensate, κ and γ_b respectively. So, the dynamics of the system is described by solving the Heisenberg-Langevin equations of motion, we get

$$\dot{\hat{c}} = -(i\Delta_c + \frac{\kappa}{2})\hat{c} + ig_0(\hat{b}_1^\dagger + \hat{b}_1)\hat{c} - iU_0 J_0\hat{c}\sum_j\hat{b}_j^\dagger\hat{b}_j + \varepsilon_l + \varepsilon_p e^{-i\delta t} + \sqrt{2\kappa}\hat{c}_{IN},$$

$$\dot{\hat{b}}_j = -\frac{E_0}{\hbar}\hat{b}_j - iJ_0[\frac{V_{cl}}{\hbar} + U_0\hat{c}^\dagger\hat{c}]\hat{b}_j - i\frac{U}{\hbar}\hat{b}_j^\dagger\hat{b}_j\hat{b}_j - \gamma_b\hat{b}_j + \sqrt{2\gamma_b}\hat{b}_{IN},$$

where, $\hat{c}_{IN}$ and $\hat{b}_{IN}$ are noise operators connected to the cavity-field and BEC, respectively. Using the ansatz $\hat{c} = c_s + \delta\hat{c}$ and $\hat{b} = b_s + \delta\hat{b}$, we can linearize the equations of motion. In case of negligible tunneling, we remove the site index j from the bosonic operators [63, 64]. Moreover, we explicate the quadrature of mechanical mode of BEC by assuming Hermitian operators, that is, $\delta\hat{q} = (\delta\hat{b} + \delta\hat{b}^\dagger)/\sqrt{2}$ and $\delta\hat{p} = (\delta\hat{b} - \delta\hat{b}^\dagger)/i\sqrt{2}$. By excluding the quantum fluctuation terms averaged to zero [65, 66, 67], the linearized set of Heisenberg-Langevin Equations of motion for condensate position operator, cavity field operator and mirror position operators along with equations for mechanical

53

resonators , is

$$
\delta\ddot{\hat{q}} + \gamma_b \delta\dot{\hat{q}} + \omega_b{}^2 \delta\hat{q} = -gF(\delta\hat{c} + \delta\hat{c}^\dagger),
$$

$$
\delta\dot{\hat{c}} = -(\frac{\kappa}{2} + i\Delta)\delta\hat{c} - ig\hat{q} + ig_0 c_s(\delta\hat{b}_1{}^\dagger + \delta\hat{b}_1) + \varepsilon_l + \varepsilon_p e^{-i\delta t},
$$

$$
\delta\dot{\hat{b}}_1 = -(i\omega_1 + \frac{\gamma_1}{2})\delta\hat{b}_1 + ig_0 c_s \delta\hat{c}^\dagger + ig_0 c_s{}^* \delta\hat{c} - ig_c \delta\hat{b}_2 + \varepsilon_1 e^{-i\delta t},
$$

$$
\delta\dot{\hat{b}}_2 = -(i\omega_2 + \frac{\gamma_2}{2})\delta\hat{b}_2 - ig_c \delta\hat{b}_1 + \varepsilon_2 e^{-i\delta t}, \tag{4.6}
$$

where, $\Delta = \Delta_c - U_0 N J_0 - g_0(b_{1s}{}^\star + b_{1s}) + gq_s$ is the effective detuning, $g = 2U_0 J_0 \sqrt{N}|c_s|^2$ is atom field coupling, $F = U_{eff} + v$, $\omega_b = \sqrt{(F)(v + 3U_{eff})}$, $U_{eff} = \frac{UN}{\hbar M}$ and $v = U_0 J_0|c_s|^2 + \frac{V_{cl}J_0}{\hbar} + \frac{E_0}{\hbar}$ are parameters for controlling atom-atom coupling, (here N represents number of atoms in M lattice sites). To calculate the first order sidebands, we use the ansatz [68, 69]

$$
\delta\hat{c} = A_1{}^- e^{-i\delta t} + A_1{}^+ e^{i\delta t},
$$

$$
\delta\hat{b}_1 = B_1{}^- e^{-i\delta t} + B_1{}^+ e^{i\delta t},
$$

$$
\delta\hat{b}_2 = B_2{}^- e^{-i\delta t} + B_2{}^+ e^{i\delta t},
$$

$$
\delta\hat{q} = E^- e^{-i\delta t} + E^+ e^{i\delta t}.
$$

Using above ansatz in the set of equation (4.6), we get a system of twelve linear

equations as

$$-gFA_1^+ - gFA_1^{-*} - r_1^- E^+ = 0,$$

$$-gFA_1^- - gFA_1^{+*} - r_1^- E^- = 0,$$

$$h_1^+ A_1^+ - iGB_1^+ - iGB_1^{-*} + igE^+ = 0,$$

$$h_1^- A_1^+ - iGB_1^- - iGB_1^{+*} + igE^- = \varepsilon_p,$$

$$h_1^+ A_1^{+*} + iGB_1^- + iGB_1^{+*} - igE^- = 0,$$

$$h_1^- A_1^{-*} + iGB_1^+ + iGB_1^{-*} - igE^+ = \varepsilon_p,$$

$$-iG^* A_1^+ - iGA_1^{-*} + k_1^+ B_1^+ + ig_c B_2^+ = 0,$$

$$-iG^* A_1^{+*} - iG^* A_1^- + k_1^- B_1^- + ig_c B_2^- = \varepsilon_1,$$

$$iGA_1^{+*} + iG^* A_1^- - ig_c B_2^- + k_1^+ B_1^{+*} = 0,$$

$$iG^* A_1^+ + iGA_1^{-*} - ig_c B_2^+ + k_1^- B_1^{-*} = 0,$$

$$k_2^+ B_2^+ + ig_c B_1^+ = 0,$$

$$k_2^- B_2^- + ig_c B_1^- = \varepsilon_2. \tag{4.7}$$

Here,

$$G = g_0 c_s \quad ; \quad h_1^\pm = \kappa/2 + i(\Delta \pm \delta),$$

$$k_1^\pm = \gamma_1/2 + i(\omega_1 \pm \delta) \quad ; \quad k_2^\pm = \gamma_2/2 + i(\omega_2 \pm \delta),$$

$$G^* = g_0 c_s^* \quad ; \quad r_1^\pm = \omega_b^2 - \delta^2 \pm i\delta\gamma_b.$$

For understanding the complete dynamics of medium (BEC) mediated FWM signal, phases for mechanical drivings ε_1 and ε_2 are introduced as,

$$\varepsilon_1 = \epsilon_1 e^{-i\varphi_1} \quad ; \quad \varepsilon_2 = \epsilon_2 e^{-i\varphi_2}.$$

55

Solving the set of linear equations in equation (4.7) for the first order side-band mode $A_1{}^+$, we get

$$A_1{}^+ \ = \ \frac{H_1}{C_1 + C_2 + C_3}\varepsilon_1 + \frac{H_2}{C_1 + C_2 + C_3}\varepsilon_2 + \frac{H_3}{C_1 + C_2 + C_3}\varepsilon_p, \qquad (4.8)$$

where,

$$H_1 \ = \ G(g_c{}^2 + k_1{}^+ k_1{}^-)(-2ig^2 F + h_1{}^- r_1{}^-),$$

$$H_2 \ = \ -Gg_c(k_1{}^+ - k_1{}^-)(2g^2 F + i h_1{}^- r_1{}^-),$$

$$H_3 \ = \ -(g^2 F k_1{}^+(g_c{}^2 + k_1{}^- k_2{}^-) - iG(k_1{}^+ - k_1{}^-)k_2{}^- r_1{}^- G^*),$$

$$C_1 \ = \ g^2 F(g_c{}^2(h_1{}^+ + h_1{}^-)k_1{}^+ - 2G^2 k_2{}^-((k_1{}^+ - k_1{}^-) + (h_1{}^+ - h_1{}^-)k_1{}^+ k_1{}^-)),$$

$$C_2 \ = \ i h_1{}^-(g_c{}^2 h_1{}^+ k_1{}^+ + h_1{}^+ k_1{}^+ k_1{}^- k_2{}^- + G^2(k_1{}^- - k_1{}^+)k_2{}^-)r_1{}^-,$$

$$C_3 \ = \ G(k_1{}^+ - k_1{}^-)k_2{}^-(2g^2 F + i h_1{}^+ r_1{}^-)G^*.$$

4.5 Numerical Results

We examine a repulsive Bose-Einstein condensate of N Rb^{87} two level atoms and take data from real experiments [70, 71]. We use experimental parameters to study enhancement in FWM signal in a Nano Electro Opto-Mechanical System (NEOMS) in the presence of Bose-Einstein condensate (BEC) trapped inside the optical cavity. The experimental parameters for the Rb^{87} condensate [71] is given in the Table 4.1. Other parameters related to cavity field, coupling strengths and mechanical resonators are same as in Section 3.2.1.

The FWM intensity is calculated using the relation,

$$FWM \ = \ \left| -\frac{\sqrt{2\kappa}}{\varepsilon_p} A_1{}^+ \right|^2.$$

Experimental parameters	
Parameters	Values
m_{bec}	$1.45 \times 10^{-25} kg$
a_{sc}	$109 a_0$
ω	$38.628 kHz$
N	$10^5 atoms$

Table 4.1: In the table, $a_0 = 0.529 \times 10^{-10} m$ is the Bohr radius.

4.5.1 FWM signal for varying atom-field coupling

In the presence of an atomic medium, i.e, Bose Einstein Condensate (BEC), a third peak appears at the resonance point (δ/ω_1) in the FWM intensity curve, as shown in Figure 4.2. When the atom-field coupling is increased, three prominent changes occur in the FWM intensity; The FWM intensity decreases for the peaks right and left to the resonance point, the intensity of the new peak at the resonance point increases and the line-width of the peak at resonance point also increases (see blue-dotdashed and red-dotted curves in 4.2). These changes occur due to the following reason; When the atom-field coupling is increased, the non-linearity in the cavity is enhanced, which significantly alters the output signal.
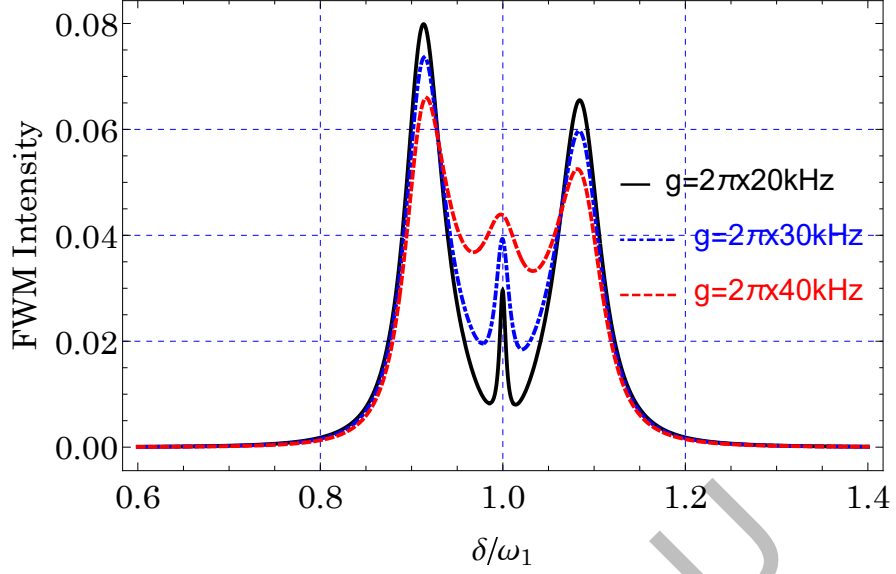
Figure 4.2: A 2-D plot for FWM Intesity (arbitrary units) as a function of normalized detuning δ/ω_1. Other parameters are $\omega_b = \omega_1$, $U_{eff} = v = \omega_b$, $\gamma_b = 0.01\gamma_1$, $\Delta_a = \omega_1$ and $\Delta = \omega_1$.

4.5.2 FWM signal in the presence of BEC

Figure 4.3 shows that the FWM signal confronts to various modifications, when the mechanical resonator MR_1 is driven. As the phase angle φ_1 is increased, the intensities of FWM peaks on both sides of the resonance point (δ/ω_1) increase. The FWM signal strength at the resonance point is independent of the phase value, as shown in Figure 4.3. For lower phase values, the FWM signal right to the resonance point is suppressed (see black-dotted and blue-dashed curves in Figure 4.3).

When MR_1 is driven, the opto-mechanical coupling strength is enhanced, due to which consistent modifications occur in the output field. Because of this reason, asymmetric suppression and amplifications are observed in the FWM signal. When the

58
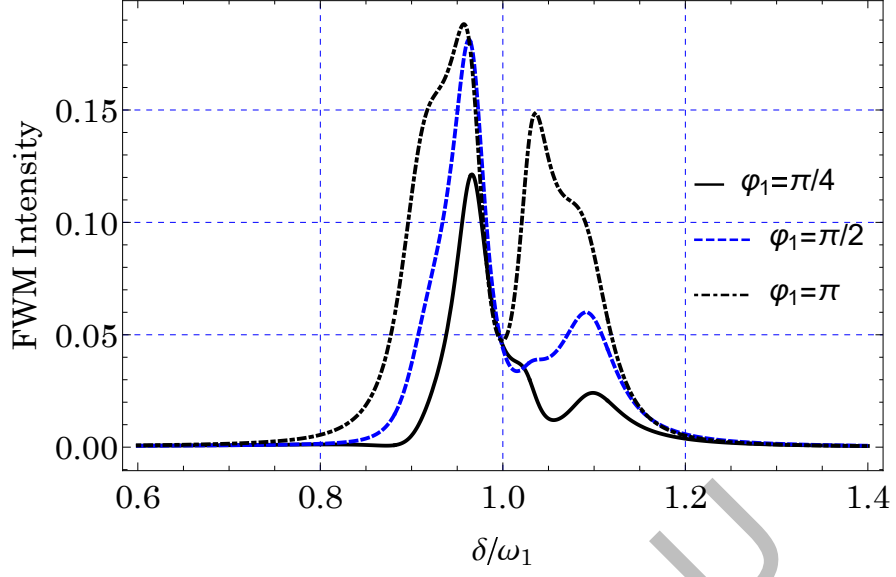
Figure 4.3: A 2-D plot for FWM Intesity (arbitrary units) as a function of normalized detuning δ/ω_1, for different values of phase angle φ_1. Other parameters are $g/2\pi = 30kHz$, $\varepsilon_1/\varepsilon_p = 0.45$, $\varepsilon_2/\varepsilon_p = 0$, $\omega_b = \omega_1$, $U_{eff} = v = \omega_b$, $\gamma_b = 0.01\gamma_1$, $\Delta_a = \omega_1$ and $\Delta = \omega_1$.

mechanical resonator MR_2 is driven instead of MR_1, anomalous changes occur in the FWM signal. At the phase angle $\varphi_2 = \pi/4$, the amplitude of the FWM peak left to the resonance point δ/ω_1 is greater than that of the peak right to the resonance point (see black-line curve in Figure 4.4). For the phase value $\varphi_2 = \pi/2$, almost symmetric FWM peaks are observed around the resonance point δ/ω_1 (see blue-dashed curve in Figure 4.4). At higher phase values, i.e $\varphi_2 = \pi$, the FWM intensity of the peak right to the resonance point is greatly amplified while the FWM signal is almost absent at the left side of the resonance point (see black-dotdashed curve in Figure 4.4).
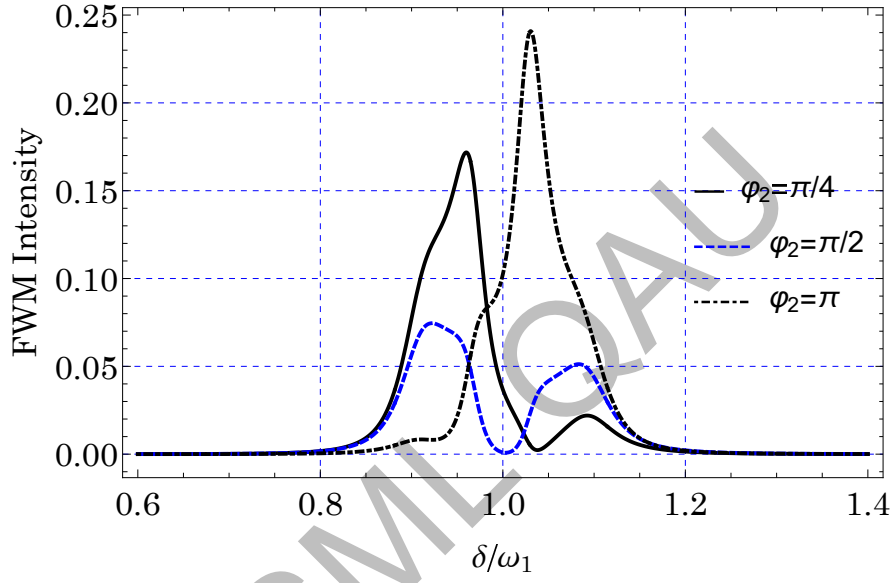
Figure 4.4: A 2-D plot for FWM Intesity (arbitrary units) as a function of normalized detuning δ/ω_1, for different values of phase angle φ_2. Other parameters are $g/2\pi = 30kHz$, $\varepsilon_1/\varepsilon_p = 0$, $\varepsilon_2/\varepsilon_p = 0.45$, $\omega_b = \omega_1$, $U_{eff} = v = \omega_b$, $\gamma_b = 0.01\gamma_1$, $\Delta_a = \omega_1$ and $\Delta = \omega_1$.

Chapter 5

Controlled Bi-stability in NEOMS

In this chapter, we explore another the non-linear effect in an nano-transducer theoretically which is bi-stability. The Nano-Opto-Electro-Mechanical System (NOEMS) comprises of a cavity with a fixed mirror that is connected to a vibrating end mirror through an opto-mechanical coupling, while the Coulomb interaction links the moving mirror to the other moving mirror. The opto-mechanical coupling that causes the non-linearity in NOEMS, also produces bi-stable behaviour in the mean intra-cavity photon number. We show that external driving fields on moveable mirrors can be used to control the optical bi-stability. Using the hybrid NOEMS, we show how to implement a system that offers an adjustable switch for regulating bi-stability under various experimental conditions. We also derive the generic bi-stability conditions in Nano-Opto-Electro-Mechanical systems.

5.1 Introduction to Bi-stability

Bi-stability in a dynamical system refers to the existence of two stable equilibrium states. When something is bi-stable, it might be in one of two states. A light switch is an example of a bi-stable mechanical device. The switch lever is intended to rest in either the "on" or "off" position, not in the middle. The electronic circuits, mechanical systems, chemical processes, non-linear optical systems, and biological and physiological systems can all exhibit the bi-stable behaviour.

When one of the mirrors in an optical cavity is moveable, the field exerts radiation pressure, which depends upon the coupling between the cavity field and the mirror. This radiation pressure alters the position of the moveable mirror, causing the optical path to shift, resulting in non-linearity in the system. Non-classical features and optical bi-stability [72, 73, 74, 75] emerges from this non-linear phenomenon, which is comparable to Kerr-medium [76, 77, 78] non-linearity.

In a pioneering work, Braginsky and his co-workers [79], hypothesised that the imposed radiation pressure by confined optical field can couple the optical and mechanical modes of a cavity resonator. There has been a steady increase in interest in opto-mechanical systems in recent years, particularly in relation to entanglement of optical and mechanical modes [80, 81, 82], opto-mechanically induced transparency [82, 83, 84, 85], and four wave mixing [74]. Hybrid quantum systems [86, 87, 88] have been developed by combining opto-mechanical resonators with other systems such as mechanical membranes [89, 90, 91, 92, 93], Bose Einstein Condensate/Fermions [93, 94, 95] and single multi-level atoms [96, 97, 98, 99, 100]. Quantum electromechan-

ical systems (QEMS) [101, 102, 103] are one type of hybrid quantum system. QEMS is a device[101, 102, 103, 104, 105] in which the quantum characteristics of the mechanical or electronic degrees of freedom becomes significant in the observable behaviour. Wineland et al. [106, 107] were the first to recognise this system, followed by Zoller and Tian [102] and Milburn and co-workers [103].

The nonlinear characteristics of the optical cavity field gives rise to optical bi-stability in the system which exhibits the phenomenon of hysteresis [106]. The optical bi-stability with Kerr effect has been studied in a basic opto-mechanical system [107, 108] as well as in hybrid opto-mechanical systems composed of trapped cold atoms [109, 110, 111, 112] and two-level atoms [113]. Besides, it has also been investigated in a hybrid electro-opto-mechanical system with coupled nano-mechanical resonators [95]. Optical bi-stability has potential applications in non-linear quantum optics, such as optical signal processing [114], optical switches [115] and optical communication devices [116]. In this work, a nano-electro-opto-mechanical system (NEOMS) [101, 114, 115, 116, 117, 118, 119, 120] made up as nano-transducer, is presented for the detail analysis of optical and mirror bi-stability. A method like this is useful for comprehending various electromagnetically-introduced transparency (EIT) window profiles [121, 122, 123], superluminal and subluminal light [93, 94], Fano resonances [121, 124, 125, 126], and Four-Wave Mixing [100, 101]. The proposed nano-electro-opto-mechanical system (NEOMS) is made from two charged mechanical resonators MR_1 and MR_2. The optical cavity field is coupled to MR_1 via opto-mechanical coupling that causes optical bi-stability in the system. Two external biased voltages V_1(-V_2) are applied to the mechanical resonators MR_1(MR_2) which results in Coulomb cou-

pling between MR$_1$ and MR$_2$. In the present work, we mainly focus on the role of external driving fields in bi-stability with the coupled mechanical resonators (MR$_s$). In experiments, this kind of cavity opto-mechanical system has been realized with a double-microdisk resonator, a nanobeam photonic crystal, or a microwave device with two micro-mechanical beams [125]. Strong mechanical driving has been utilized to make hybrid quantum spin-phonon devices [127] and ultra-strong exciton-phonon coupling [128].

5.2 Hamiltonian of the System

Figure 5.1 depicts the basic Nano Electro Opto-Mechanical System (NEOMS), which has a fixed mirror and a moving end mirror MR_1 which combine to form an opto-mechanical system. The mechanical resonator MR_1 interacts to the cavity field via radiation pressure force. A second mirror (mechanical resonator MR_2) is introduced into the cavity which interacts with the mechanical resonator MR_1 through phonon-phonon coupling.

The second mirror MR_2 allows more control over the cavity field and gives a lot of options for learning about non-linear processes in Cavity-based Electro-Opto-Mechanical Systems.

The total Hamiltonian of the system, under the rotating reference frame at the frequency ω_l, is

$$\hat{H} = \hat{H}_{mc} + \hat{H}_{dr} + \hat{H}_{int}. \tag{5.1}$$
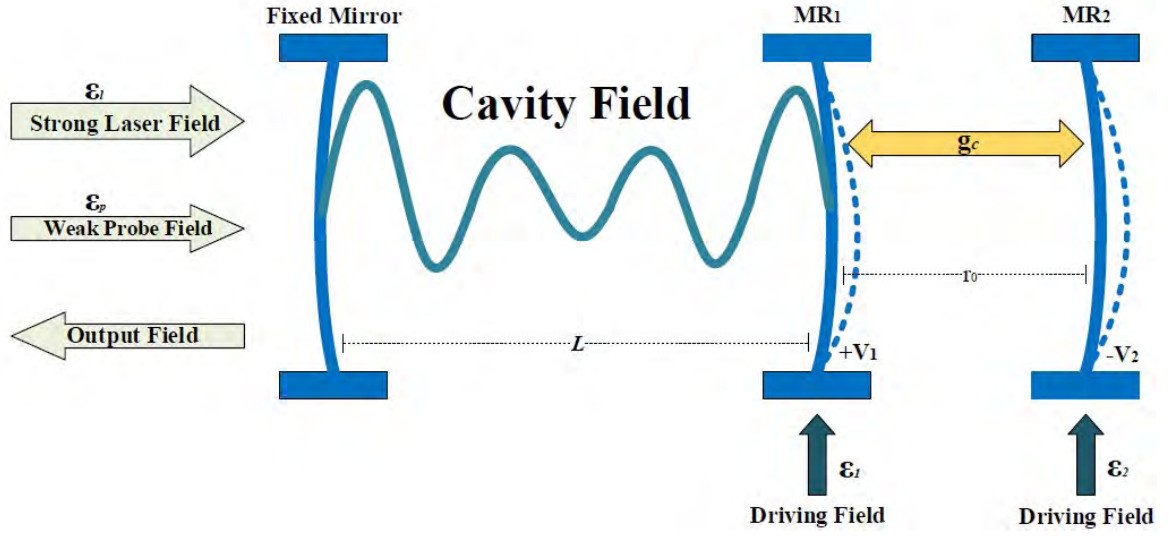
Figure 5.1: The Schematic representation of the Nano Electro Opto-Mechanical System (NEOMS): MR_1 is coupled with the cavity field through opto-mechanical coupling g_0 and to the second mechanical resonator MR_2 through the Coulomb coupling strength g_c. A strong pump field ε_l and a weak probe field ε_p are pumped into the cavity. MR_1 is charged by biased voltage $+V_1$ and MR_2 is charged by $-V_2$, r_0 is the equilibrium distance between MR_1 and MR_2 which are selectively driven by ε_1 and ε_2.

Where $\hat{H}_{mc}$ is mirror filed Hamiltonian defined as:

$$\hat{H}_{mc} = \hbar\Delta_c \hat{c}^\dagger \hat{c} + \left[\frac{\hat{p_1}^2}{2m_1} + \frac{1}{2}m_1\omega_1^2 \hat{q}^2_1 \right] + \left[\frac{\hat{p_2}^2}{2m_2} + \frac{1}{2}m_2\omega_2^2 \hat{q}_2^2 \right] \tag{5.2}$$

,

where, $\Delta_c = \omega_c - \omega_l$ is detuning of the cavity field frequency. The first term represents the Single-mode of cavity field with frequency ω_c and annihilation (creation) operator $\hat{c}$ ($\hat{c}^\dagger$). The second and third term represent the free Hamiltonian of moving

65

mirrors (MR_1 and MR_2), where operators, $\hat{q}_i$, $\hat{p}_i$, ω_i and m_i represent its position, momentum, resonance frequency and effective mass respectively.

While, $\hat{H}_{dr}$ is the combined Hamiltonian of the strong laser field of amplitude ε_l and weak probe field of amplitude ε_p along with the external driving fields with amplitudes ε_1 and ε_2 is expressed as:

$$\hat{H}_{dr} = i\hbar\varepsilon_l(\hat{c}^\dagger - \hat{c}) + i\hbar\left(\varepsilon_p e^{-i\delta t}\hat{c}^\dagger - \varepsilon_p^* e^{i\delta t}\hat{c}\right) + i\hbar\left[\sum_{j=1}^{2}\left(\varepsilon_j\hat{q}_j e^{-i\delta t+i\varphi_j} - \varepsilon_j\hat{q}_j^\dagger e^{-i\delta t-i\varphi_j}\right)\right] (5.3)$$

Where, $\delta_c = \omega_p - \omega_l$ is the detuning of probe field frequency where ω_l is pump field frequency.

The Classical light fields (pump and probe fields) with frequencies ω_l and ω_p are represent in first two terms. The strong laser power ε_l induced in the cavity with $9mW$ strength. So it is considered as a real value in above equation. While ε_p is a very weak probe field used to test the non-linearity inside the cavity, is considered as a complex valued quantity whose real and imaginary parts examine the damping and oscillation of the field respectively. Here, the strength of laser power is related to ε_l and ε_p by $\varepsilon_l = \sqrt{2\kappa\wp_l/\hbar\omega_l}$ and $\varepsilon_p = \sqrt{2\kappa\wp_p/\hbar\omega_p}$. The last term represents the Hamiltonian of external modulating fields on MR_1 and MR_2, here ε_j $(j = 1, 2)$ is the amplitude and φ_j is the corresponding phase. The terms b_j and $b_j{}^\dagger$ are annihilation and creation operators for the positions of MR_1 and MR_2 respectively. The small oscillations of the MRs from their mean positions can be represented as $q_j = \sqrt{\frac{\hbar}{2m_j\omega_j}}(b_j + b_j{}^\dagger)$ $(j = 1, 2)$. Similarly, using the relation $\dot{q}_j = p_j/m_j$, the oscillations in the momenta of the mirrors can be represented as $p_j = \sqrt{\frac{\hbar m_j}{2\omega_j}}(\dot{b}_j + \dot{b}_j{}^\dagger)$, here, $\dot{q}_j = \frac{d}{dt}(q_j)$. We will take expectation values of all the operators as we deal with the mean response of the coupled system to the probe field.

66

Furthermore, $\hat{H}_{int}$ is the interaction Hamiltonian for opto-mechanical coupling between the cavity field and MR_1 and the Coulomb interaction between MR_1 and MR_2 is defined as:

$$\hat{H}_{int} = -\hbar g_o \hat{c}^\dagger \hat{c} \hat{q}_1 + \hbar g_c \hat{q}_1 \hat{q}_2. \tag{5.4}$$

Here, fisrt term represents opto-mechanical coupling between MR_1 and the Cavity field and second term represents the coulomb coupling between the mechanical resonators. Where, g_0 is opto-mechanical coupling strength and is given by $g_0 = \left(\frac{\omega_c}{L}\right)\sqrt{\frac{\hbar}{2m_1\omega_1}}$ and g_c is Coulomb coupling strength and is given by $g_c = \frac{k_e q_1 q_2}{r_0{}^3}\sqrt{\frac{\hbar}{2m_1 m_2 \omega_1 \omega_2}}$. The equilibrium spacing between two resonators is $r_0 = 2mm$. In terms of mirror annihilation(creation) operator $b_j(b_j{}^\dagger)$, equation (5.2) and equation (5.4) can be written as

$$
\begin{aligned}
H_{mc} &= \hbar\Delta_c c^\dagger c + \hbar\omega_1 b_1{}^\dagger b_1 + \hbar\omega_2 b_2{}^\dagger b_2, \\
H_{int} &= -\hbar G_0 c^\dagger c(b_1 + b_1{}^\dagger) + \hbar G_c(b_1{}^\dagger b_2 + b_1 b_2{}^\dagger)
\end{aligned}
\tag{5.5}
$$

Here, $G_0 = g_0\sqrt{\frac{\hbar}{2m_1\omega_1}}$ and $G_c = g_c\sqrt{\frac{1}{2m_1 m_2 \omega_1 \omega_2}}$.

5.3   Mathematical Treatment

A strong laser field of frequency ω_l and a weak probe field of frequency ω_p are applied to the optical cavity, and two external driving fields ε_1 and ε_2 are applied to the mechanical resonators MR_1 and MR_2, respectively. the Heisenberg–Langevin Equations of motion

in terms of $c(c^\dagger)$, $b_1(b_1{}^\dagger)$ and $b_2(b_2{}^\dagger)$ are written as

$$
\begin{aligned}
\dot{c} &= -(i\Delta_c + \frac{\kappa}{2})c + iG_0(b_1{}^\dagger + b_1)c + \varepsilon_l + \varepsilon_p e^{-i\delta t} + \sqrt{2\kappa}c_{in}(t), \\
\dot{b_1} &= -(i\omega_1 + \frac{\gamma_1}{2})b_1 + iG_0 c^\dagger c - iG_c b_2 + \varepsilon_1 e^{-i\delta t - i\varphi_1} + \sqrt{2\gamma_1}\xi_1(t), \\
\dot{b_2} &= -(i\omega_2 + \frac{\gamma_2}{2})b_2 - iG_c b_1 + \varepsilon_2 e^{-i\delta t - i\varphi_2} + \sqrt{2\gamma_2}\xi_2(t)
\end{aligned}
$$

$$(5.6)$$

Here, $\hat{c}_{in}(t)$ represents the input vacuum noise with zero mean value associated with cavity field, while terms $\hat{\xi}_1(t)$ and $\hat{\xi}_1(t)$ are Brownian noise operators associated with the damping of the MR_1 and MR_2 respectively. The symbols κ and γ_i $(i = 1, 2)$ denote the decays terms associated with the cavity and the MR_i $(i = 1, 2)$ respectively. Using mean field approximation [121] the mean values of the noise terms are averaged to zero, considering only the dissipation and fluctuation terms, we arrive at the equations,

$$
\begin{aligned}
\langle \dot{c} \rangle &= -(i\Delta_c + \frac{\kappa}{2})\langle c \rangle + iG_0(\langle b_1{}^\dagger \rangle + \langle b_1 \rangle)\langle c \rangle + \varepsilon_l + \varepsilon_p e^{-i\delta t}, \\
\langle \dot{b_1} \rangle &= -(i\omega_1 + \frac{\gamma_1}{2})\langle b_1 \rangle + iG_0\langle c^\dagger \rangle\langle c \rangle - iG_c\langle b_2 \rangle + \varepsilon_1 e^{-i\delta t - i\varphi_1}, \\
\langle \dot{b_2} \rangle &= -(i\omega_2 + \frac{\gamma_2}{2})\langle b_2 \rangle - iG_c\langle b_1 \rangle + \varepsilon_2 e^{-i\delta t - i\varphi_2}.
\end{aligned}
$$

$$(5.7)$$

Here, we use the assumption [121, 125]: $\langle h \rangle = h_s + h_- e^{-i\delta t} + h_+ e^{i\delta t}$, where, h_s denotes any of the steady-state solutions c_s, q_{is} and p_{is}, in order to acquire the steady-state solutions of the above equations. Here, h_+ and h_- are of the same order as ε_p. If we have the case of $h_s \gg h_\pm$, then we can treat $h_\pm$ as perturbations for the solution of equation (5.7). Now by substituting the ansatz into equation (5.7), we obtain the

following (steady-state) solutions:

$$
\begin{aligned}
c_s &= \frac{\varepsilon_l + \varepsilon_p}{i\Delta + \frac{\kappa}{2}} \\
b_{1s} &= \frac{iG_0|c_s|^2 - iG_c b_{2s} + \varepsilon_1 e^{-i\phi_1}}{i\omega_1 + \frac{\gamma_1}{2}} \\
b_{2s} &= \frac{-iG_c b_{1s} + \varepsilon_2 e^{-i\phi_2}}{i\omega_2 + \frac{\gamma_2}{2}}.
\end{aligned}
\tag{5.8}
$$

Here, $\Delta = \Delta_c - G_0 q_{1s}$ is the effective detuning. Also, $\wp_p \ll \wp_l$, hence, for the simulation only strong laser power is considered.

5.4 Occurrence of Optical Bi-stability

Optical bi-stability is experimentally observed in micro-cavities [129]. Here in our scheme bi-stable behavior is due to the non-linearity which emerges from opto-mechanical coupling strength G_0 as well as Coulomb coupling strength G_c. By solving the steady state values of cavity field photon number in equation (5.8) we have,

$$
|\varepsilon_l + \varepsilon_p|^2 = |c_s|^2 \left[\frac{\kappa^2}{4} + (\Delta_c - G_0(b_{1s}^* + b_{1s}))^2 \right], \tag{5.9}
$$

where $|c_s|^2 = c_s c_s^*$. This equation indicates the occurrence of bi-stable behavior.

It is clear from equation (5.9) that bi-stability in photon number vanishes if we have $G = 0$. By rearranging the equation (5.9), we obtain a third order polynomial of the steady-state intra-cavity photon numbers as follow:

$$
a_1 x^3 + a_2 x^2 + a_3 x + a_4 = 0, \tag{5.10}
$$

69

where,

$$x = |c_s|^2,$$

$$a_1 = G_0{}^2\alpha_1{}^2,$$

$$a_2 = 2\alpha_1(\Gamma + \Delta_c G_0),$$

$$a_3 = \left(\frac{\kappa^2}{4} + \Delta_c{}^2 + G_0\Gamma(G_0\Gamma + 2\Delta_c)\right),$$

$$a_4 = -|\varepsilon_l + \varepsilon_p|^2.$$

Here, $\alpha_1 = \beta_1 + \beta_1^*$, $\Gamma = \alpha_2\varepsilon_2 + \alpha_3\varepsilon_1$, $\alpha_2 = \beta_2 e^{-i\phi_2} + \beta_2^* e^{i\phi_2}$, $\alpha_3 = \beta_3 e^{-i\phi_1} + \beta_3^* e^{i\phi_1}$, where , $\beta_1 = \frac{i(i\omega_2 + \gamma_2/2)G_0}{(i\omega_1 + \gamma_1/2)(i\omega_2 + \gamma_2/2) + G_c{}^2}$, $\beta_2 = -\frac{G_c}{G_0}\frac{\beta_1}{(i\omega_2 + \gamma_2/2)}$ and $\beta_3 = \frac{-i\beta_1}{G_0}$. This equation has three roots, two of which are for stable regimes and the third one is for the unstable regime of the steady-state photon number. The respective branches of the bi-stable curve have been found by using the solutions of the cubic polynomial equation $ay^3 + by^2 + cy + d = 0$ with inflection and critical points, i.e., $y_c = \frac{-b \pm \sqrt{b^2 - 3ac}}{3a}$ and $y_{inf} = -b/3a$. Using the solutions for y_c and y_{inf}, we can write the critical and inflection points of the equation (5.10) as,

$$x_{c\pm} = \frac{-a_2/a_1 \pm \sqrt{(a_2/a_1)^2 - 3a_3/a_1}}{3}, \ x_{inf} = -a_2/3a_1, \tag{5.11}$$

where $x_{c-}(x_{c+})$ and x_{inf} are the critical points of lower(upper) stable and unstable branches of the bi-stable curve. The range of bi-stability window is determined by these critical points and at these points the driving laser field power $\wp_l$ has a corresponding window also. We assume that our proposed NOEMS works in resolved-sideband regime, i.e., $\kappa \ll \omega_1$. The strength of the laser field directly affects the resolved sideband

regime, therefore the photon number increases by increasing the strength of the laser field. So, for a specific range of values of the strong laser power, the steady-state photon number displays the phenomenon of bi-stability. When the strength of the driving field is increased, the cavity field detuning reaches to a certain value, called the critical detuning. At this critical value, the outset of the bi-stable behavior in the system can be seen. The critical value of the cavity detuning can be found by using equation (5.10) as,

$$\Delta_c = \sqrt{3}\kappa. \tag{5.12}$$

This is the threshold value of the cavity detuning Δ_c. The value of Δ_c should always be greater than threshold value. To investigate the control of optical and mirror bi-stability in NOEMS, we choose the parametric values from the recent experiments [96, 130, 131]. The length of the cavity of proposed Nano-electro-opto-mechanical system (NEOMS) is taken as L = 25cm. For simplicity, we choose identical mechanical resonators (MRs) with masses $m_1(m_2)$= 145ng, oscillation frequencies $\omega_1(\omega_2)$= $2\pi \times$ 947kHz and decay rates $\gamma_1(\gamma_2)$= $2\pi \times$ 140kHz. The cavity decay rate is considered as $\kappa = 2\pi \times$ 215kHz. The cavity field frequency is calculated by the relation $\omega_c = 2\pi c/\lambda_l$,where c is speed of light, and $\lambda_l = 1064$ nm is the wavelength of the driving field. We choose $\Delta_c = 3\kappa$ and $\omega_l = \omega_c - \omega_1$, and the power of the pump field is taken as 9mW. As we can see that the value of mechanical resonator frequency is greater than cavity decay rate, hence the system stays in the resolved sideband regime.

The bifurcation diagram for the steady-state solution of equation (5.9) is illustrated in Figure 5.2 where the steady-state photon number is plotted as a function of the input laser power by taking the value of cavity field detuning $\Delta_c > \sqrt{3}\kappa$. The critical

71

points x_{c-} and x_{c+} indicate the corresponding lower and upper stable branches and the inflection points P and Q indicate the corresponding unstable branch of the curve. When we start scanning the system with a low value of the laser field, and gradually increase the laser power $\wp_l$, the photon intensity of intra-cavity field initially follows the lower stable branch S_1 of the curve which further extends to the first critical point x_{c-}. If we further increase the strength of driving laser power to a value of $7.6 mW$, the value of steady-state photon number jumps to the upper stable branch S_2, which extends from the second critical point x_{c+} to infinity. The central branch represented by the blue-dashed line is unstable and stretches from the inflection point P to the another inflection point Q. The slope of unstable branch is negative, therefore it cannot be observed experimentally.

On the other hand, if we start scanning with a higher value of the driving field, and gradually decrease the laser power $\wp_l$, the intra-cavity photon number will start decreasing by following the upper stable branch initially, however, when it reaches to the inflection point P, it will jump to the lower stable branch at second critical point x_{c-} and continue to decrease further.

Now, we present a detailed analysis of controllable bi-stability that primarily depends on the system parameters including, coupling frequencies and strength of external driving fields. Figure 5.3 shows the variations in the S-shaped bi-stability curve of the intra-cavity photon numbers $|c_s|^2$ against the laser power $\wp_l$ for different values of opto-mechanical coupling strength G_0. We can notice that the bifurcation curves overlap for different values of opto-mechanical coupling frequency. As we increase the opto-mechanical coupling strength, the mechanical back-action of MR_1 raises the ra-
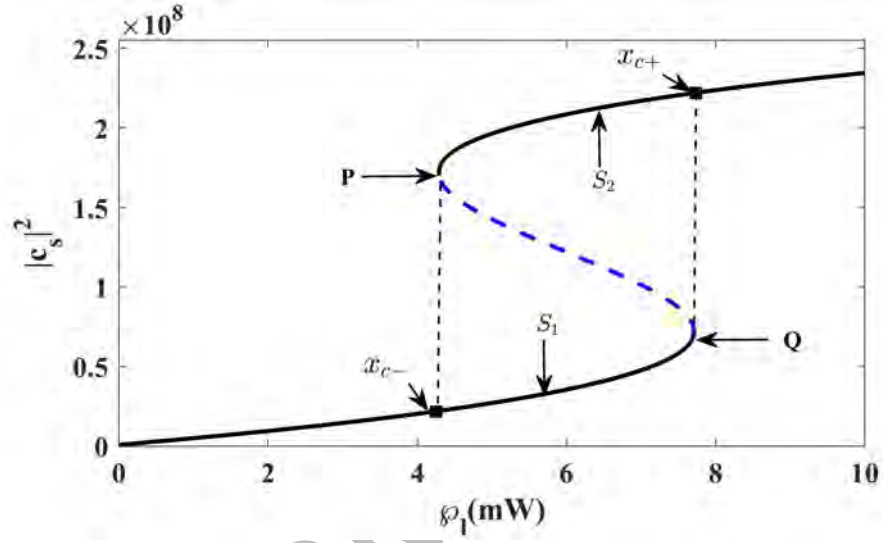
Figure 5.2: Plot of mean intra-cavity photon number $|c_s|^2$ as a function of the driving laser power $|\wp_l|$. Other system parameters used for this particular case are $m_1 = m_2$ = 145 ng, $\omega_1 = \omega_2 = 2\pi \times 947$ kHz, $\varepsilon_1 = \varepsilon_2 = 0$, $G_0 = 2\pi \times 5$ kHz, $\Delta_c = 3.6\kappa$ and $\kappa = 2\pi \times 215$ kHz.

diation pressure force, which causes scattering of photons in the cavity. In the lower coupling regime i.e., $G_0/2\pi = 6$ kHz (black solid line), the bifurcation curve follows the upper stable branch. When the frequency of opto-mechanical coupling is further increased i.e., $G_0/2\pi = 7$ kHz (black dashed curve), the lower stable path is followed by the upper stable path. In addition to the variation of photon numbers, the width of bi-stable curve also decreases at the same time by increasing the opto-mechanical coupling frequency.

Further increasing the frequency of opto-mechanical coupling strength G_0, the second lower stable path follows the third lower stable path and vice versa. We observe that the bi-stability curve continuously varies as well as the photon number decreases with the variation of opto-mechanical coupling G_0. This variation of photon number is also known as flip-flop phenomenon [132]. This kind of process provides an elegant technique to control the intensity of intra-cavity photons. Hence, this control parameter provides an experimental realization of controllable optical switch.

Now, we explore the effect of Coulomb coupling strength G_c on optical bi-stability. For this reason, we plot the bifurcation curve of the intra-cavity photon number $|c_s|^2$ as a function of input laser power $\wp_l$ for different values of Coulomb coupling strength G_c, in Figure 5.4. The bias gates $+V_1$ and $-V_2$ are used to tailor the system for varied Coulomb coupling G_c values. The Coulomb coupling strength i.e., $G_c = 0.2$ MHz (see black solid curve) is not strong enough to change the radiation pressure inside the cavity when the bias gate across each mirror is low. As a result, we have the maximum amount of photons and the system remains in upper stable branch. When the charges on the resonators are increased by increasing the bias gates $+V_1$ and -

Figure 5.3: Plot of mean intra-cavity photon number $|c_s|^2$ as a function of the driving laser power $|\wp_l|$ for different values of opto-mechanical coupling strength G_0. Other system parameters are the same as used in Figure 5.2

.

V_2 across the resonators MR_1 and MR_2 respectively, the Coulomb coupling strength is enhanced which, in turn, increases the radiation pressure force inside the optical cavity. Therefore, the non-linearity in the system is boosted up and as a result the intra-cavity photon number $|c_s|^2$ is suppressed inside the optical cavity. This behavior of the system is depicted in Figure 5.4 for $G_c = 0.4$ MHz (see red dashed curve) and $G_c = 0.6$ MHz (see blue long-dashed curve). This study reveals that Coulomb coupling G_c has a considerable impact on the bistable behaviour of the steady-state photon number, and that parametric modulation of Coulomb coupling can be used to create a tunable optical switch.

Now, we probe the behavior of bi-stable curve of intra-cavity photon number $|c_s|^2$ as a function of input laser power $\wp_l$ for different values of cavity detuning Δ_c. For
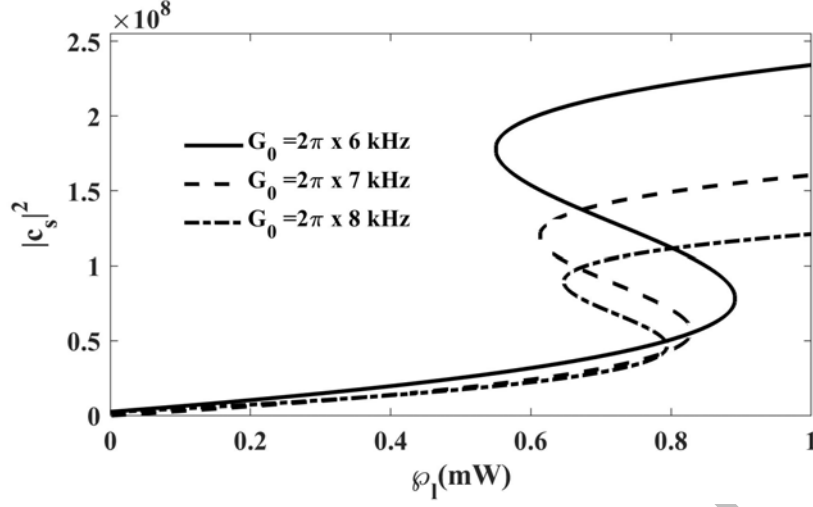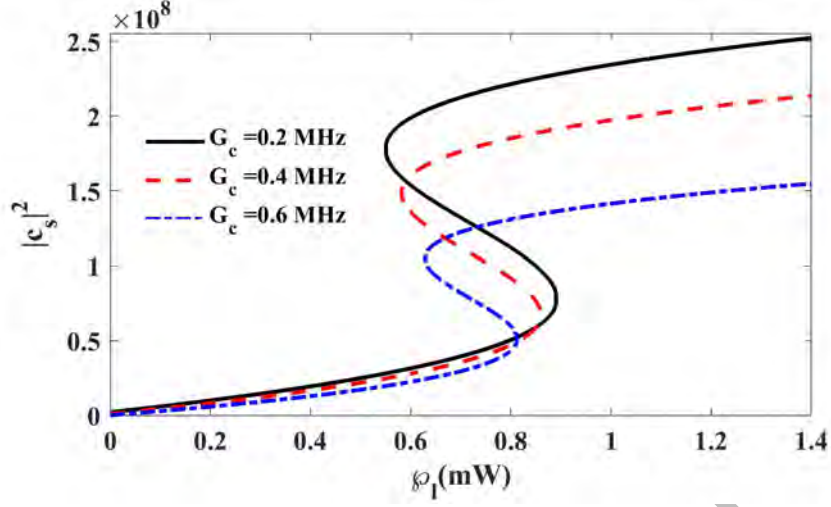
Figure 5.4: The intra-cavity photon number $|c_s|^2$ as a function of the driving laser power $|\wp_l|$ is plotted for different values of Coulomb coupling strength G_c. Other system parameters are same as used in Figure 5.2.

this purpose, we illustrate the effect of the variations in cavity field detuning on the intra-cavity photon number $|c_s|^2$, in Figure 5.5. The stable and unstable points are shifted at different values of photon number by increasing the cavity field detuning frequency. Another prominent effect occurs by increasing Δ_c i.e., the width of bi-stable curve increases. For lower values of cavity field detuning, i.e, $\Delta_c = 1.8\kappa$, the bi-stable behavior almost vanishes (see red solid curve). This is due to the fact that the threshold bi-stability occurs in the system at the critical detuning $\Delta_c = \sqrt{3}\kappa$. It can be observed that the upper stable path of the bifurcation curve jumps to the next upper stable branch for higher values of cavity field detuning (see blue dashed and black dot-dashed curves). A similar transition takes place from the upper stable path to the lower one with the decreasing strength of input laser field. These features reveal that
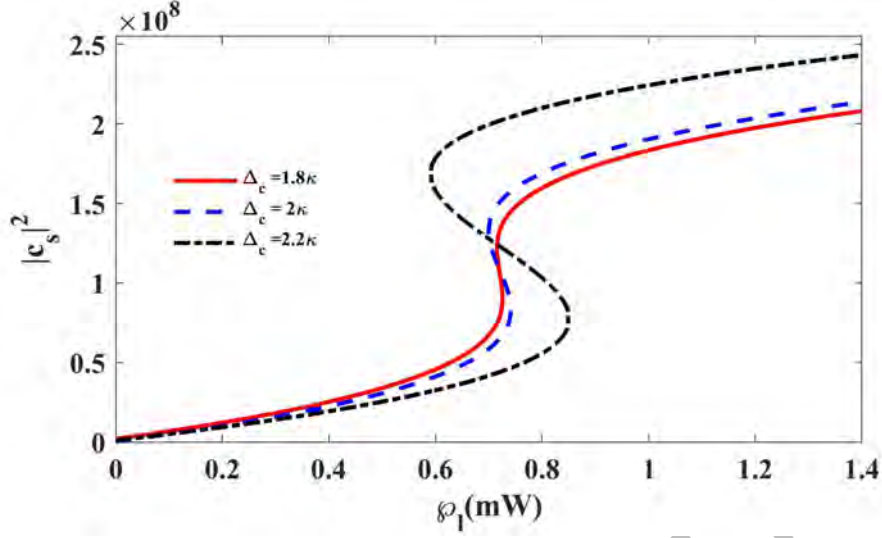
Figure 5.5: Variation of mean intra-cavity photon number $|c_s|^2$ for bi-stability as a function of input laser power $|\wp_l|$ for different values of cavity detuning Δ_c. The remaining parameters are the same as used in Figure 5.2.

the origin of the bi-stability is the characteristic non-linearities of cavity field detuning and the laser power. This indicates that we can develop a controllable optical switch based on cavity field detuning and the input laser power.

5.4.1 Effect of External Driving Fields on Optical Bi-stability

In the previous numerical simulations, we studied the behavior of bi-stable (bifurcation) curve of the steady-state photon number in the absence of external mechanical driving fields, i.e., ε_1 and ε_2. Now, we introduce external mechanical pumps to drive the micro-resonators MR_1 and MR_2 and check for the abrupt changes in the bi-stability of the system. So, we drive the mechanical resonators MR_s with a mechanical pump (acoustic molecule) $\varepsilon_j = \epsilon_j e^{-i\phi_1}$ $(j = 1, 2)$ and explore its effect on the intra-cavity

77

photon number $|c_s|^2$.

When a mechanical pump field is applied to MR_1 only, by keeping the amplitude ϵ_1 constant and varying the phase angle ϕ_1, it leads to phase-sensitive optical behaviors of the NEOMS. This behavior is shown in Figure 5.6(a). When we increase the phase angle ϕ_1 from $\pi/4$ to π, the steady-state intra-cavity photon intensity is amplified (see purple, purple dashed and red dot-dashed curves). The width of bi-stable (bifurcation) curve also increases by increasing the phase angle ϕ_1 of mechanical pump ε_1 on MR_1. An additional effect is also seen in the plot of bi-stability i.e., the curves overlap and the intersection point of the three different curves are same (see Figure 5.6(a)). Moreover, the first upper stable branches follow the next upper stable path and vice versa. A similar transition occurs in the lower stable branches. Now, if we drive the second mechanical resonator MR_2 only, i.e., $\varepsilon_2 \neq 0$ and $\varepsilon_1 = 0$, keeping the amplitude ϵ_2 constant and varying the phase angle ϕ_2, the bi-stable behavior of the system confronts with some minor changes in the upper stable branch of the curve, as shown in Figure 5.6(b). The first upper stable path follows the second upper stable path and vice versa, as we increase the phase angle ϕ_2 from $\pi/4$ to π (see blue solid, blue dashed and black long-dashed curves). In this case, the intra-cavity photon intensity is suppressed by increasing the phase angle ϕ_2. Moreover, the same transition does not occur in the lower stable branches. The external driving field on MR_2 only effects the Coulomb coupling strength g_c between the mirrors. The Coulomb coupling strength g_c has no direct effect on the radiation pressure force inside the cavity. Therefor, the lower stable path for intra-cavity photon intensity is independent of the phase angle ϕ_2. Similar behaviors of the bi-stable curve can be seen in Figure 5.6(c) and Figure 5.6(d) by

78

(a) For different values of ϕ_1

(b) For different values of ϕ_2

(c) For different values of ε_1

(d) For different values of ε_2
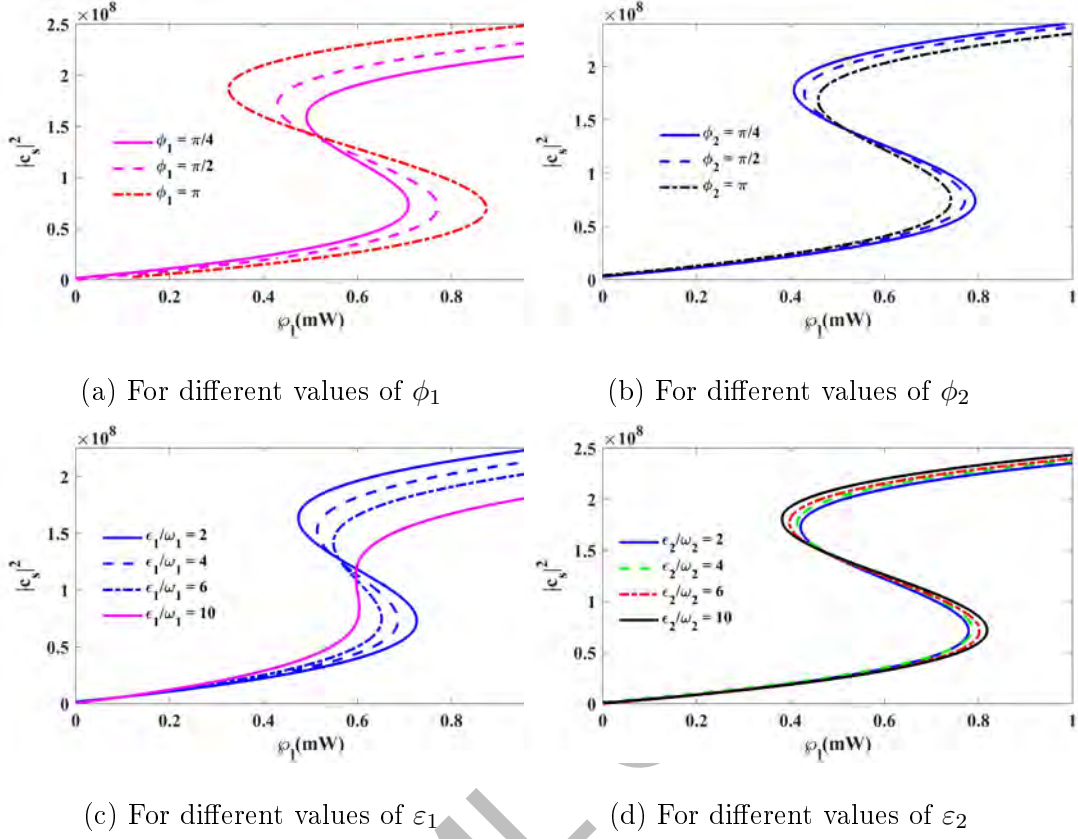
Figure 5.6: Plots of mean intra-cavity photon number $|c_s|^2$ versus the driving laser power $|\wp_l|$. Controlled bi-stable behavior for different values of amplitudes and phase angles of driving fields of MR_1 and MR_2. Other system parameters are same as used in Figure 5.2 and Figure 5.3.

selectively driving the mechanical resonators MR_1 and MR_2, keeping the phase angle $\phi_1(\phi_2)$ constant and varying the amplitude $|\varepsilon_1|(|\varepsilon_2|)$ of MR_s.

5.5 Occurance of Mirror Bi-stability

In order to determine the bistable behavior of steady-state position q_{1s} as a function of input laser power $\wp_l$, we use the relation $(b_{1s}^* + b_{1s}) = \sqrt{\frac{2m_1\omega_1}{\hbar}}q_{1s}$ and rewrite the equation (5.8) in terms of q_{1s} as follows:

$$|\varepsilon_l + \varepsilon_p|^2 = |c_s|^2 \left[\frac{\kappa^2}{4} + \left(\Delta_c - \sqrt{\frac{2m_1\omega_1}{\hbar}}G_0 q_{1s} \right)^2 \right]. \qquad (5.13)$$
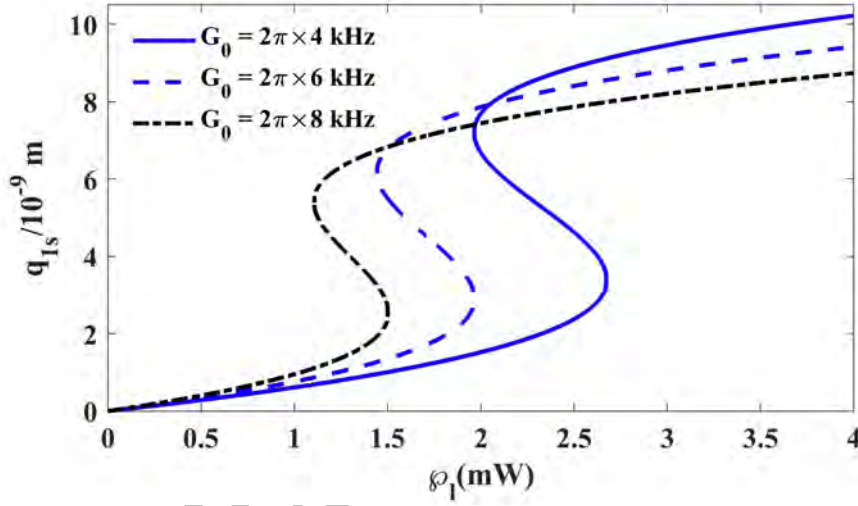
Figure 5.7: Plot of steady state displacement q_{1s} versus the driving laser field power $|\wp_l|$ by varying the optomechanical coupling strength G_0. Other system parameters used are $m_1 = m_2 = 145$ ng, $\omega_1 = \omega_2 = 2\pi \times 947$ kHz, $\varepsilon_1 = \varepsilon_2 = 0$, $G_c = 0$, $\Delta_c = 3.6\kappa$ and $\kappa = 2\pi \times 215$ kHz.

The bi-stable behavior of steady-state position q_{1s} as a function of input laser power $\wp_l$ is depicted in Figure 5.7 for different values of opto-mechanical coupling strength G_0. In a weak coupling regime i.e., $G_0/2\pi = 4$ kHz (blue solid curve), the bi-stability in the system appears at a higher value of input laser power $\wp_l = 2.4$ mW. However, when

the system is driven in a strong opto-mechanical coupling regime i.e., $G_0/2\pi = 6, 8$ kHz (see blue dashed and black dot-dashed curves), the bi-stability occurs at lower values of input laser power and the lower stable branch jumps to the upper stable path and continues to follow it, as the input laser power is increased. Moreover, the bi-stability curves overlap for higher values of laser power. This feature gives a control over the mechanical motion of micro-resonator MR_1 for different values of input laser power.

Now, we investigate the effect of Coulomb coupling strength G_c and external mechanical pump field ε_1 on the steady-state position q_{1s}. For this reason, we plot the steady-state displacement q_{1s} as a function of input laser power $\wp_l$ for several values of Coulomb coupling strength G_c in Figure 5.8(a). The steady-state solution shows a bistable (bifurcation) curve at a higher value of laser power for $G_c = 0.2$ MHz (see magenta solid curve). As we increase the bias gate V_1 on the mirror MR_1, the curve shifts to the left and the bistability occurs at lower values of laser power (see red dashed and red solid curves). Furthermore, no overlapping occurs and the first lower stable path follows the second stable branch and vice versa. Similar transitions can be seen in the upper stable branches. When an external modulating field ε_1 is applied on the mirror MR_1 only by keeping the phase angle $\phi_1 = 0$ and varying the amplitude $\epsilon_1/\omega_1 = 2, 3.4, 4.8$, the first lower stable path follows the second stable path and it continues to follow the third stable branch and so on (see black solid, dashed and dot-dashed curves in Figure 5.8(b). The upper stable branches do not exhibit any changes by varying the amplitude of external mechanical pump field on MR_1. To study the effects of Coulomb force and mechanical pump on MR_2, we solved 5.8 for the steady-state displacement q_{2s}. The plot of steady-state solution for q_{2s} shows a bistable

81

(a) For varying frequency of Coulomb coupling G_c

(b) For varying amplitude of driving field ε_1
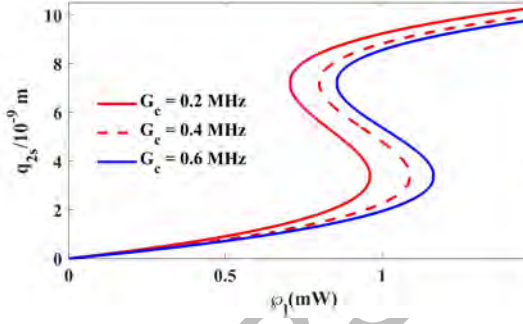
(c) For varying frequency of Coulomb coupling G_c
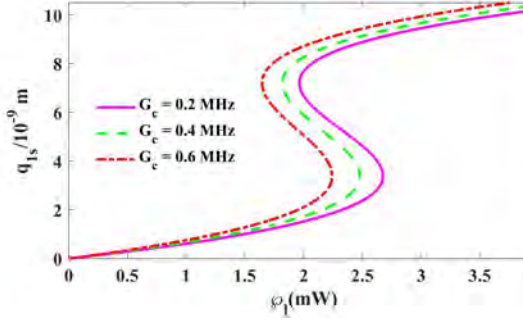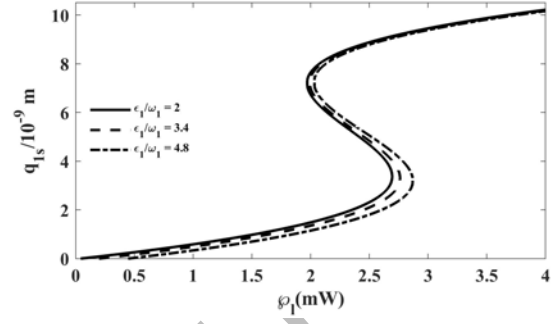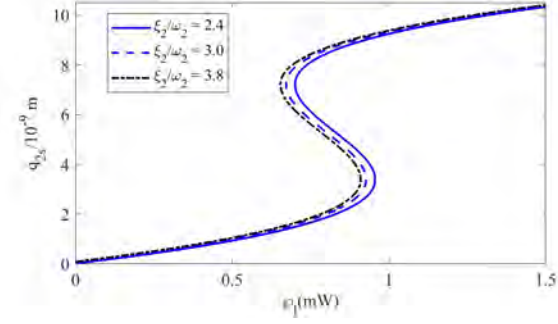
(d) For varying amplitude of driving field ε_2

Figure 5.8: Plots of steady state displacement q_{1s} versus the driving laser power $|\wp_l|$ by varying the Coulomb coupling strength G_c and amplitude $\epsilon_1(\epsilon_2)$ of driving field $\varepsilon_1(\varepsilon_2)$ on $\mathrm{MR}_1(\mathrm{MR}_2)$. Other system parameters are same as used Figure 5.7.

behavior which is depicted in Figure 5.8(c) and 5.8(d). The upper stable branch of the red solid curve ($G_c = 0.2$ MHz jumps down to the upper stable path of red dashed curve ($G_c = 0.4$ MHz) and vice versa. In this case the bistability curve produces a reverse effect of Figure 5.8(a). When an external mechanical driving field ε_2 is applied on MR_2 only, the system shows slight changes in the stable points of the bifurcation curve by increasing the amplitude of driving field $\epsilon_2/\omega_2 = 2.4, 3.0, 3.8$ and keeping the phase angle $\phi_2 = 0$ (see Figure 5.8(d)). Furthermore, amplitude of steady-state displacement q_{2s} decreases for the lower stable branch as we increase the amplitude of external modulating field ε_2 on MR_2. From the above discussions, it is cleared that a controllable bistable optical switching of steady-state photon intensity and mechanical displacements can be achieved by adjusting the coupling frequencies and selectively driving the mechanical resonators MR_1 and MR_2.

Chapter 6

Conclusion

In the first part of the dissertation, we investigate the phenomenon of Four-Wave Mixing in an opto-mechanical system in the presence of a switchable mechanical driving field on the moving-end mirror (MR_1). Asymmetric amplifications and suppressions have been observed in the output light signal (FWM).In addition, it has been shown that the FWM signal can be controlled by varying the amplitude and phase of mechanical driving on MR_1.

The Four-Wave Mixing phenomenon has been studied in a typical Nano Electro Opto-Mechanical System (NEOMS), in the second part of the thesis. We show that the second mechanical resonator (MR_2) provides an extra control over the FWM signal. It has been seen that the selective mechanical drivings of both MR_s have a significant effect on the FWM spectra. These switchable mechanical drivings impart a tunable FWM signal at the output. Moreover, it has been observed that the intensities of FWM peaks can be amplified and suppressed by varying the amplitude and phase of mechanical drivings of MR_s.

The third part of the dissertation discusses effect of atomic medium on the FWM signal. For this purpose a trapped Bose-Einstein condensate (BEC) in a Nano-Electro-Opto-Mechanical System (NEOMS) has been studied by selectively driving the mechanical resonators MR_1 and MR_2. The medium-enhanced FWM signal has been observed to show inconsistent modifications by varying the phase angle of mechanical driving fields of MR_s. Moreover, it has been observed that the FWM signal can be greatly enhanced by driving the mechanical resonator (MR_2) only.

In the fourth part, we present a powerful scheme to experimentally realize an optical switch primarily based on optical bi-stability in a Nano-Electro-Opto-Mechanical System (NEOMS). We report an optical and a mirror bi-stability as a function of input laser power, coupling frequencies and external mechanical pump fields on MR_s. In the examined system, the coupling frequencies and the switchable mechanical driving fields allow a threshold value of cavity field detuning and laser power which can be utilized in developing tunable optical switches and all-optical transistors.

So, we theoretically studied different parameters to control the light which contributes in the development of optical transmitter, optical switches and all optical transistors.

Bibliography

[1] Gerry, Christopher, Peter Knight, and Peter L. Knight. "Introductory Quantum Optics." Cambridge University Press, (2005).

[2] Blencowe, Miles. "Quantum electromechanical systems." Physics Reports 395, no. 3 (2004): 159-222.

[3] Schwab, Keith C., and Michael L. Roukes. "Putting mechanics into quantum mechanics." Physics Today 58, no. 7 (2005): 36-42.

[4] Aspelmeyer, Markus, and Keith Schwab. "Focus on mechanical systems at the quantum limit." New Journal of Physics 10, no. 9 (2008): 095001.

[5] Kippenberg, Tobias J., and Kerry J. Vahala. "Cavity opto-mechanics." Optics Express 15, no. 25 (2007): 17172-17205.

[6] Vedral, Vlatko. "Quantum entanglement." Nature Physics 10, no. 4 (2014): 256-258.

[7] Camacho, Ryan M., Praveen K. Vudyasetu, and John C. Howell. "Four-wave-mixing stopped light in hot atomic rubidium vapour." Nature Photonics 3, no. 2 (2009): 103-106.

[8]   Hammerer, Klemens, Margareta Wallquist, Claudiu Genes, Max Ludwig, Florian Marquardt, Philipp Treutlein, Peter Zoller, Jinwu Ye, and H. Jeff Kimble. "Strong coupling of a mechanical oscillator and a single atom." Physical Review Letters 103, no. 6 (2009): 063005.

[9]   Sohail, Amjad, Yang Zhang, Jun Zhang, and Chang-shui Yu. "Optomechanically induced transparency in multi-cavity optomechanical system with and without one two-level atom." Scientific Reports 6, no. 1 (2016): 1-8.

[10] He, Qing, Fazal Badshah, Liping Li, Lianbei Wang, Shi-Lei Su, and Erjun Liang. "Transparency, Stokes, and Anti-Stokes Processes in a Multimode Quadratic Coupling System with Parametric Amplifier." Annalen Der Physik 533, no. 5 (2021): 2000612.

[11] Liu, L. W., D. J. Gengzang, Y. Q. Shi, Q. Chen, X. L. Wang, and P. Y. Wang. "Controllable Four-Wave Mixing Based on Hybrid BEC-Optomechanical Systems." Acta Physica Polonica, A. 136, no. 3 (2019): 444-453.

[12] Harris, Stephen E., J. E. Field, and A. Imamoğlu. "Nonlinear optical processes using electromagnetically induced transparency." Physical Review Letters 64, no. 10 (1990): 1107.

[13] Li, Yong-qing, and Min Xiao. "Enhancement of nondegenerate four-wave mixing based on electromagnetically induced transparency in rubidium atoms." Optics Letters 21, no. 14 (1996): 1064-1066.

[14] Gong, Z. R., H. Ian, Yu-xi Liu, C. P. Sun, and Franco Nori. "Effective Hamiltonian approach to the Kerr nonlinearity in an optomechanical system." Physical Review A 80, no. 6 (2009): 065801.

[15] Schliesser, Albert, Rémi Rivière, Georg Anetsberger, Olivier Arcizet, and Tobias J. Kippenberg. "Resolved-sideband cooling of a micromechanical oscillator." Nature Physics 4, no. 5 (2008): 415-419.

[16] Imoto, Nobuyuki, H. A. Haus, and Y. Yamamoto. "Quantum nondemolition measurement of the photon number via the optical Kerr effect." Physical Review A 32, no. 4 (1985): 2287.

[17] Qiu, Z. Q., and Samuel D. Bader. "Surface magneto-optic Kerr effect." Review of Scientific Instruments 71, no. 3 (2000): 1243-1255.

[18] Liu, Chien, Zachary Dutton, Cyrus H. Behroozi, and Lene Vestergaard Hau. "Observation of coherent optical information storage in an atomic medium using halted light pulses." Nature 409, no. 6819 (2001): 490-493.

[19] Safavi-Naeini, Amir H., T. P. Alegre, Jasper Chan, Matt Eichenfield, Martin Winger, Qiang Lin, Jeff T. Hill, Darrick E. Chang, and Oskar Painter. "Electromagnetically induced transparency and slow light with optomechanics." Nature 472, no. 7341 (2011): 69-73.

[20] Chang, Yue, T. Shi, Yu-xi Liu, C. P. Sun, and Franco Nori. "Multistability of electromagnetically induced transparency in atom-assisted optomechanical cavities." Physical Review A 83, no. 6 (2011): 063826.

[21] Shahidani, S., M. H. Naderi, and M. Soltanolkotabi. "Control and manipulation of electromagnetically induced transparency in a nonlinear optomechanical system with two movable mirrors." Physical Review A 88, no. 5 (2013): 053813.

[22] Kowalski, K., V. Cao Long, K. Dinh Xuan, M. Głódź, B. Nguyen Huy, and J. Szonert. "Electromagnetically induced transparency." Physics Today 50, no. 7 (1997): 135.

[23] Sohail, Amjad, Yang Zhang, Jun Zhang, and Chang-shui Yu. "Optomechanically induced transparency in multi-cavity optomechanical system with and without one two-level atom." Scientific Reports 6, no. 1 (2016): 1-8.

[24] Lemonde, Marc-Antoine, Nicolas Didier, and Aashish A. Clerk. "Nonlinear interaction effects in a strongly driven optomechanical cavity." Physical Review Letters 111, no. 5 (2013): 053602.

[25] Rempe, G., R. J. Thompson, R. J. Brecha, W. D. Lee, and H. J. Kimble. "Optical bistability and photon statistics in cavity quantum electrodynamics." Physical Review Letters 67, no. 13 (1991): 1727.

[26] Payne, M. G., and L. Deng. "Quantum entanglement of Fock states with perfectly efficient ultraslow single-probe photon four-wave mixing." Physical Review Letters 91, no. 12 (2003): 123602.

[27] Venkatesh, B. Prasanna, Jonas Larson, and D. H. J. O'Dell. "Band-structure loops and multistability in cavity QED." Physical Review A 83, no. 6 (2011): 063606.

[28] Joshi, Amitabh, and Min Xiao. "Optical multistability in three-level atoms inside an optical ring cavity." Physical Review Letters 91, no. 14 (2003): 143904.

[29] Phuc, Nguyen Thanh, Yuki Kawaguchi, and Masahito Ueda. "Quantum mass acquisition in spinor Bose-Einstein condensates." Physical Review Letters 113, no. 23 (2014): 230401.

[30] Yamamoto, Yoshihisa, and Yoshiro Takahashi. "Bose-Einstein Condensation: A Platform for Quantum Simulation Experiments." In Principles and Methods of Quantum Information Technologies, pp. 265-307. Springer, Tokyo, (2016): 265-307.

[31] Jiang, Cheng, Hongxiang Liu, Yuanshun Cui, Xiaowei Li, Guibin Chen, and Bin Chen. "Electromagnetically induced transparency and slow light in two-mode optomechanics." Optics Express 21, no. 10 (2013): 12165-12173.

[32] Tian, Lin, and Peter Zoller. "Coupled ion-nanomechanical systems." Physical Review Letters 93, no. 26 (2004): 266403.

[33] Huang, Sumei, and G. S. Agarwal. "Normal-mode splitting and antibunching in Stokes and Anti-Stokes processes in cavity optomechanics: radiation-pressure-induced four-wave-mixing cavity optomechanics." Physical Review A 81, no. 3 (2010): 033830.

[34] Glasser, Ryan T., Ulrich Vogl, and Paul D. Lett. "Stimulated generation of superluminal light pulses via four-wave mixing." Physical Review Letters 108, no. 17 (2012): 173902.

[35] Wang, Zhiping, Benli Yu, Jun Zhu, Zhigang Cao, Shenglai Zhen, Xuqiang Wu, and Feng Xu. "Atom localization via controlled spontaneous emission in a five-level atomic system." Annals of Physics 327, no. 4 (2012): 1132-1145.

[36] Kazemi, Seyedeh Hamideh, and Mohammad Mahmoudi. "Optomechanical second-order sideband effects in a Laguerre–Gaussian rotational-cavity system." Physica Scripta 95, no. 4 (2020): 045107.

[37] Gröblacher, Simon, Klemens Hammerer, Michael R. Vanner, and Markus Aspelmeyer. "Observation of strong coupling between a micromechanical resonator and an optical cavity field." Nature 460, no. 7256 (2009): 724-727.

[38] Hill, Jeff T., Amir H. Safavi-Naeini, Jasper Chan, and Oskar Painter. "Coherent optical wavelength conversion via cavity optomechanics." Nature Communications 3, no. 1 (2012): 1-7.

[39] Munsch, Mathieu, Andreas V. Kuhlmann, Davide Cadeddu, Jean-Michel Gérard, Julien Claudon, Martino Poggio, and Richard J. Warburton. "Resonant driving of a single photon emitter embedded in a mechanical oscillator." Nature Communications 8, no. 1 (2017): 1-7.

[40] Wang, Dawei, Tee-Hiang Cheng, Yong-Kee Yeo, Zhaowen Xu, Yixin Wang, Gaoxi Xiao, and Jianguo Liu. "Performance comparison of using SOA and HNLF as FWM medium in a wavelength multicasting scheme with reduced polarization sensitivity." Journal of Lightwave Technology 28, no. 24 (2010): 3497-3505.

[41] Kong, Xiaoyi, and Yuefeng Zhao. "All optical wavelength conversion of dual users CO-OFDM system based on FWM in cascade HNLFs." Optical Fiber Technology 63 (2021): 102480.

[42] Sharma, Vishal, and Ramandeep Kaur. "Implementation of DWDM system in the presence of four wave mixing (FWM) under the impact of channel spacing." Optik-International Journal for Light and Electron Optics 124, no. 17 (2013): 3112-3114.

[43] D'ottavi, A., Francois Girardin, L. Graziani, F. Martelli, P. Spano, Antonio Mecozzi, S. Scotti, R. Dall'Ara, J. Eckner, and G. Guekos. "Four-wave mixing in semiconductor optical amplifiers: A practical tool for wavelength conversion." IEEE Journal of selected topics in Quantum Electronics 3, no. 2 (1997): 522-528.

[44] Fukuda, Hiroshi, Koji Yamada, Tetsufumi Shoji, Mitsutoshi Takahashi, Tai Tsuchizawa, Toshifumi Watanabe, Jun-ichi Takahashi, and Sei-ichi Itabashi. "Four-wave mixing in silicon wire waveguides." Optics Express 13, no. 12 (2005): 4629-4637.

[45] Payne, M. G., and L. Deng. "Quantum entanglement of Fock states with perfectly efficient ultraslow single-probe photon four-wave mixing." Physical Review Letters 91, no. 12 (2003): 123602.

[46] Camacho, Ryan M., Praveen K. Vudyasetu, and John C. Howell. "Four-wave-mixing stopped light in hot atomic rubidium vapour." Nature Photonics 3, no. 2 (2009): 103-106.

[47] Aso, Osamu, Masateru Tadakuma, and Shu Namiki. "Four-wave mixing in optical fibers and its applications." dEp 1 (1999): 63-68.

[48] Phillips, William D. "Nobel Lecture: Laser cooling and trapping of neutral atoms." Reviews of Modern Physics 70, no. 3 (1998): 721.

[49] Aspect, A., B. Desruelle, V. Boyer, S. G. Murdoch, G. Delannoy, P. Bouyer, G. Birkl, and M. Lécrivain. "Evaporative cooling and BEC in a high magnetic field." In Bose-Einstein Condensation in Atomic Gases, IOS Press, (1999): 503-519.

[50] Wineland, David J., Jean Dalibard, and C. Cohen-Tannoudji. "Sisyphus cooling of a bound atom." JOSA B 9, no. 1 (1992): 32-42.

[51] Anderson, Mike H., Jason R. Ensher, Michael R. Matthews, Carl E. Wieman, and Eric A. Cornell. "Observation of Bose-Einstein condensation in a dilute atomic vapor." Science 269, no. 5221 (1995): 198-201.

[52] Cohen-Tannoudji, Claude, and William D. Phillips. "New mechanisms for laser cooling." Phys. Today 43, no. 10 (1990)): 33-40.

[53] Ketterle, Wolfgang, and N. J. Van Druten. "Evaporative cooling of trapped atoms." In Advances in Atomic, Molecular, and Optical Physics, vol. 37, Academic Press, (1996): 181-236.

[54] Ketterle, Wolfgang. "Nobel lecture: When atoms behave as waves: Bose-Einstein condensation and the atom laser." Reviews of Modern Physics 74, no. 4 (2002): 1131.

[55] Sackett, C. A., C. C. Bradley, M. Welling, and Randall G. Hulet. "Bose–Einstein condensation of lithium." Applied Physics B 65, no. 4 (1997): 433-440.

[56] Neuman, Keir C., and Steven M. Block. "Optical trapping." Review of Scientific Instruments 75, no. 9 (2004): 2787-2809.

[57] Marangos, Jonathan P. "Electromagnetically induced transparency." Journal of Modern Optics 45, no. 3 (1998): 471-503.

[58] Peters, Thorsten, Benjamin Wittrock, Frank Blatt, Thomas Halfmann, and Leonid P. Yatsenko. "Thermometry of ultracold atoms by electromagnetically induced transparency." Physical Review A 85, no. 6 (2012): 063416.

[59] Safavi-Naeini, Amir H., T. P. Alegre, Jasper Chan, Matt Eichenfield, Martin Winger, Qiang Lin, Jeff T. Hill, Darrick E. Chang, and Oskar Painter. "Electromagnetically induced transparency and slow light with optomechanics." Nature 472, no. 7341 (2011): 69-73.

[60] Glasser, Ryan T., Ulrich Vogl, and Paul D. Lett. "Stimulated generation of superluminal light pulses via four-wave mixing." Physical Review Letters 108, no. 17 (2012): 173902.

[61] Kühner, Till D., Steven R. White, and Hartmut Monien. "One-dimensional Bose-Hubbard model with nearest-neighbor interaction." Physical Review B 61, no. 18 (2000): 12474.

[62] Konukoglu, Ender, Ben Glocker, Darko Zikic, and Antonio Criminisi. "Neighbourhood approximation using randomized forests." Medical Image Analysis 17, no. 7 (2013): 790-804.

[63] Lafuente, Luis, and José A. Cuesta. "Density functional theory for nearest-neighbor exclusion lattice gases in two and three dimensions." Physical Review E 68, no. 6 (2003): 066120.

[64] Morsch, Oliver, and Markus Oberthaler. "Dynamics of Bose-Einstein condensates in optical lattices." Reviews of Modern Physics 78, no. 1 (2006): 179.

[65] Louisell, W. H., A. Yariv, and A. E. Siegman. "Quantum fluctuations and noise in parametric processes. I." Physical Review 124, no. 6 (1961): 1646.

[66] Bhattacherjee, Aranya B. "Cavity quantum optomechanics of ultracold atoms in an optical lattice: normal-mode splitting." Physical Review A 80, no. 4 (2009): 043607.

[67] Akram, M. Javed, M. Miskeen Khan, and Farhan Saif. "Tunable fast and slow light in a hybrid optomechanical system." Physical Review A 92, no. 2 (2015): 023846.

[68] Bhattacharya, M., P-L. Giscard, and P. Meystre. "Entanglement of a Laguerre-Gaussian cavity mode with a rotating mirror." Physical Review A 77, no. 1 (2008): 013827.

[69] Bhattacharya, M., P-L. Giscard, and Pierre Meystre. "Entangling the rovibrational modes of a macroscopic mirror using radiation pressure." Physical Review A 77, no. 3 (2008): 030303.

[70] Huepe, Cristian, Stéphane Metens, Guy Dewel, Pierre Borckmans, and Marc-Etienne Brachet. "Decay rates in attractive Bose-Einstein condensates." Physical Review Letters 82, no. 8 (1999): 1616.

[71] Söding, J., D. Guéry-Odelin, P. Desbiolles, F. Chevy, H. Inamori, and J. Dalibard. "Three-body decay of a rubidium Bose–Einstein condensate." Applied Physics B 69, no. 4 (1999): 257-261.

[72] Tredicucci, Alessandro, et al. "Optical bistability of semiconductor microcavities in the strong-coupling regime." Physical Review A 54.4 (1996): 1843.

[73] Dorsel, A., et al. "Optical bistability and mirror confinement induced by radiation pressure." Physical Review Letters 51.17 (1983): 1550.

[74] Meystre, Pierre, et al. "Theory of radiation-pressure-driven interferometers." JOSA B 2.11 (1985): 1830-1840.

[75] Huttenhower, Curtis, et al. "Structure, function and diversity of the healthy human microbiome." Nature 486.7402 (2012): 207-214.

[76] Fabre, Claude, et al. "Quantum-noise reduction using a cavity with a movable mirror." Physical Review A 49.2 (1994): 1337.

[77] Aldana, Samuel, Christoph Bruder, and Andreas Nunnenkamp. "Equivalence between an optomechanical system and a Kerr medium." Physical Review A 88.4 (2013): 043826.

[78] Agrawal, Govind P. "Nonlinear fiber optics." In Nonlinear Science at the Dawn of the 21st Century, Springer, Berlin, Heidelberg, (2000): 195-211.

[79] Braginskii, Vladimir Borisovich, and Anatoliǐ Borisovich Manukin. "Measurement of weak forces in physics experiments." UCP (1977): 161.

[80] Vitali, D., P. Tombesi, M. J. Woolley, A. C. Doherty, and G. J. Milburn. "Entangling a nanomechanical resonator and a superconducting microwave cavity." Physical Review A 76, no. 4 (2007): 042336.

[81] Genes, Claudiu, A. Mari, P. Tombesi, and D. Vitali. "Robust entanglement of a micromechanical resonator with output optical fields." Physical Review A 78, no. 3 (2008): 032316.

[82] Abdi, M. and Barzanjeh, Sh. and Tombesi, P. and Vitali, D. "Effect of phase noise on the generation of stationary entanglement in cavity optomechanics." Physical Review A 84.3 (2011): 032325.

[83] Agarwal, Girish S., and Sumei Huang. "Electromagnetically induced transparency in mechanical effects of light." Physical Review A 81, no. 4 (2010): 041803.

[84] Weis, R., and S. Deléglise Riviere. "E. Gavartin, O. Arcizet, A. Schliesser, and TJ Kippenberg." Science 330 (2010): 1520.

[85] C. Jiang, J.-J. Li, W. He, K.-D. Zhu, and Euro., Phys. Lett. 91 (2010): 1-17.

[86] Carmele, Alexander, et al. "Opto-nanomechanics strongly coupled to a Rydberg superatom: coherent versus incoherent dynamics." New Journal of Physics 16.6 (2014): 063042.

[87] B. Rogers, N. L. Gullo, G. D. Chiara, G. M. Palma, and M. Paternostro, Quantum Meas. Quantum Metrol. 2 (2014): 11-43.

[88] Bariani F., S. Singh, L. F. Buchmann, M. Vengalattore, and Pierre Meystre. "Hybrid optomechanical cooling by atomic Λ systems." Physical Review A 90, no. 3 (2014): 033838.

[89] Safavi-Naeini, A. H., T. M. Alegre, and J. Chan. "M. Eichen eld, M. Winger, Q. Lin, JT Hill, DE Chang, and O. Painter." Nature (London) 472 (2011): 69.

[90] Rocheleau, T., T. Ndukum, C. Macklin, and J. B. Hertzberg. "AA Clerk, and KC Schwab." Nature 463 (2010): 72.

[91] Schwab, Keith C., and Michael L. Roukes. "Putting mechanics into quantum mechanics." Physics Today 58, no. 7 (2005): 36-42.

[92] McGee, S. A., D. Meiser, C. A. Regal, K. W. Lehnert, and M. J. Holland. "Mechanical resonators for storage and transfer of electrical and optical quantum states." Physical Review A 87, no. 5 (2013): 053818.

[93] Akram, Muhammad Javed, and Farhan Saif. "Complex dynamics of nano-mechanical membrane in cavity optomechanics." Nonlinear Dynamics 83.1-2 (2016): 963-970.

[94] Brennecke, Ferdinand, Stephan Ritter, Tobias Donner, and Tilman Esslinger. "Cavity optomechanics with a Bose-Einstein condensate." Science 322, no. 5899 (2008): 235-238.

[95] Kanamoto, Rina, and P. Meystre. "Optomechanics of a quantum-degenerate Fermi gas." Physical review letters 104, no. 6 (2010): 063601.

[96] Yang, Shuai, M. Al-Amri, and M. Suhail Zubairy. "Dicke quantum phase transition with a degenerate Fermi gas in an optical cavity." Journal of Physics B: Atomic, Molecular and Optical Physics 47, no. 13 (2014): 135503.

[97] Bariani, Francesco, Johannes Otterbach, Huatang Tan, and Pierre Meystre. "Single-atom quantum control of macroscopic mechanical oscillators." Physical Review A 89, no. 1 (2014): 011801.

[98] Kiyani, K. H., S. C. Chapman, Yu V. Khotyaintsev, M. W. Dunlop, and F. Sahraoui. "Global scale-invariant dissipation in collisionless plasma turbulence." Physical Review Letters 103, no. 7 (2009): 075006.

[99] Restrepo, Juan, Cristiano Ciuti, and Ivan Favero. "Single-polariton optomechanics." Physical Review Letters 112.1 (2014).

[100] Saif, Farhan. "Corrigendum to "Classical and quantum chaos in atom optics".[Phys. Rep. 419 (2005) 207-258]." Physics Reports 425, no. 5-6 (2006): 369-369.

[101] Fink, J. M., M. Göppl, M. Baur, R. Bianchetti, Peter J. Leek, Alexandre Blais, and Andreas Wallraff. "Climbing the Jaynes–Cummings ladder and observing its nonlinearity in a cavity QED system." Nature 454, no. 7202 (2008): 315-318.

[102] Tian, Lin. "Optoelectromechanical transducer: Reversible conversion between microwave and optical photons." Annalen der Physik 527, no. 1-2 (2015): 1-14.

[103] Tian, Lin, and Peter Zoller. "Coupled ion-nanomechanical systems." Physical Review Letters 93.26 (2004): 266403.

[104] Hensinger, W. K., D. Wahyu Utami, H-S. Goan, K. Schwab, C. Monroe, and G. J. Milburn. "Ion trap transducers for quantum electromechanical oscillators." Physical Review A 72, no. 4 (2005): 041405.

[105] Tian, Lin. "Adiabatic state conversion and pulse transmission in optomechanical systems." Physical Review Letters 108.15 (2012): 153604.

[106] Bennett, Steven D., Jesse Maassen, and Aashish A. Clerk. "Scattering approach to backaction in coherent nanoelectromechanical systems." Physical Review Letters 105, no. 21 (2010): 217206.

[107] Wineland, David J., C. Monroe, Wayne M. Itano, Dietrich Leibfried, Brian E. King, and Dawn M. Meekhof. "Experimental issues in coherent quantum-state manipulation of trapped atomic ions." Journal of research of the National Institute of Standards and Technology 103, no. 3 (1998): 259.

[108] Leibfried, D., and R. Blatt. "C. Monroe y D. Wineland." Rev. of Mod. Phys 75 (2003): 281.

[109] Teufel, J. D., J. W. Harlow, C. A. Regal, and K. W. Lehnert. "Dynamical backaction of microwave fields on a nanomechanical oscillator." Physical Review Letters 101, no. 19 (2008): 197203.

[110] Anetsberger, Georg, Olivier Arcizet, Quirin P. Unterreithmeier, Rémi Rivière, Albert Schliesser, Eva Maria Weig, Jörg Peter Kotthaus, and Tobias J. Kippenberg. "Near-field cavity optomechanics with nanomechanical oscillators." Nature Physics 5, no. 12 (2009): 909-914.

[111] Park, Young-Shin, and Hailin Wang. "Resolved-sideband and cryogenic cooling of an optomechanical resonator." Nature physics 5, no. 7 (2009): 489-493.

[112] Chang, Darrick E., Vladan Vuletić, and Mikhail D. Lukin. "Quantum nonlinear optics—photon by photon." Nature Photonics 8, no. 9 (2014): 685-694.

[113] Gröblacher, Simon, Klemens Hammerer, Michael R. Vanner, and Markus Aspelmeyer. "Observation of strong coupling between a micromechanical resonator and an optical cavity field." Nature 460, no. 7256 (2009): 724-727.

[114] Li, Hao-Kun, Xue-Xin Ren, Yong-Chun Liu, and Yun-Feng Xiao. "Photon-photon interactions in a largely detuned optomechanical cavity." Physical Review A 88, no. 5 (2013): 053850.

[115] Wang, Ying-Dan, and Aashish A. Clerk. "Using dark modes for high-fidelity optomechanical quantum state transfer." New Journal of Physics 14, no. 10 (2012): 105010.

[116] McRae, Terry G., Kwan H. Lee, Glen I. Harris, Joachim Knittel, and Warwick P. Bowen. "Cavity optoelectromechanical system combining strong electrical actuation with ultrasensitive transduction." Physical Review A 82, no. 2 (2010): 023825.

[117] Bennett, Steven D., Lynda Cockins, Yoichi Miyahara, Peter Grütter, and Aashish A. Clerk. "Strong electromechanical coupling of an atomic force microscope cantilever to a quantum dot." Physical Review Letters 104, no. 1 (2010): 017203.

[118] Lee, Kwan H., Terry G. McRae, Glen I. Harris, Joachim Knittel, and Warwick P. Bowen. "Cooling and control of a cavity optoelectromechanical system." Physical Review Letters 104, no. 12 (2010): 123604.

[119] McGee, S. A., D. Meiser, C. A. Regal, K. W. Lehnert, and M. J. Holland. "Mechanical resonators for storage and transfer of electrical and optical quantum states." Physical Review A 87, no. 5 (2013): 053818.

[120] Tsang, Mankei. "Cavity quantum electro-optics." Physical Review A 81.6 (2010): 063837.

[121] Regal, C. A., and K. W. Lehnert. "From cavity electromechanics to cavity optomechanics." In Journal of Physics: Conference Series, vol. 264, no. 1, IOP Publishing, (2011): 012025.

[122] Akram, Muhammad Javed, Fazal Ghafoor, and Farhan Saif. "Electromagnetically induced transparency and tunable fano resonances in hybrid optomechanics." Journal of Physics B: Atomic, Molecular and Optical Physics 48, no. 6 (2015): 065502.

[123] Ma, Peng-Cheng, Jian-Qi Zhang, Yin Xiao, Mang Feng, and Zhi-Ming Zhang. "Tunable double optomechanically induced transparency in an optomechanical system." Physical Review A 90, no. 4 (2014): 043825.

[124] Wang, Hui, Xiu Gu, Yu-xi Liu, Adam Miranowicz, and Franco Nori. "Optomechanical analog of two-color electromagnetically induced transparency: Photon transmission through an optomechanical device with a two-level system." Physical Review A 90, no. 2 (2014): 023817.

[125] Agarwal, Girish S., and Sumei Huang. "Electromagnetically induced transparency in mechanical effects of light." Physical Review A 81, no. 4 (2010): 041803.

[126] Safavi-Naeini, A. H., T. M. Alegre, and J. Chan. "M. Eichen eld, M. Winger, Q. Lin, JT Hill, DE Chang, and O. Painter." Nature (London) 472 (2011): 69.

[127] Carretta, S., A. Chiesa, F. Troiani, D. Gerace, G. Amoretti, and P. Santini. "Quantum information processing with hybrid spin-photon qubit encoding." Physical Review Letters 111, no. 11 (2013): 110501.

[128] Roden, Jan, Alexander Eisfeld, Wolfgang Wolff, and Walter T. Strunz. "Influence of complex exciton-phonon coupling on optical absorption and energy transfer of quantum aggregates." Physical Review Letters 103, no. 5 (2009): 058301.

[129] Jiang, Cheng, Hongxiang Liu, Yuanshun Cui, Xiaowei Li, Guibin Chen, and Xuemin Shuai. "Controllable optical bistability based on photons and phonons in a two-mode optomechanical system." Physical Review A 88, no. 5 (2013): 055801.

[130] Chen, Hua-Jun, Hong-Wei Wu, Jian-Yong Yang, Xue-Chao Li, Ya-Juan Sun, and Yuan Peng. "Controllable optical bistability and four-wave mixing in a photonic-molecule optomechanics." Nanoscale Research Letters 14, no. 1 (2019): 1-10.

[131] Ullah, Kamran. "Electro-optomechanical switch via tunable bistability and four-wave mixing." Chinese Physics B 28, no. 11 (2019): 114209.

[132] Li, Kangkang, Renan Bu, Xiuxiu Wang, Haixia Chen, Dan Zhang, Xinghua Li, and Yanpeng Zhang. "Flip-flop converter of dual-bistability using cavity and parametric amplified four-wave mixing." Scientific Reports 8, no. 1 (2018): 1-8.

Turnitin Originality Report

OPERATIONAL CHARACTERISTICS OF NANO-ELECTRO-OPTO-MECHANICAL   turnitin
TRANSDUCER   by Asma Javaid .

From CL QAU (DRSML)

- Processed on 03-Mar-2022 09:51 PKT
- ID: 1775283080
- Word Count: 17120

Similarity Index
11%
Similarity by Source

Internet Sources:
   4%
Publications:
   9%
Student Papers:
   2%

sources:

1 3% match (publications)
Kamran Ullah, "Electro-optomechanical switch via tunable bistability and four-wave mixing", Chinese Physics B, 2019

2 1% match ()
Akram, M, Javed, Naseer, Khalid, Saif, Farhan, "Efficient tunable switch from slow light to fast light in quantum opto-electromechanical system", 2015

3 1% match (Internet from 14-Apr-2019)
https://link.springer.com/content/pdf/10.1007/s11433-016-0346-4.pdf

4 1% match (publications)
Tian-Xiang Lu, Ya-Feng Jiao, Hui-Lai Zhang, Farhan Saif, Hui Jing, "Selective and switchable optical amplification with mechanical driven oscillators", Physical Review A, 2019

5 1% match (student papers from 09-Jun-2017)
Submitted to Higher Education Commission Pakistan on 2017-06-09

6 < 1% match (publications)
Kamran Ullah, "Electro-optomechanical switch via tunable bistability and four-wave mixing", Chinese Physics B, 2019

7 < 1% match ()
Bai, Cheng-Hua, Wang, Dong-Yang, Wang, Hong-Fu, Zhu, Ai-Dong, Zhang, Shou, "Modulation of entanglement between two oscillators separated in space with an optical parametric amplifier", 2016

8 < 1% match (Internet from 04-Apr-2021)
https://arxiv.org/pdf/1109.6316.pdf

9 < 1% match (student papers from 26-Nov-2019)
Submitted to Higher Education Commission Pakistan on 2019-11-26

10 < 1% match (student papers from 05-Apr-2015)
Submitted to Higher Education Commission Pakistan on 2015-04-05

11 < 1% match (student papers from 19-Jan-2017)
Submitted to Higher Education Commission Pakistan on 2017-01-19

12 < 1% match (publications)
Li, , "A Circuit Cavity Electromechanical System", Generalized Optomechanics and Its Applications Quantum Optical Properties of Generalized Optomechanical System, 2013.

13 < 1% match (student papers from 02-May-2021)
Submitted to American College of the Middle East on 2021-05-02